Identification of PDL1 Drivers in Models of Head and Neck Squamous Cell Carcinoma by Genome Wide Screening

by

Jacqueline Mann

A dissertation submitted in partial fulfillment
of the requirements for the degree of
Doctor of Philosophy
(Molecular and Cellular Pathology)
in the University of Michigan
2020

Doctoral Committee:

Assistant Professor J.Chad Brenner, Co-Chair
Professor Alexey Nesvizhskii, Co-Chair
Professor Thomas Carey
Professor Nicholas Lukacs

Jacqueline Mann

jacmann@umich.edu

ORCID iD: 0000-0002-6786-7990

Dedication

For my friends, my family members, and all others who suffer from cancer.

Acknowledgements

First, I would like to thank Dr. Chad Brenner for welcoming me into his lab, for his encouragement and guidance along this journey, and for his enduring optimism in the face of any challenge, as this was often exactly what I needed in a mentor.

I would also like to thank my committee members for their support throughout this process. Dr. Tom Carey, Dr. Nick Lukacs, and my co-mentor Dr. Alexey Nesvizhskii have all encouraged and helped me in finding my way through graduate school and beyond, and I am so grateful they were willing to take the time to help mold my scientific thinking and advise me as I transition to the next phase of my career.

Thank you to the Molecular and Cellular Pathology Program, especially Dr. Zaneta Nikolovska-Coleska and Laura Labut, for the support and resources they work so tirelessly to provide in order to create such a strong training environment. Thank you also to the Proteome Informatics of Cancer Training Program, which expanded the scope of my learning tremendously.

Thank you to the MCP and PIBS students I have met during my time at U of M. It has been such a privilege to learn alongside and from so many fun and talented people.

A huge thank you to the many members of the Brenner lab and broader Head and Neck Oncology research team who contributed to this project and who provided endless scientific and moral support. Sue, Nicole, Elizabeth, Aditi, Sammi, Becky, Jiayu, Cate, Apurva- thank you so much for all your contributions to this work and for the fun and supportive lab environment you all helped to create. Thank you to Megan, who was truly another mentor to me throughout my time in the Brenner lab. Thank you to Brittany, a great friend and talented researcher, for all of her hard work in contributing to this project and keeping the lab running smoothly. Thank you to Molly- a brilliant and supportive colleague and friend. It was my good fortune that the only desk available when Molly joined the lab was next to mine, as I cannot imagine this past year in the lab without her.

Another huge thank you to the undergraduate and high school students who have worked with me over the years, including Mamadou Bah, Judy Kafelghazal, Julia Eisenberg, Tala Al Saghir, Gregory Crump, Isabel Murray, Hasnat Ahmed, and Erin Scheftz. I can't wait to see where life takes these smart and dedicated students. I thank them for all the time and effort they put into research in our laboratory, and for the refreshing positivity they brought to the work.

I would also like to thank my early scientific mentors at Chelmsford Public Schools and the University of Vermont, including Dr. Paula Deming at UVM. I would not be the scientist I am today had Dr. Deming not taken the time to personally train me, provided me with countless opportunities for growth, and supported all of my ambitions. Recalling her confidence in me has

bolstered me on many occasions, and I hope to pay forward the time and effort she invested in my education.

Thank you also to my wonderful friends in Ann Arbor and across the country who have brought so much joy and levity into my life. In particular, I could not have completed this process without the incredible support I have received from some of my oldest and dearest friends. Annie Accettella, Liz Cantrell, and Claire O'Connell: I have yet to find the words to express in full my gratitude for your unwavering support from the happiest to the most difficult moments. You are my second family.

Finally, I would like to thank my very first teachers- my parents, who, despite my interests being vastly different from their own (e.g. all furry/scaly/slimy creatures), fostered my every curiosity, encouraged me in every pursuit, and gifted me the most invaluable freedom in knowing I could be whomever I chose. Anything I accomplish is, above all else, a reflection of the infinitely loving and supportive world the Kudla and Mann families have built around me.

Table of Contents

List of Tables

List of Figures

Abstract

Head and neck squamous cell carcinoma (HNSCC) is the sixth most common cancer worldwide and as only approximately 50% of patients survive five years after diagnosis, new treatment options are urgently needed. A complex array of molecular and microenvironmental alterations are believed to play a role in HNSCC pathogenesis, including suppression of antitumor immunity by expression of the immune checkpoint signal Programmed Death Ligand 1 (PDL1). The advancement of predictive and prognostic biomarkers, as well as rationally designed and personalized treatment regimens, will be especially crucial to improving outcomes across the spectrum of HNSCC subtypes. In an effort to comprehensively understand disease heterogeneity and mechanisms regulating immune escape, we have profiled various genetic, transcriptomic, and immunologic features of HNSCC.

The focus of this work was on the regulation of PDL1, a target for immunotherapy that has garnered significant attention in recent years. We aimed to provide a more complete portrait of the molecular pathways contributing to immunosuppression in HNSCC, and to identify signals that could be exploited as biomarkers and therapeutic targets. We utilized multiple genome wide screening techniques to select HNSCC cells with altered PDL1 expression and validated several hits nominated by these screens, most notably FGFR and TLR2 signaling. We expect these findings to contribute to a broader understanding of PDL1 checkpoint regulation in models and tumors with diverse genetic and phenotypic characteristics, and that this knowledge will ultimately lead to novel biomarkers and therapeutic combinations to improve patient outcomes.

Chapter 1 Introduction

1.1 Surveilling the Potential for Precision Medicine- Driven PD1/PDL1 Targeted Therapy in HNSCC[1]

Abstract

Immunotherapy is becoming an accepted treatment modality for many patients with cancer and is now approved for use in platinum-refractory recurrent or metastatic head and neck squamous cell carcinoma (HNSCC). Despite these successes, a minority of patients with HNSCC receiving immunotherapy respond to treatment, and few undergo a complete response. Thus, there is a critical need to identify mechanisms regulating immune checkpoints in HNSCC in the hopes of predicting responders, and so that novel combination strategies can be developed for non-responders. Here, we review the immunotherapy and molecular genetics literature to describe what is known about immune checkpoints in common genetic subsets of HNSCC. We highlight several highly recurrent genetic lesions that may serve as biomarkers or targets for combination immunotherapy in HNSCC.

Introduction

Over the last decade, research in head and neck squamous cell carcinoma (HNSCC) has shown that suppression of the host immune system plays a key role in the development and

[1] This section was published in the Journal of Cancer in collaboration with the following authors: Rebecca Hoesli, Nicole Michmerhuizen, Samantha Devenport, Megan Ludwig, Taylor Vandenberg, Chloe Matovina, Nadine Jawad, Michelle Mierzwa, Andrew Shuman, Matthew Spector, and Chad Brenner.

progression of HNSCC. Many critical components of both the innate and adaptive immune systems are dysfunctional in patients with HNSCC, including the activity of natural killer cells, the function of antigen presenting machinery, and the maturation of dendritic cells [1-4]. Additionally, in the composition of functioning cells such as T lymphocytes, there is a shift towards immunosuppression, with higher numbers of the immunosuppressive regulatory T cells and immunosuppressive cytokines, while the overall number of lymphocytes is decreased [5-9]. Many of these defects feedback amongst themselves, resulting in the release of cytokines and recruitment of immunosuppressive cells, further promoting the immunosuppressive environment. Importantly, this immunosuppression appears to play pivotal roles in both HNSCCs driven by high risk human papilloma virus (HPV) and HPV negative disease.

In addition to these defects, HNSCCs, like other immunosuppressive cancers, have co-opted beneficial physiologic signaling pathways to aid in immune evasion. In the intact immune system, there is a necessary equilibrium between activation and suppression of the immune system. This balance prevents excessive activation of the immune system resulting in autoimmune diseases, as well as pathologic suppression resulting in opportunistic infections. Various co-stimulatory and co-inhibitory signaling pathways are involved in maintaining this equilibrium, including the CTLA-4 and programmed death-1 (PD-1):programmed death ligand-1 (PDL1) pathways, which serve as checkpoints to mitigate excessive inflammation. Both of these pathways are thought to have been exploited by HNSCC in order to enhance the immunosuppressive environment, preventing immune surveillance and tumor destruction [10, 11]. Therapies targeting the co-inhibitory receptor CTLA-4 were among the earliest immunotherapies for cancer, and following their success in the clinic, additional targets, including the PD-1:PD-1

pathway, were quickly advanced [10]. This review will focus on the various genetic alterations and molecular pathways that may contribute to dysregulation of the PD-1:PDL1 pathway.

Immune Checkpoints and PD1/PDL1 Signaling

The PD-1/PDL1 pathway is an important co-inhibitory pathway involved in the regulation of the human immune response. This pathway serves as an immune checkpoint, providing protection against excessive tissue damage induced by inflammation [10], and is especially important in regulating antigen-specific effector T-cell activity in peripheral tissues. The PD-1 receptor is a transmembrane protein expressed by T cells, B cells, and many types of tumor-infiltrating lymphocytes (TILs). PD-1 can bind either of two ligands: PDL1 or PDL2, both of which are cell surface proteins of the B7 family [12, 13]. Upon ligand binding, generation and activation of effector T cells, particularly CD8+ T cells, is dramatically suppressed [14]. Expression of PDL1 can be stimulated by interferon-γ (IFN-γ), a cytokine produced primarily by effector lymphocytes [15]. In general, interferons function as lines of communication between the innate and adaptive immune responses by activating immature dendritic cells and CD8+ T cells. IFN-γ is largely responsible for inducing inflammation, a critical component of the immune response. Cancer cells are thought to induce an immune response, and inflammation is common within the tumor microenvironment. However, it is hypothesized that cancer cells can develop an "adaptive immune resistance" to increased levels of inflammation by upregulating PDL1 in response to IFN-γ, thereby protecting themselves against immune attack by promoting T cell anergy and apoptosis [16, 17]. An interesting connection has also emerged between HPV infection, now recognized as a common initiator of oropharyngeal cancer, and immunosuppression. Major sites of HPV infection, such as the tonsillar crypts, may be prone to harboring high levels of foreign antigens [18]. It is plausible that activation of immunosuppressive mechanisms to stifle

excessive inflammation also creates a permissive environment for both persistent HPV and associated tumors to flourish [18]. It has also been postulated that immunosuppressive pathways initiated by HPV itself allow for malignant transformation at the site of infection [19].

Although the PD-1/PDL1 pathway was discovered more than two decades ago, the therapeutic potential associated with targeting this pathway in cancer was not immediately recognized. As the immunosuppressive function of the PD-1/PDL1 interaction was revealed and PDL1 expression was observed in tumor cells, researchers hypothesized that blockade of this pathway could help facilitate eradication of tumors and impede tumor metastasis [20]. This hypothesis was first tested in melanoma, in which treatment with monoclonal antibodies (mAbs) directed against PD-1 showed promising results. In a meta-analysis of 5 multi-center randomized control trials including 2,828 patients, patients treated with an anti- PD-1 mAb experienced superior progression free survival (PFS) ranging from 3.7 to 6.9 months as compared with 2.2 to 4.2 months in the control group. Six-month PFS was significantly improved for patients treated with anti-PD-1 therapy, with a hazard ratio (HR) of 0.55 [21]. There was also a statistically significant improvement in overall response rate (ORR) with an odds ratio (OR) of 3.89 [21]. Two anti-PD-1 antibodies, pembrolizumab and nivolumab, have since been approved by the FDA for the treatment of advanced melanoma due to convincing data demonstrating increased ORR, as well as improved PFS and OS [11].

Currently, five mAb therapies targeting the PD-1/PDL1 pathway are under investigation for use in HNSCC. Pembrolizumab and Nivolumab target PD-1, while MEDI4736, Atezolizumab, and Avelumab target PDL1. Pembrolizumab has shown considerable promise for use in patients with recurrent and/or metastatic HNSCC. An 18.2% ORR has been reported with a severe adverse reaction rate of 7.6%, leading to the August 2016 approval of Pembrolizumab

for platinum-refractory recurrent or metastatic HNSCC patients [22]. Interestingly, ORR was independent of HPV status and PDL1 status [23]. A phase 3 trial is also currently underway for Nivolumab versus either Cetuximab, Docetaxel, or Methotrexate for recurrent/metastatic HNSCC (Clinical Trial: NCT02105636). Preliminary results show a doubling in the one year overall survival rate to 36% in Nivolumab treated patients. Median overall survival was 7.5 months in the Nivolumab group as compared to 5.1 months in the standard treatment group. Interestingly, both HPV positive and HPV negative patients benefit with the median survival for HPV positive patients increasing from 4.4 to 9.1 months, and that of HPV negative patients increasing from 5.8 to 7.5 months [24]. Due to its early success, additional trials evaluating the efficacy of Nivolumab in combination with chemotherapy and/or radiation for definitive therapy in locoregionally advanced HNSCC are currently underway (NCT02764593).

Of the mAbs against PDL1, MEDI4736 or Durvalumab, is currently being evaluated in a phase 3 trial of Durvalumab alone versus Durvalumab plus an anti-CTLA-4 inhibitor (tremelimumab) versus standard treatment (NCT02369874) [25]. Atezolizumab and Avelumab are currently in several Phase 1b/2 trials evaluating the safety and efficacy of these inhibitors in advanced solid tumor malignancies, as listed in Table1.1. Several ongoing trials are investigating their use alone and in combination with other targeted therapies.

Given the enthusiasm for drugs targeting the PD1/PDL1 pathways in the management of recurrent HNSCC, it is reasonable to expect that new protocols will be developed expanding the application of immunotherapy in this context. An enhanced understanding of PD-1 and PDL1 expression and modulation, in addition to other factors predicting response to PD-1/PDL1 blockade, will be essential to the rational design of future trials. Here, we review potential

modulators of PDL1 expression, as well as important considerations associated with targeting PDL1 in HNSCC patients.

PD-1 and PDL1 expression in HNSCC

While several studies have evaluated expression of PDL1 in HNSCC by immunohistochemistry, results are highly variable. Thus, the clinical significance of PDL1 expression in tumor cells remains unclear. PDL1 staining may be membranous and/or diffuse, and often appears at the interface of tumor cells and T cells. PDL1 expression is reported in 51-87% of HNSCC tumors across several reports and criteria for PDL1 "positivity" are highly variable [18, 26-31]. Small sample size, inconsistent representation of different disease sites, prior therapy, or the antibody used to detect PDL1 may contribute to discrepancies among these studies. Intratumoral heterogeneity and temporal changes in PDL1 expression may also lead to false negatives [32]. HPV associated cancers are more likely to express PDL1, but PDL1 expression has not been directly correlated with survival despite the better prognosis observed among these cancers. However, tumor infiltration with high numbers of PD-1 expressing CD8+ T cells is associated with longer overall survival; the mechanism and implications thereof remain unclear [29, 33].

Potential for intrinsic modulation of PDL1 by oncogenic pathways

JAK2/STAT1 mediated induction of PDL1 expression on the surface of tumor cells has been demonstrated in response to IFN-γ, and, recently, epidermal growth factor (EGF) [34]. The finding that EGF can promote PDL1 expression was especially interesting given that the EGF receptor (EGFR) is highly overexpressed in HNSCC. This observation highlights the possibility that other signals, including common oncogenic drivers, may contribute to immunosuppression by promoting PDL1 expression. Elucidating the molecular mechanisms governing PDL1 expression in the context of HNSCC may provide a compelling rationale for combining

immunotherapy with other agents targeting upstream regulators of the PDL1/PD-1 pathway. While mechanisms regulating PDL1 have been examined in other cancers, few studies have addressed intrinsic modulation of PDL1 in HNSCC, especially in the context of emerging precision medicine paradigms that match targeted therapies with specific genetic lesions [35-39]. Interestingly, several potentially targetable pathways including EGFR, phosphatidylinositol 3-kinase (PI3K)/Akt, MAPK, p53, STAT and HIF-1α are commonly deregulated in HNSCC and could potentially influence the expression of PDL1 (**Figure 1.1**). There is potential to exploit newly discovered relationships between PDL1 regulation and other well-described drug targets, and rapidly translate these findings, as many of these pathways are already being targeted in clinical trials (**Table 1.2**).

EGFR

EGFR is overexpressed in >90% of HNSCCs by a variety of genetic mechanisms including amplification (~10% of cases) [40-43]. It is therefore not surprising that targeting EGFR has become an important strategy in the management of HNSCC. Several small molecule inhibitors of EGFR signaling are currently being investigated, and clinical success has been achieved with biologics such as Cetuximab, a chimeric IgG1 mAb against EGFR [44]. As both EGFR- and PD-1/PDL1-targeted therapies have advanced, evidence has emerged for a potential confluence of these two pathways. In NSCLC, where immune checkpoint inhibitors have been more extensively studied and exploited, an interesting relationship between EGFR and PDL1 has been noted. Specifically, tumors with activating genetic aberrations to EGFR were more likely to have PDL1 overexpression than those without [45, 46], and treatment of these tumors with the small molecule EGFR inhibitor gefitinib caused a substantial reduction in PDL1 expression suggesting a direct

mechanistic link between the two molecules [46]. Surprisingly, refractory NSCLC tumors arising after gefitinib treatments also have elevated PDL1 expression [47], suggesting that immune escape is an important mechanism to overcoming EGFR inhibitor response. More recently, Concha-Benavente et. al. noted a similar relationship in HNSCC models showing that Cetuximab-mediated EGFR inhibition caused a reduction in adaptive PDL1 expression through modulation of the JAK2/STAT1 effectors [34].

The postulate that EGFR activation can promote immune escape through regulation of PDL1 expression is especially interesting given the prevalence of Cetuximab-based therapies in HNSCC. The logical hypothesis addresses whether these two therapies can be combined, particularly given the poor observed response to Cetuximab as a single agent. It is unclear if combination Cetuximab + PD1/PDL1 checkpoint inhibitors would provide an incremental effect, as Cetuximab inhibits PDL1 expression thereby removing the immunotherapy target, perhaps suggesting the need for sequential use of the drugs. However, by activating T-cells to clear any tumor cells that are innately resistant to Cetuximab (or the EGFR-based modulation of PDL1), this combination may effectively clear heterogeneous tumor cell populations, although this remains to be proven *in vivo*. Clinical trials assessing these combinations in advanced HNSCC patients are currently being evaluated and sequential trials assessing PDL1 inhibition following Cetuximab failure are already ongoing (NCT02255097). An additional facet of mAb therapies is the potential for antibody-dependent cellular cytotoxicity (ADCC), a mechanism for the clearance of IgG1-coated target cells. ADCC is triggered by engagement of Fc receptors on immune effector cells with the Fc region of IgG1. Cetuximab induces ADCC in an EGFR-dependent manner in cell culture and in murine models [48-51], and although the contribution of ADCC to the anti-tumor effects of Cetuximab in humans is not fully understood, evidence of

increased ADCC has been reported. In a study of 22 HNSCC and colorectal cancer patients, Bertino et al observed more pronounced increases in ADCC in patients who experienced clinical benefit from Cetuximab than in those who did not [52]. ADCC may play a key role in the clinical efficacy of EGFR targeted mAbs, and could have important implications for combination immunotherapeutic strategies. For example, it is possible that the combined effects of relief from T-cell anergy, stimulation of natural killer cells, and inhibition of EGFR signaling in addicted cells may amplify the anti-tumor function of either strategy alone. EGFR-based therapies may therefore have important mechanistic consequences on PD1/PDL1-based therapies in HNSCC, and these molecules may serve as important companion diagnostics for adjunctive immunotherapy.

PI3K/AKT

The PI3K pathway, based on data from The Cancer Genome Atlas and other analyses, has been identified as the most frequently mutated of any oncogenic and targetable pathway in HNSCC [53-55]. Activating mutations and/or amplification of PIK3CA, which encodes PI3K's catalytic subunit and alpha isoform, was the most frequent alteration observed in the PI3K pathway. Aberration of this gene was reported in 37% of the TCGA HNSCC cohort [53]. As a whole, alterations in the PI3K pathway contribute to tumor progression and increased cell growth and viability; they are also more commonly observed in advanced stage disease [56, 57].

Various interferons have been shown to activate the PI3K pathway as well as to induce the expression of PDL1. In response to interferon, PI3K signaling is required for phosphorylation of STAT1 at the serine 727 residue and for the associated increase in gene transcription [58, 59]. PKC (δ and ε isoforms) and/or NF-κB may serve as downstream mediators of this response [15, 60-

[63]. Chen et al. showed that PDK2 signaling, which can be initiated by the PI3K-PKC pathway, is responsible for interferon-induced PDL1 expression in oral squamous cell carcinoma [15], and Kondo et al. demonstrated the dependence of interferon-induced PDL1 expression on NF-κB in myodysplastic syndrome blast cells [64]. Additionally, in dermal fibroblasts, interferon treatment led to translocation of NF-κB to the nucleus and transient phosphorylation of ERK and AKT. This effect was abrogated upon treatment with PI3K and MEK but not PKC inhibitors [60]. BRAF-inhibitor resistant melanoma cells also display inducible PDL1 expression that is dependent on NF-κB. In contrast to observations in dermal fibroblasts, however, the PI3K and MAPK pathways were not significant mediators of this response [65]. Ferris and colleagues reported that PI3K inhibitors wortmannin and BYL719 blocked AKT phosphorylation but failed to reverse the extrinsic interferon- or intrinsic EGFR-mediated increases in PDL1 expression in HNSCC cell lines [34]. These data indicate that the role of PI3K, NF-κB, and PKC may be cell-type specific and therefore motivate further studies of the signaling mechanisms in HNSCCs.

The PI3K pathway is also commonly activated in HNSCC via loss of PTEN, which functions as a "brake" on PI3K signaling. The PTEN tumor suppressor has been associated with PDL1 expression in other cancer types. Transgenic mouse models of lung SCC with loss of both PTEN and Lkb1, for example, developed tumors with elevated levels of PDL1 [66]. Parsa et al. showed that loss of PTEN in glioblastoma patients correlated with increased PDL1 expression and that PDL1 translation was S6K1-mediated [67]. Furthermore, a negative correlation between PTEN and PDL1 expression has been identified in pancreatic and colorectal cancer samples [68, 69]. miRNAs may also be an important component of this response as the upregulation of miRNAs, including miR-21, -20b, and 130b, in colorectal and esophageal cancers has been shown to suppress PTEN gene transcription [69, 70].

MAPK

In HNSCC, genetic alterations in MAPK family members are relatively rare. Only 5% of patients in the TCGA cohort displayed mutations or copy number changes in HRAS, with other alterations in this pathway (such as those affecting KRAS and MAPK1) occurring even less frequently [53]. In spite of this, signaling of the Ras-MEK-ERK pathway is often aberrant in HNSCC due to overexpression of EGFR or activation of other RTKs [71].

The signaling functions of the MAPK pathway, like those of the PI3K pathway, are important in interferon-induced changes in PDL1 expression. MAPK acts in coordination with the JAK/STAT pathway to regulate gene transcription, and inhibitors of MAPK pathway members (including MEK, ERK, and JNK) block these effects [72]. Consistent with this, Liu et al. showed that PMA, a known MEK/ERK pathway activator, could increase PDL1 expression in multiple myeloma; similarly, blocking MEK/ERK via pharmacological methods or siRNA knockdown resulted in decreased interferon-induced PDL1 expression [73]. Melanoma cells resistant to BRAF inhibition also displayed MAPK activation and increased PDL1 expression via c-Jun and STAT3, and this effect was reversed by MEK inhibitors [74]. Similar evidence for the role of the MAPK pathway in inducing PDL1 expression was identified in bladder cancer, where inhibitors of ERK and JNK blocked the induction of PDL1 expression by LPS treatment [75]. MAPK signaling also modulates PDL1 expression in anaplastic large cell lymphoma (via ALK) and in Hodgkin's lymphoma (via p38 MAPK and MEK1/2) [76].

Recent studies of breast cancer cell lines and murine models, however, have indicated that MEK inhibitor trametinib might induce PDL1 expression and therefore be useful in priming patients for immunotherapy treatment [77]. Further studies in BRAF-mutant and WT melanoma as well as

KRAS-mutant NSCLC cells showed varying PDL1 transcript levels following trametinib treatment [78]. Combination MAPK and PDL1 inhibitor treatments have been proposed and tested in vitro and in vivo, and combination therapies are currently being evaluated in clinical trials (such as NCT02027961 and NCT01988896 for BRAF-mutant melanoma and NSCLC patients, respectively) [79].

While these dual therapies might be effective in HNSCC, further work regarding both the specific mechanism of MAPK pathway activation in PDL1 expression and the modulation of PDL1 levels by MAPK inhibitors are necessary. Initial studies by Ferris and colleagues suggest that MEK inhibitors do not significantly alter PDL1 expression in HNSCC cell lines, but that JAK2 and STAT1 might be critical mediators of immunogenicity [34]. Additional research will aid in selecting patients who are the most likely to respond to combination MAPK-immunotherapy treatments, and one trial is currently underway in advanced solid malignancies including HNSCC (NCT02586987).

p53

The TP53 gene, encoding the p53 tumor suppressor, is the most commonly mutated gene in HNSCC [80]. Cortez et al recently reported that p53 can regulate PDL1 production via miR-34. p53 deficient or mutant tumors express significantly higher PDL1 levels than wild type p53 tumors [81]. In cell lines, p53 induced miR-34 repressed PDL1 expression. Interestingly, injection of miR-34 mimics, such as the drug MRX34, reduces PDL1 expression and increases immune response to tumorous growth. When MRX34 was paired with radiation therapy (XRT), a common anti-cancer treatment that induces the adaptive immune response to promote tumor regression, exponential increases in CD8+ tumor-infiltrating cell expression were found [81].

Understanding the relationship between the p53 pathway and its effects on PDL1 expression may allow physicians to better tailor treatment of tumors with p53 mutations.

STAT3

The STAT signaling pathway is known to play an important role in many cellular processes, including division, apoptosis, and motility. Involvement of the transcriptional activator STAT3 has been reported in the development and growth of tumors [82], and recent studies aim to elucidate the role of STAT3 in PDL1 expression on tumor cells [83]. STAT3 inhibition reduces PDL1 expression in NSCLC [84]. Similarly, in multiple types of lymphoma, PDL1 expression is enhanced by STAT3 and is decreased upon STAT3 inhibition [85, 86]. As activated STAT3 was elevated in HNSCC tumors compared to normal epithelium [87], elucidating a role for STAT3 in regulating PDL1 in HNSCC may shed light on potential therapeutic targets or factors influencing the ability of these tumors to respond to PD-1 blockade. However, a recent study found no correlation between STAT3 and PDL1 expression in HPV positive HNSCC, and only a weak correlation in HPV negative HNSCC [34].

HIF-1α

Hypoxia inducible factors (HIFs) are transcriptional regulators integral to the response to hypoxia in solid tumors, and are believed to be critical to metastasis [88]. Under hypoxic conditions, tumors utilize HIF-1α to upregulate glycolysis and to increase blood flow to the tumor by promoting angiogenesis. Recently, HIF-1α was suggested to play a role in PDL-1 expression [89]. Specifically, in myeloid derived stem cells (MDSCs), HIF-1α binds directly to the HRE-4 site in the proximal promoter of PDL1 [89]. Another PDL1 proximal promoter site, HRE-2,

has also been shown to bind with HIF-1 in mammary cells [90]. Hypoxia-induced PDL1 expression has been demonstrated in MDSCs, macrophages, dendritic cells, and tumor cells including breast and prostate cancer cell lines [89, 90], and this effect was HIF-1α dependent. While no direct link has been established between HIF-1 and PDL1 in HNSCC, given the reported overexpression of HIF-1α in HNSCC tissue vs adjacent normal tissue [91] and the poor prognosis associated with low intratumoral oxygen levels in HNSCC [92], a more detailed understanding of the potential for interplay between immune evasion and hypoxia could reveal novel mechanisms of HNSCC pathogenesis.

Additional Targets

Finally, there are additional genomic mutations in head and neck squamous cell carcinomas noted in the data from The Cancer Genome Atlas HNSCC cohort that make attractive targets for investigation in the development of immunotherapies. In addition to those described above, defects of note include mutations affecting other components of the innate and adaptive immune response, including antigen processing machinery and HLA, as well as tumor necrosis factor (TNF) receptor-associated factor 3 (TRAF3). HLA molecules play a key role in tumor identification and antigen presentation in the functioning immune system. HLA associates with degraded tumor peptides and β2-microglobulins, and once properly folded, the HLA complex consisting of the HLA protein chains, β2-microglobulins, and tumor peptides is transported to the cell surface, where it is recognized by T cells [3]. However, in one study of head and neck cancers, approximately 40% of primary tumors had at least selective loss of HLA class I antigens, and 15% had complete loss [93]. Although no current therapies target this defect, it

remains an attractive target for immunotherapies, as it could play an important role in activating T cells against tumor antigens.

TRAF3 plays an important role in regulating the crossroads between the anti-viral, anti-inflammatory, and cancer pathways by modulating toll-like receptors, TNF receptors, and producing interferons and anti-inflammatory cytokines [94]. They have been implicated in multiple myeloma in humans, and in one study of transgenic mice, overexpression was associated with autoimmunity and a predisposition to developing squamous cell carcinoma [95]. In the data from The Cancer Genome Atlas, TRAF3 mutation was a distinguishing mutation of HPV positive tumors [80]. No current therapies have been developed, but like HLA mutations, it remains as attractive area for investigation.

HPV and PDL1

Human papillomavirus (HPV), a known risk factor for HNSCC, has been linked to PD-1 pathway activation in several settings. In a 2013 study, Yang et. al described a correlation between PD-1 on T cells, persistent high risk (HR)-HPV infection, and the development of cervical intraepithelial neoplasia (CIN) [96]. A positive correlation between PDL1 expression and CIN grade was also observed in HR-HPV positive patients, suggesting that the PD-1:PDL1 pathway may play a role in permitting HR-HPV-related CIN progression [96].

With rates of HPV associated oropharyngeal cancers rapidly rising, it has become clear that the distinct pathogenesis of these cancers may warrant the development of alternate treatment protocols [97]. HPV associated HNSCCs generally have favorable clinical outcomes independently predicted by HPV status [98, 99]. The oropharyngeal tumors that result from HPV infection grow in the tonsillar crypts and near the base of tongue, which are also the most common sites of HPV infection. PDL1 expression is also found in deep tonsillar crypts in both

normal and HNSCC patients [18]. It is therefore plausible that a dampened effector T cell response within these crypts may yield an environment especially permissive to both initial HPV infection and SCC tumorigenesis.

HPV positive HNSCCs are able to grow and evade anti-tumor immunity despite high levels of inflammation. In order to evaluate the relevance of PD-1:PDL1 pathway in the development of HPV associated HNSCC, Lyford-Pike et. al analyzed PD-1 expression on TILs and peripheral blood mononuclear cells (PBMCs) isolated from patients with HPV positive HNSCC versus those from patients with a nonmalignant tonsillar pathology (such as hypertrophy or tonsillitis), and identified a population of PD-1 expressing CD8+ TILs in HPV positive HNSCC tumors. Such a population was not observed in T-cells infiltrating nonmalignant inflamed tonsils. Furthermore, the PD-1 expressing CD8+ TILs exhibited diminished ability to produce IFN-γ in response to stimulation with PMA/ionomycin compared to TILs not expressing PD-1, indicating the functional suppression of affected T-lymphocytes. Lyford-Pike also showed PDL1 expression localized to the interface of the tumor and CD8+ TILs [18]. This study implies that the PD-1:PDL1 pathway is likely important in both persistence of the initial HPV infection and suppression of anti-tumor immunity during tumorigenesis. Because high levels of membranous PDL1 expression were observed within tumors, HPV positive HNSCC patients are logical candidates for PD-1:PDL1-targeted therapy. Furthermore, a recent study in mice demonstrated improved anti-tumor activity in large HPV-induced tumors when immunization against HPV16 genes E6 and E7 was combined with an anti-PD-1 antibody [100].

Taken together, these data support the idea that blocking PD-1:PDL1 interactions may be a potential therapeutic option for HPV-infected patients. Indeed, early reports from the CheckMate-141 trial indicate enhanced benefit from Nivolumab in HPV positive patients.

Additionally, in the context of cervical lesions, HPV-induced malignant progression correlates with low or undetectable T cell response to HPV antigens [101]. Anti-tumor vaccines currently in clinical trials aim to stimulate an immune response against HPV specific antigens, such as viral oncoproteins E6 and E7, which function in malignant transformation to inactivate p53 and pRb, respectively

(NCT02865135, NCT02864147, NCT02002182, NCT02596243, NCT02163057) [102, 103]. It is possible that future immunotherapeutic protocols for the management of HPV positive HNSCC may achieve maximal benefit by combining vaccines to promote generation of tumor-specific effector T cells with anti-PD-1/PDL1 mAbs to relieve immunosuppression.

Predicting response to PD-1 blockade

PDL1 expression was initially considered a logical potential biomarker predicting response to anti-PD-1 therapy, but the many factors complicating its detection have limited its current utility, and no correlation between PDL1 expression and response to immunotherapy has been observed [29]. Thus, new methods for predicting potential responders are needed. Immunotherapy trials for other cancers may yield insight into potential biomarkers for response to PD-1 blockade in HNSCC. As in HNSCC, a main risk factor for non-small cell lung cancer (NSCLC) is smoking, which is associated with higher nonsynonymous mutation burden [104]. Recently, Rizvi et al reported improved objective response, durable clinical benefit, and progression free survival in Pembrolizumab-treated NSCLC patients with more non-synonymous mutations and a molecular smoking signature [105]. Not surprisingly, mutational load positively correlated with higher neoantigen levels, which were also associated with improved treatment efficacy. A similar trend of high mutational load was observed in bladder cancer patients responsive to PD-1 blockade [106]. It therefore seems likely that the neoantigens produced by

highly mutated tumors could potentially improve the ability of T-cells to recognize tumor cells following release from PDL1-mediated immunosuppression. Smoking status has not yet been reported for HNSCC patients treated with anti- PD-1 mAbs, and further investigation will be necessary to determine whether the correlations observed in NSCLC are recapitulated in the HNSCC setting.

In advanced melanoma patients who responded to pembrolizumab, tumors had less diverse T cell populations at baseline, but the number of expanded clones after treatment was 10 fold higher than in patients with disease progression [107]. These data suggest that a pre-existing T-cell repertoire poised to target tumor cells but negatively regulated by PD-1: PDL1 may predict response to PD-1 blockade. Again, this mechanism has yet to be investigated in HNSCC patients.

Limitations

Given the recent approval of anti-PD-1 therapy in the treatment of recurrent HNSCC, immunotherapy represents an exciting new avenue in the management of a disease with a limited armamentarium of systemic treatment options. It is also important, however, to consider the current limitations of immune checkpoint blockade. Improvements to OS, ORR, and PFS have been reported in patients treated with nivolumab and pembrolizumab, but many patients do not respond to immunotherapy, and no criteria currently exist to aid in selection of patients likely benefit from PD-1 blockade. Additionally, many patients, such as those with preexisting autoimmune disease, are not considered candidates for immunotherapy due to concern for unacceptable toxicity.

If and when immunotherapy is extended beyond the metastatic/recurrent setting, important new considerations will arise. Anti-PD-1 is currently administered in the context of

HNSCC recurrence to patients who have already received XRT, which may sensitize tumors to immune attack. In murine models, XRT increases type I IFN levels in tumors, thereby promoting T-cell effector function. XRT also induced IFN- dependent up-regulation of the CXCR3 chemokine, which enhanced the recruitment of T cells to tumors [108]. It is also speculated that the high mutational load in XRT treated tumors leads to higher neoantigen levels, and therefore improved detection by T cells. If these mechanisms are found to be at play, the utility of PD-1 blockade as a frontline monotherapy may be limited. However, further investigation of a role for RT in sensitizing cancers to anti-tumor immunity may provide rationale for protocols combining XRT with immune checkpoint blockade. Several studies in mice, as well as anecdotal evidence in humans, support the hypothesis that XRT and immunotherapy may synergize to promote tumor clearance by the immune system. Concurrent immune checkpoint therapy and XRT induced anti-tumor T-cell responses in mice, even outside the radiation field [109]. Instances of abscopal effects of XRT have been observed in melanoma patients also treated with immune checkpoint inhibitors [110, 111].

Conclusions

The exploitation of anti-tumor immunity in the treatment of cancer is a promising and rapidly expanding field, but more research is needed to understand mechanisms mediating response to immunotherapy and expand the population of patients who will benefit from this strategy. While anti-PD-1/PDL1 therapy has improved outcomes in comparison to the standard of care for a subset of patients with HNSCC, the proportion of responding patients, as well as the degree of benefit, remains modest. The future of anti-PD-1/PDL1 therapy in the treatment of HNSCC relies upon a better understanding of the dysregulated pathways in HNSCC that may alter its efficacy. With a vast and growing array of targeted therapies in development for the

treatment of cancer, countless opportunities for modulation of PDL1 can be envisioned. Trials capitalizing on mechanistic discoveries by combining anti-PD-1 therapy with other precision-medicine approaches may maximize the results seen with immunotherapy.

Figures

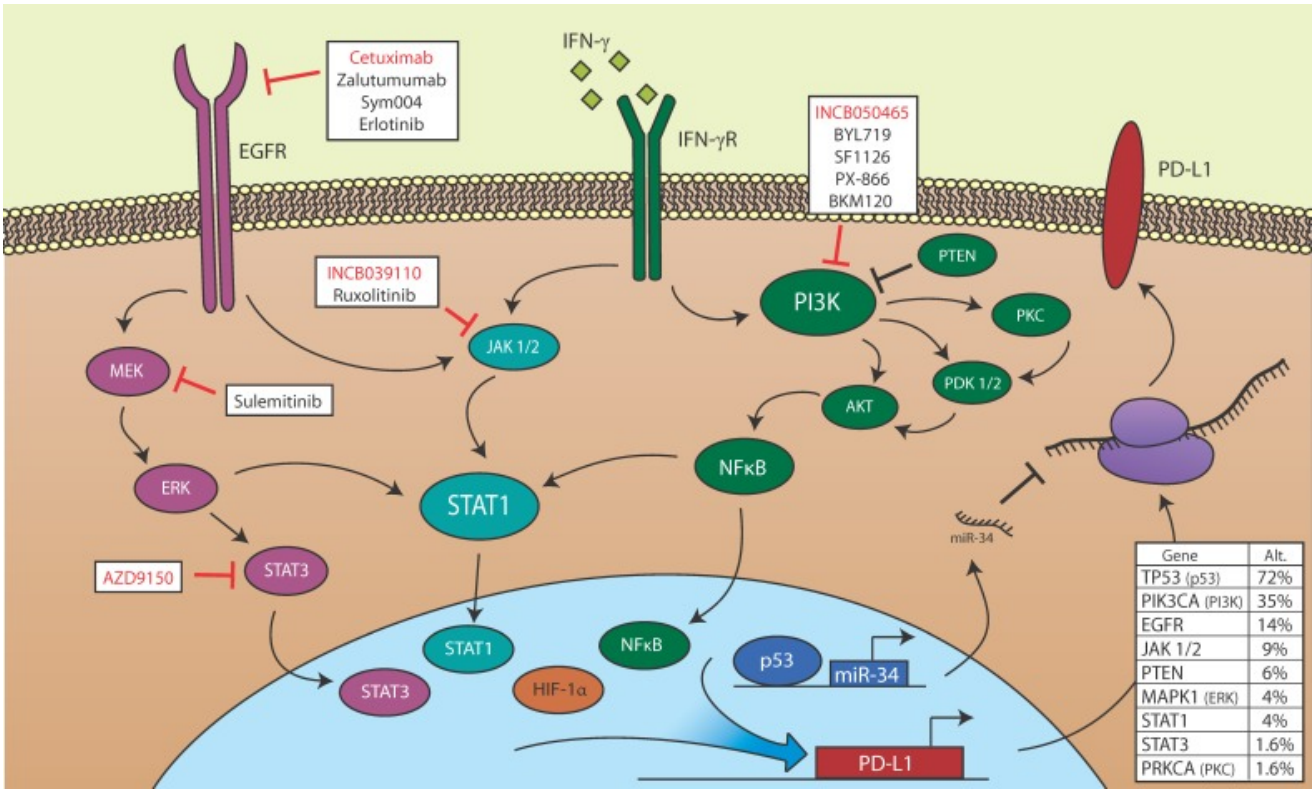

Figure 1-1 Potential for PDL1 modulation in HNSCC.

Members of the EGFR, STAT, PI3K, p53, and HIF-1α signaling pathways, all of which may be de-regulated in HNSCC, are shown. EGFR is aberrantly activated in HNSCC and may promote PDL1 transcription via JAK/STAT or MEK/ERK signaling. IFN-γ induces PDL1 transcription in HSCC via JAK/STAT signaling, and may also activate the PI3K signaling pathway, which regulates PDL1 transcription in other cancers. HIF-1α binds directly to the PDL1 promoter and correlates with high PDL1 expression. p53 loss of function is common in HNSCC, and wild type p53 blocks PDL1 translation via transcription of miR-34. Also shown are targeted small molecule inhibitors and biologics currently being evaluated in active clinical trials open to HNSCC patients. Red text indicates inhibitors for which efficacy in combination with PD-1/PDL1 blockade is being evaluated. Table (lower right) is based upon data generated by the TCGA Research Network (http://cancergenome.nih.gov). The middle column denotes the percentage of 504 cases with alternations (mutations or copy number variations) in the indicated gene. Within this dataset, 35 of 106 cases in which p16 was assessed were designated HPV positive. The rightmost column denotes the percentage of HPV positive cases with alterations in the indicated gene.

Tables

Table 1-1. Clinical trials, immunotherapy combinations.

List of current trials evaluating the use of targeted therapies towards the PD-1/PDL1 pathway in combination with other immunotherapy treatments in HNSCC.

Trial	Phase	Therapy	Description	Target	Condition
NCT02655822	Phase I/Ib	CPI-444 + Atezolizumab	Evaluate the safety and preliminary efficacy of CPI-444 (small molecule immune checkpoint inhibitor of adenosine A2A receptor) in combination with Atezolizumab	PDL1 Adenosine A2A receptor	Advanced malignancies (including HNSCC)
NCT02543645	Phase I/II	Atezolizumab + Varlilumab	Evaluate safety and preliminary efficacy of Atezolizumab + Varlilumab (anti-CD27 mAb)	PDL1 CD27	Advanced malignancies (including HNSCC)
NCT02554812	Phase 1b/2	Avelumab + PF-05082566 or PF-04518600	Evaluate safety, pharmacokinetics, and pharmacodynamics of Avelumab + PF-05082566 (stimulatory mAb towards CD137) versus Avelumab + PF-04518600 (stimulatory mAb towards CD134)	PDL1 CD-137 CD-134	Advanced solid malignancies (including HNSCC)
NCT02301130	Phase I	MEDI4736 + Mogamulizumab versus Mogamulizumab + Tremelimumab	Evaluate the safety and preliminary efficacy of MEDI4736 + Mogamulizumab (C-C chemokine receptor 4 (CCR4) inhibitor) versus Mogamulizumab +	PDL1 C-C chemokine receptor 4 (CCR4)	Advanced solid tumors (including HNSCC)

			Tremelimumab (CTLA-4 inhibitor)	CTLA-4 receptor	
NCT02658214	Phase I	MEDI4736 + Tremelimumab + Paclitaxel + Carboplatin	Evaluate the safety, tolerability, and preliminary efficacy of MEDI4736 + Tremelimumab (CTLA-4 inhibitor) + Paclitaxel + Carboplatin	PDL1 CTLA-4 receptor	Chemotherapy naïve locally advanced unresectable or metastatic HNSCC and other solid tumors
NCT02262741	Phase I	MEDI4736 + Tremelimumab	Evaluate the safety, tolerability, and efficacy of MEDI4736 + Tremelimumab (CTLA-4 inhibitor)	PDL1 CTLA-4 receptor	Recurrent or metastatic HNSCC
NCT02291055	Phase I/II	MEDI4736 +/- ADXS11-001	Evaluate safety and tolerability of MEDI4736 +/- ADXS11-001 (Listeria monocytogenes cancer vaccine)	PDL1 Cancer vaccine against HPV-16 E7	Recurrent or metastatic HNSCC
NCT02643303	Phase I/II	MEDI4736 + Tremelimumab + PolyICLC	Evaluate the safety and efficacy of MEDI4736 + Tremelimumab (CTLA-4 inhibitor) + PolyICLC (Toll-like receptor agonist)	PDL1 CTLA-4 receptor Toll-like receptor	Advanced biopsy accessible tumors (including HNSCC)
NCT02319044	Phase II	MEDI4736 versus Tremelimumab versus MEDI4736 + Tremelimumab	Evaluate safety and preliminary efficacy of MEDI4736 versus Tremelimumab (CTLA-4 inhibitor) versus MEDI4736 + Tremelimumab	PDL1 CTLA-4 receptor	Recurrent or metastatic HNSCC
NCT02551159	Phase III	MEDI4736 + Tremelimumab	Evaluate safety and efficacy of MEDI4736 with and without Tremelimumab (CTLA-4 inhibitor) versus standard of care	PDL1 CTLA-4 receptor	Recurrent or metastatic HNSCC without prior

					systemic chemotherapy
NCT02369874	Phase III	MEDI4736 + Tremelimumab	Evaluate safety and efficacy of MEDI4736 + Tremelimumab (CTLA-4 inhibitor) versus MEDI4736 alone versus standard of care	PDL1 CTLA-4 receptor	Previously treated recurrent or metastatic HNSCC
NCT02124850	Phase Ib	Nivolumab + Cetuximab + Motolimod	Evaluate change in immune biomarkers and tumor markers after treatment with Cetuximab + Motolimod (small molecule agonist of toll-like receptor 8) versus Nivolumab + Cetuximab + Motolimod	PD-1 EGF receptor Toll-like receptor 8	Stage II, III, or IVa HNSCC
NCT02488759	Phase I/II	Nivolumab +/- Ipilimumab	Evaluate safety and preliminary efficacy of Nivolumab +/- Ipilimumab	PD-1 CTLA-4 receptor	Virus associated malignancy (including HPV+ HNSCC)
NCT02335918	Phase I/II	Nivolumab + Varlilumab	Evaluate safety, tolerability, and preliminary efficacy of Nivolumab + Varlilumab (anti-CD27 mAb)	PD-1 CD27	Refractory solid tumors (including HNSCC)
NCT02741570	Phase III	Nivolumab + Ipilimumab	Evaluate safety and efficacy of Nivolumab + Ipilimumab versus Cetuximab + Cisplatin/Carboplatin + Fluorouracil	PD-1 CTLA-4 receptor EGF receptor	Recurrent or metastatic HNSCC, without prior treatment with systemic cancer therapy
NCT02636036	Phase I	Pembrolizumab + Enadenotucirev	Evaluate safety of Pembrolizumab + Enadenotucirev (oncolytic virus)	PD-1 Targeted viral therapy	Metastatic or advanced solid tumors

					(including HNSCC)
NCT02475213	Phase I	Pembrolizumab + Enoblituzumab	Evaluate safety of Pembrolizumab + Enoblituzumab (mAB towards B7-H3)	PD-1 B7-H3	Refractory malignancies including recurrent or metastatic HNSCC that expresses B7-H3
NCT02626000	Phase I	Pembrolizumab + Talimogene laherparepvec	Evaluate the safety and preliminary efficacy of pembrolizumab + Talimogene laherparepvec (oncolytic virus)	PD-1 Targeted viral therapy	Recurrent or metastatic HNSCC

Table 1-2. Clinical trials, PD1/PDL1 inhibitors plus small molecule inhibitors.

List of current trials evaluating the use of targeted therapies towards the PD-1/PDL1 pathway in combination with small molecule inhibitor treatments in HNSCC.

Trial	Phase	Therapy	Description	Target	Condition
NCT02471846	Phase Ib	Atezolizumab + GDC-0919	Evaluate safety, tolerability, pharmokinetics, and preliminary efficacy of Atezolizumab + GDC-0919 (indoleamine 2,3-dioxygenase (IDO) pathway inhibitor)	PDL1 Indoleamine 2,3-dioxygenase pathway	Locally advanced or metastatic solid tumors (including HNSCC)
NCT02264678	Phase I	MEDI4736 + AZD6738 vs. AZD6738 + Carboplatin vs.	Evaluate the safety, tolerability, pharmacokinetics, and preliminary anti-tumor activity of MEDI4736 + AZD6738 (ATR kinase inhibitor) vs. AZD6738 + Carboplatin vs. AZD6738 +	PDL1 ATR kinase Nuclear enzyme poly(ADP-ribose)	Advanced solid malignancies

		AZD6738 + Olaparib	Olaparib (nuclear enzyme poly(ADP-ribose) polymerase (PARP) inhibitor)	polymerase (PARP)	(including HNSCC)
NCT02586987	Phase I	MEDI4736 + Selumetinib	Evaluate the safety, tolerability, pharmacokinetics, and preliminary efficacy of MEDI4736 + Selumetinib (mitogen-activated protein kinase (MEK or MAPK/ERK kinase) 1 and 2 inhibitor)	PDL1 MAP/ERK kinase	Advanced solid tumors (including HNSCC)
NCT02499328	Phase 1b/2	MEDI4736 + AZD5069 or AZD9150	Evaluate safety, tolerability, and preliminary efficacy of AZD5069 (CXC2 inhibitor) versus AZD9150 (STAT3 inhibitor) alone and in combination with MEDI4736 (PD-L1 inhibitor)	PDL1 CXC2 STAT3	Recurrent or metastatic HNSCC
NCT02318277	Phase I/II	MEDI4736 + Epacadostat	Evaluate the safety, tolerability, pharmacokinetics, and preliminary efficacy of MEDI4736 + Epacadostat (indoleamine 2,3-dioxygenase (IDO1) inhibitor)	PDL1 Indoleamine 2,3-dioxygenase	Advanced solid tumors (including HNSCC)
NCT02526017	Phase I	Nivolumab + FPA-008	Evaluate safety and preliminary efficacy of Nivolumab + FPA-008 (colony stimulating factor-1 receptor (CSF1R) inhibitor)	PD-1 Colony stimulating factor-1 receptor	Advanced solid tumors (including HNSCC)
NCT02124850	Phase Ib	Nivolumab + Cetuximab + Motolimod	Evaluate change in immune biomarkers and tumor markers after treatment with Cetuximab + Motolimod (small molecule agonist of toll-like receptor 8) versus Nivolumab + Cetuximab + Motolimod	PD-1 EGF receptor Toll-like receptor 8	Stage II, III, or IVa HNSCC
NCT02834247	Phase Ib	Nivolumab + TAK-659	Evaluate maximum tolerated dose, safety, and preliminary efficacy of Nivolumab + TAK-659 (Spleen tyrosine kinase (SYK) inhibitor)	PD-1 Spleen tyrosine kinase	Advanced solid tumors

					(including HNSCC)
NCT02327078	Phase I/II	Nivolumab + Epacadostat	Evaluate safety tolerability, and preliminary efficacy of Nivolumab + Epacadostat (indoleamine 2,3-dioxygenase (IDO1) inhibitor)	PD-1 Indoleamine 2,3 dioxygenase	Advanced malignancies (including HNSCC)
NCT02646748	Phase I	Pembrolizumab + INCB039110 versus Pembrolizumab + INCB050465	Evaluate the safety, tolerability, and preliminary efficacy of pembrolizumab + INCB039110 (Jak inhibitor specific for Jak1) versus INCB050465 (PI3K-delta inhibitor)	PD-1 JAK1 PI3K-delta	Advanced solid tumors (including HNSCC)
NCT02452424	Phase 1/2a	Pembrolizumab + PLX3397	Evaluate safety and preliminary efficacy of combined therapy of Pembrolizumab and PLX3397 (colony-stimulating factor-1 receptor (CSF1R) inhibitor)	PD-1	Melanoma Solid tumors (including HNSCC)
NCT02501096	Phase 1b/2	Pembrolizumab + Lenvatinib	Evaluate safety and preliminary efficacy of Pembrolizumab + Lenvatinib (tyrosine kinase inhibitor)	PD-1 Tyrosine kinase	Solid malignancies (including HNSCC)
NCT02178722	Phase I/II	Pembrolizumab + INCB024360	Evaluate safety, toxicity, and preliminary efficacy of Pembrolizumab + Epacadostat (indoleamine 2,3-dioxygenase (IDO1) inhibitor)	PD-1 Indoleamine 2,3-dioxygenase	Selected cancers including HNSCC
NCT02538510	Phase I/II	Pembrolizumab + Vorinostat	Evaluate safety and preliminary efficacy of Pembrolizumab + Vorinostat (Histone Deacetylase Inhibitor)	PD-1 Histone deacetylase	Recurrent or Metastatic HNSCC or salivary gland carcinoma

NCT02454179	Phase II	Pembrolizumab + ACP-196	Evaluate efficacy of Pembrolizumab + ACP-196 (Acalabrutinib, Bruton's tyrosine kinase inhibitor)	PD-1 Tyrosine kinase	Recurrent, metastatic, or unresectable HNSCC

Bibliography

1. Bauernhofer T, Kuss I, Henderson B, Baum AS, Whiteside TL. Preferential apoptosis of CD56dim natural killer cell subset in patients with cancer. European journal of immunology. 2003;33:119–24.
2. Dasgupta S, Bhattacharya-Chatterjee M, O'Malley BW, Chatterjee SK. Inhibition of NK Cell Activity through TGF-β1 by Down-Regulation of NKG2D in a Murine Model of Head and Neck Cancer. The Journal of Immunology. 2005;175:5541–50.
3. Ferris RL, Whiteside TL, Ferrone S. Immune escape associated with functional defects in antigen-processing machinery in head and neck cancer. Clinical cancer research: an official journal of the American Association for Cancer Research. 2006;12:3890–5.
4. Almand B, Resser JR, Lindman B, Nadaf S, Clark JI, Kwon ED. et al. Clinical significance of defective dendritic cell differentiation in cancer. Clinical cancer research: an official journal of the American Association for Cancer Research. 2000;6:1755–66.
5. Kuss I, Hathaway B, Ferris RL, Gooding W, Whiteside TL. Decreased absolute counts of T lymphocyte subsets and their relation to disease in squamous cell carcinoma of the head and neck. Clinical cancer research: an official journal of the American Association for Cancer Research. 2004;10:3755–62.
6. Chen Z, Malhotra PS, Thomas GR, Ondrey FG, Duffey DC, Smith CW. et al. Expression of proinflammatory and proangiogenic cytokines in patients with head and neck cancer. Clinical cancer research: an official journal of the American Association for Cancer Research. 1999;5:1369–79.
7. Ferris RL. Immunology and Immunotherapy of Head and Neck Cancer. Journal of Clinical Oncology; 2015.
8. Schaefer C, Kim GG, Albers A, Hoermann K, Myers EN, Whiteside TL. Characteristics of CD4+CD25+ regulatory T cells in the peripheral circulation of patients with head and neck cancer. British journal of cancer. 2005;92:913–20.
9. Strauss L, Bergmann C, Szczepanski M, Gooding W, Johnson JT, Whiteside TL. A unique subset of CD4+CD25highFoxp3+ T cells secreting interleukin-10 and transforming growth factor-beta1 mediates suppression in the tumor microenvironment. Clinical cancer research: an official journal of the American Association for Cancer Research. 2007;13:4345–54.
10. Pardoll DM. The blockade of immune checkpoints in cancer immunotherapy. Nat Rev Cancer. 2012;12:252–64.

11. Ascierto PA, Marincola FM. 2015: The Year of Anti-PD-1/PD-L1s Against Melanoma and Beyond. EBioMedicine. 2015;2:92–3.
12. Freeman GJ, Long AJ, Iwai Y, Bourque K, Chernova T, Nishimura H. et al. Engagement of the PD-1 immunoinhibitory receptor by a novel B7 family member leads to negative regulation of lymphocyte activation. The Journal of experimental medicine. 2000;192:1027–34.
13. Ishida Y, Agata Y, Shibahara K, Honjo T. Induced expression of PD-1, a novel member of the immunoglobulin gene superfamily, upon programmed cell death. The EMBO journal. 1992;11:3887–95.
14. Okiyama N, Katz SI. Programmed cell death 1 (PD-1) regulates the effector function of CD8 T cells via PD-L1 expressed on target keratinocytes. Journal of autoimmunity. 2014;53:1–9.
15. Chen J, Feng Y, Lu L, Wang H, Dai L, Li Y. et al. Interferon-gamma-induced PD-L1 surface expression on human oral squamous carcinoma via PKD2 signal pathway. Immunobiology. 2012;217:385–93.
16. He J, Hu Y, Hu M, Li B. Development of PD-1/PD-L1 Pathway in Tumor Immune Microenvironment and Treatment for Non-Small Cell Lung Cancer. Scientific reports. 2015;5:13110.
17. Taube JM, Anders RA, Young GD, Xu H, Sharma R, McMiller TL. et al. Colocalization of inflammatory response with B7-h1 expression in human melanocytic lesions supports an adaptive resistance mechanism of immune escape. Science translational medicine. 2012;4:127ra37.
18. Lyford-Pike S, Peng S, Young GD, Taube JM, Westra WH, Akpeng B. et al. Evidence for a role of the PD-1:PD-L1 pathway in immune resistance of HPV-associated head and neck squamous cell carcinoma. Cancer Res. 2013;73:1733–41.
19. Garcia-Pineres AJ, Hildesheim A, Herrero R, Trivett M, Williams M, Atmetlla I. et al. Persistent human papillomavirus infection is associated with a generalized decrease in immune responsiveness in older women. Cancer Res. 2006;66:11070–6.
20. Okazaki T, Honjo T. PD-1 and PD-1 ligands: from discovery to clinical application. International immunology. 2007;19:813–24.
21. Lin Z, Chen X, Li Z, Luo Y, Fang Z, Xu B. et al. PD-1 Antibody Monotherapy for Malignant Melanoma: A Systematic Review and Meta-Analysis. PloS one. 2016;11:e0160485.
22. Nivolumab Doubles Survival for Patients with HNSCC. Cancer Discov. 2016;6:Of3.
23. Seiwert TY. et al. Antitumor activity and safety of pembrolizumab in patients (pts) with advanced squamous cell carcinoma of the head and neck (SCCHN): Preliminary results from KEYNOTE-012 expansion cohort. J Clin Oncol. 2015:abstrLBA6008.. ASCO Annual Meeting. 2015; 33.
24. Gillison M, Blumenschein G, Fayette J. et al. Nivolumab (nivo) vs investigator's choice (IC) for recurrent or metastatic (R/M) head and neck squamous cell carcinoma (HNSCC): CheckMate-141. AACR Annual Meeting. 2016:AbstractCT099.
25. Seiwert TY, Weiss J, Baxi SS, Ahn M, Fayette J, Gillison ML, A phase 3, randomized, open-label study of first-line durvalumab (MEDI4736) ± tremelimumab versus standard of care (SoC; EXTREME regimen) in recurrent/metastatic (R/M) SCCHN: KESTREL. suppl; abstr TPS6101. J Clin Oncol, 2016 ASCO Annual Meeting; 2016. p. 34.
26. Lin Y-M, Sung W-W, Hsieh M-J, Tsai S-C, Lai H-W, Yang S-M. et al. High PD-L1 Expression Correlates with Metastasis and Poor Prognosis in Oral Squamous Cell Carcinoma. PloS one. 2015;10:e0142656.

27. Strome SE, Dong H, Tamura H, Voss SG, Flies DB, Tamada K. et al. B7-H1 blockade augments adoptive T-cell immunotherapy for squamous cell carcinoma. Cancer Res. 2003;63:6501–5.
28. Ukpo OC, Thorstad WL, Lewis JS Jr. B7-H1 expression model for immune evasion in human papillomavirus-related oropharyngeal squamous cell carcinoma. Head and neck pathology. 2013;7:113–21.
29. Badoual C, Hans S, Merillon N, Van Ryswick C, Ravel P, Benhamouda N. et al. PD-1-Expressing Tumor-Infiltrating T Cells Are a Favorable Prognostic Biomarker in HPV-Associated Head and Neck Cancer. Cancer Research. 2013;73:128–38.
30. Cho Y-A, Yoon H-J, Lee J-I, Hong S-P, Hong S-D. Relationship between the expressions of PD-L1 and tumor-infiltrating lymphocytes in oral squamous cell carcinoma. Oral Oncology. 2011;47:1148–53.
31. Hsu MC, Hsiao JR, Chang KC, Wu YH, Su IJ, Jin YT. et al. Increase of programmed death-1-expressing intratumoral CD8 T cells predicts a poor prognosis for nasopharyngeal carcinoma. Modern pathology: an official journal of the United States and Canadian Academy of Pathology, Inc. 2010;23:1393–403.
32. Taube JM, Klein A, Brahmer JR, Xu H, Pan X, Kim JH. et al. Association of PD-1, PD-1 ligands, and other features of the tumor immune microenvironment with response to anti-PD-1 therapy. Clinical cancer research: an official journal of the American Association for Cancer Research. 2014;20:5064–74.
33. Wansom D, Light E, Thomas D, Worden F, Prince M, Urba S. et al. Infiltrating lymphocytes and human papillomavirus-16-associated oropharyngeal cancer. The Laryngoscope. 2012;122:121–7.
34. Concha-Benavente F, Srivastava RM, Trivedi S, Lei Y, Chandran U, Seethala RR. et al. Identification of the Cell-Intrinsic and -Extrinsic Pathways Downstream of EGFR and IFNgamma That Induce PD-L1 Expression in Head and Neck Cancer. Cancer Res. 2016;76:1031–43.
35. Birkeland AC, Ludwig ML, Meraj TS, Brenner JC, Prince ME. The Tip of the Iceberg: Clinical Implications of Genomic Sequencing Projects in Head and Neck Cancer. Cancers. 2015;7:2094–109.
36. Birkeland AC, Uhlmann WR, Brenner JC, Shuman AG. Getting personal: Head and neck cancer management in the era of genomic medicine. Head & neck; 2015.
37. Birkeland AC, Yanik M, Tillman BN, Scott MV, Foltin SK, Mann JE, Identification of Targetable ERBB2 Aberrations in Head and Neck Squamous Cell Carcinoma. JAMA otolaryngology- head & neck surgery; 2016.
38. Giefing M, Wierzbicka M, Szyfter K, Brenner JC, Braakhuis BJ, Brakenhoff RH. et al. Moving towards personalised therapy in head and neck squamous cell carcinoma through analysis of next generation sequencing data. European journal of cancer. 2016;55:147–57.
39. Tillman BN, Yanik M, Birkeland AC, Liu CJ, Hovelson DH, Cani AK. et al. Fibroblast growth factor family aberrations as a putative driver of head and neck squamous cell carcinoma in an epidemiologically low-risk patient as defined by targeted sequencing. Head & neck. 2016;38(Suppl 1):E1646–52.
40. Temam S, Kawaguchi H, El-Naggar AK, Jelinek J, Tang H, Liu DD. et al. Epidermal growth factor receptor copy number alterations correlate with poor clinical outcome in patients with head and neck squamous cancer. Journal of clinical oncology: official journal of the American Society of Clinical Oncology. 2007;25:2164–70.

41. Grandis JR, Tweardy DJ. Elevated Levels of Transforming Growth Factor α and Epidermal Growth Factor Receptor Messenger RNA Are Early Markers of Carcinogenesis in Head and Neck Cancer. Cancer Research. 1993;53:3579–84.
42. Birkeland AC, Brenner JC. Personalizing Medicine in Head and Neck Squamous Cell Carcinoma: The Rationale for Combination Therapies. Medical research archives; 2015. p. 3.
43. Birkeland AC, Ludwig ML, Spector ME, Brenner JC. The potential for tumor suppressor gene therapy in head and neck cancer. Discovery medicine. 2016;21:41–7.
44. Bonner JA, Harari PM, Giralt J, Azarnia N, Shin DM, Cohen RB. et al. Radiotherapy plus Cetuximab for Squamous-Cell Carcinoma of the Head and Neck. New England Journal of Medicine. 2006;354:567–78.
45. Tang Y, Fang W, Zhang Y, Hong S, Kang S, Yan Y. et al. The association between PD-L1 and EGFR status and the prognostic value of PD-L1 in advanced non-small cell lung cancer patients treated with EGFR-TKIs. Oncotarget. 2015;6:14209–19.
46. Lin K, Cheng J, Yang T, Li Y, Zhu B. EGFR-TKI down-regulates PD-L1 in EGFR mutant NSCLC through inhibiting NF-kappaB. Biochemical and biophysical research communications. 2015;463:95–101.
47. Han JJ, Kim DW, Koh J, Keam B, Kim TM, Jeon YK. et al. Change in PD-L1 Expression After Acquiring Resistance to Gefitinib in EGFR-Mutant Non-Small-Cell Lung Cancer. Clinical lung cancer. 2016;17:263–70.e2.
48. Kurai J, Chikumi H, Hashimoto K, Yamaguchi K, Yamasaki A, Sako T. et al. Antibody-Dependent Cellular Cytotoxicity Mediated by Cetuximab against Lung Cancer Cell Lines. Clinical Cancer Research. 2007;13:1552.
49. Hara M, Nakanishi H, Tsujimura K, Matsui M, Yatabe Y, Manabe T. et al. Interleukin-2 potentiation of cetuximab antitumor activity for epidermal growth factor receptor-overexpressing gastric cancer xenografts through antibody-dependent cellular cytotoxicity. Cancer Science. 2008;99:1471–8.
50. Kasper S, Breitenbuecher F, Reis H, Brandau S, Worm K, Kohler J. et al. Oncogenic RAS simultaneously protects against anti-EGFR antibody-dependent cellular cytotoxicity and EGFR signaling blockade. Oncogene. 2013;32:2873–81.
51. Yang X, Zhang X, Mortenson ED, Radkevich-Brown O, Wang Y, Fu Y-X. Cetuximab-mediated Tumor Regression Depends on Innate and Adaptive Immune Responses. Mol Ther. 2013;21:91–100.
52. Bertino EM, McMichael EL, Mo X, Trikha P, Davis M, Paul B. et al. A Phase I Trial to Evaluate Antibody-Dependent Cellular Cytotoxicity of Cetuximab and Lenalidomide in Advanced Colorectal and Head and Neck Cancer. Molecular Cancer Therapeutics. 2016;15:2244.
53. Cancer Genome Atlas Network. Comprehensive genomic characterization of head and neck squamous cell carcinomas. Nature. 2015;517:576–82.
54. Lui VW, Hedberg ML, Li H, Vangara BS, Pendleton K, Zeng Y. et al. Frequent mutation of the PI3K pathway in head and neck cancer defines predictive biomarkers. Cancer Discov. 2013;3:761–9.
55. Michmerhuizen NL, Birkeland AC, Bradford CR, Brenner JC. Genetic determinants in head and neck squamous cell carcinoma and their influence on global personalized medicine. Genes & cancer. 2016;7:182–200.
56. Osaki M, Oshimura M, Ito H. PI3K-Akt pathway: its functions and alterations in human cancer. Apoptosis. 2004;9:667–76.

57. Isaacsson Velho PH, Castro G Jr, Chung CH. Targeting the PI3K Pathway in Head and Neck Squamous Cell Carcinoma. Am Soc Clin Oncol Educ Book; 2015. pp. 123–8.
58. Nguyen H, Ramana CV, Bayes J, Stark GR. Roles of phosphatidylinositol 3-kinase in interferon-gamma-dependent phosphorylation of STAT1 on serine 727 and activation of gene expression. J Biol Chem. 2001;276:33361–8.
59. Kaur S, Uddin S, Platanias LC. The PI3' kinase pathway in interferon signaling. J Interferon Cytokine Res. 2005;25:780–7.
60. Lee SK, Seo SH, Kim BS, Kim CD, Lee JH, Kang JS. et al. IFN-gamma regulates the expression of B7-H1 in dermal fibroblast cells. J Dermatol Sci. 2005;40:95–103.
61. Le Good JA, Ziegler WH, Parekh DB, Alessi DR, Cohen P, Parker PJ. Protein kinase C isotypes controlled by phosphoinositide 3-kinase through the protein kinase PDK1. Science. 1998;281:2042–5.
62. Choudhury GG. A linear signal transduction pathway involving phosphatidylinositol 3-kinase, protein kinase Cepsilon, and MAPK in mesangial cells regulates interferon-gamma-induced STAT1alpha transcriptional activation. J Biol Chem. 2004;279:27399–409.
63. DeVries TA, Kalkofen RL, Matassa AA, Reyland ME. Protein kinase Cdelta regulates apoptosis via activation of STAT1. J Biol Chem. 2004;279:45603–12.
64. Kondo A, Yamashita T, Tamura H, Zhao W, Tsuji T, Shimizu M. et al. Interferon-gamma and tumor necrosis factor-alpha induce an immunoinhibitory molecule, B7-H1, via nuclear factor-kappaB activation in blasts in myelodysplastic syndromes. Blood. 2010;116:1124–31.
65. Gowrishankar K, Gunatilake D, Gallagher SJ, Tiffen J, Rizos H, Hersey P. Inducible but not constitutive expression of PD-L1 in human melanoma cells is dependent on activation of NF-kappaB. PLoS One. 2015;10:e0123410.
66. Xu C, Fillmore CM, Koyama S, Wu H, Zhao Y, Chen Z. et al. Loss of Lkb1 and Pten leads to lung squamous cell carcinoma with elevated PD-L1 expression. Cancer Cell. 2014;25:590–604.
67. Parsa AT, Waldron JS, Panner A, Crane CA, Parney IF, Barry JJ. et al. Loss of tumor suppressor PTEN function increases B7-H1 expression and immunoresistance in glioma. Nat Med. 2007;13:84–8.
68. Zhang Y, Zhang J, Xu K, Xiao Z, Sun J, Xu J. et al. PTEN/PI3K/mTOR/B7-H1 signaling pathway regulates cell progression and immuno-resistance in pancreatic cancer. Hepatogastroenterology. 2013;60:1766–72.
69. Zhu J, Chen L, Zou L, Yang P, Wu R, Mao Y. et al. MiR-20b, -21, and -130b inhibit PTEN expression resulting in B7-H1 over-expression in advanced colorectal cancer. Hum Immunol. 2014;75:348–53.
70. Yu T, Cao R, Li S, Fu M, Ren L, Chen W. et al. MiR-130b plays an oncogenic role by repressing PTEN expression in esophageal squamous cell carcinoma cells. BMC Cancer. 2015;15:29.
71. Ludwig ML, Birkeland AC, Hoesli R, Swiecicki P, Spector ME, Brenner JC. Changing the paradigm: the potential for targeted therapy in laryngeal squamous cell carcinoma. Cancer biology & medicine. 2016;13:87–100.
72. Uddin S, Majchrzak B, Woodson J, Arunkumar P, Alsayed Y, Pine R. et al. Activation of the p38 mitogen-activated protein kinase by type I interferons. J Biol Chem. 1999;274:30127–31.
73. Liu J, Hamrouni A, Wolowiec D, Coiteux V, Kuliczkowski K, Hetuin D. et al. Plasma cells from multiple myeloma patients express B7-H1 (PD-L1) and increase expression after

stimulation with IFN-{gamma} and TLR ligands via a MyD88-, TRAF6-, and MEK-dependent pathway. Blood. 2007;110:296–304.
74. Jiang X, Zhou J, Giobbie-Hurder A, Wargo J, Hodi FS. The activation of MAPK in melanoma cells resistant to BRAF inhibition promotes PD-L1 expression that is reversible by MEK and PI3K inhibition. Clinical cancer research: an official journal of the American Association for Cancer Research. 2013;19:598–609.
75. Qian Y, Deng J, Geng L, Xie H, Jiang G, Zhou L. et al. TLR4 signaling induces B7-H1 expression through MAPK pathways in bladder cancer cells. Cancer Invest. 2008;26:816–21.
76. Yamamoto R, Nishikori M, Tashima M, Sakai T, Ichinohe T, Takaori-Kondo A. et al. B7-H1 expression is regulated by MEK/ERK signaling pathway in anaplastic large cell lymphoma and Hodgkin lymphoma. Cancer Sci. 2009;100:2093–100.
77. Loi S, Dushyanthen S, Beavis PA, Salgado R, Denkert C, Savas P. et al. RAS/MAPK Activation Is Associated with Reduced Tumor-Infiltrating Lymphocytes in Triple-Negative Breast Cancer: Therapeutic Cooperation Between MEK and PD-1/PD-L1 Immune Checkpoint Inhibitors. Clin Cancer Res. 2016;22:1499–509.
78. Liu L, Mayes PA, Eastman S, Shi H, Yadavilli S, Zhang T. et al. The BRAF and MEK Inhibitors Dabrafenib and Trametinib: Effects on Immune Function and in Combination with Immunomodulatory Antibodies Targeting PD-1, PD-L1, and CTLA-4. Clin Cancer Res. 2015;21:1639–51.
79. Hughes PE, Caenepeel S, Wu LC. Targeted Therapy and Checkpoint Immunotherapy Combinations for the Treatment of Cancer. Trends Immunol. 2016;37:462–76.
80. The Cancer Genome Atlas N. Comprehensive genomic characterization of head and neck squamous cell carcinomas. Nature. 2015;517:576–82.
81. Cortez MA, Ivan C, Valdecanas D, Wang X, Peltier HJ, Ye Y. et al. PDL1 Regulation by p53 via miR-34. JNCI Journal of the National Cancer Institute. 2016;108:djv303.
82. Chan KS, Sano S, Kiguchi K, Anders J, Komazawa N, Takeda J. et al. Disruption of Stat3 reveals a critical role in both the initiation and the promotion stages of epithelial carcinogenesis. The Journal of clinical investigation. 2004;114:720–8.
83. Wolfle SJ, Strebovsky J, Bartz H, Sahr A, Arnold C, Kaiser C. et al. PD-L1 expression on tolerogenic APCs is controlled by STAT-3. European journal of immunology. 2011;41:413–24.
84. Fujita Y, Yagishita S, Hagiwara K, Yoshioka Y, Kosaka N, Takeshita F. et al. The clinical relevance of the miR-197/CKS1B/STAT3-mediated PD-L1 network in chemoresistant non-small-cell lung cancer. Molecular therapy: the journal of the American Society of Gene Therapy. 2015;23:717–27.
85. Hao Y, Chapuy B, Monti S, Sun HH, Rodig SJ, Shipp MA. Selective JAK2 Inhibition Specifically Decreases Hodgkin Lymphoma and Mediastinal Large B-cell Lymphoma Growth In Vitro and In Vivo. Clinical cancer research: an official journal of the American Association for Cancer Research. 2014;20:2674–83.
86. Green MR, Monti S, Rodig SJ, Juszczynski P, Currie T, O'Donnell E. et al. Integrative analysis reveals selective 9p24.1 amplification, increased PD-1 ligand expression, and further induction via JAK2 in nodular sclerosing Hodgkin lymphoma and primary mediastinal large B-cell lymphoma. Blood. 2010;116:3268–77.
87. Grandis JR, Drenning SD, Zeng Q, Watkins SC, Melhem MF, Endo S. et al. Constitutive activation of Stat3 signaling abrogates apoptosis in squamous cell carcinogenesis in vivo. Proceedings of the National Academy of Sciences of the United States of America. 2000;97:4227–32.

88. Lu X, Kang Y. Hypoxia and hypoxia-inducible factors: master regulators of metastasis. Clinical cancer research: an official journal of the American Association for Cancer Research. 2010;16:5928–35.
89. Noman MZ, Desantis G, Janji B, Hasmim M, Karray S, Dessen P. et al. PD-L1 is a novel direct target of HIF-1alpha, and its blockade under hypoxia enhanced MDSC-mediated T cell activation. The Journal of experimental medicine. 2014;211:781–90.
90. Barsoum IB, Smallwood CA, Siemens DR, Graham CH. A mechanism of hypoxia-mediated escape from adaptive immunity in cancer cells. Cancer Res. 2014;74:665–74.
91. Beasley NJ, Leek R, Alam M, Turley H, Cox GJ, Gatter K. et al. Hypoxia-inducible factors HIF-1alpha and HIF-2alpha in head and neck cancer: relationship to tumor biology and treatment outcome in surgically resected patients. Cancer Res. 2002;62:2493–7.
92. Brizel DM, Dodge RK, Clough RW, Dewhirst MW. Oxygenation of head and neck cancer: changes during radiotherapy and impact on treatment outcome. Radiotherapy and oncology: journal of the European Society for Therapeutic Radiology and Oncology. 1999;53:113–7.
93. Ferris RL, Hunt JL, Ferrone S. Human leukocyte antigen (HLA) class I defects in head and neck cancer: molecular mechanisms and clinical significance. Immunologic research. 2005;33:113–33.
94. Guven-Maiorov E, Keskin O, Gursoy A, VanWaes C, Chen Z, Tsai CJ. et al. TRAF3 signaling: Competitive binding and evolvability of adaptive viral molecular mimicry. Biochimica et biophysica acta. 2016;1860:2646–55.
95. Zapata JM, Llobet D, Krajewska M, Lefebvre S, Kress CL, Reed JC. Lymphocyte-specific TRAF3 transgenic mice have enhanced humoral responses and develop plasmacytosis, autoimmunity, inflammation, and cancer. Blood. 2009;113:4595–603.
96. Yang W, Song Y, Lu YL, Sun JZ, Wang HW. Increased expression of programmed death (PD)-1 and its ligand PD-L1 correlates with impaired cell-mediated immunity in high-risk human papillomavirus-related cervical intraepithelial neoplasia. Immunology. 2013;139:513–22.
97. Ang KK, Harris J, Wheeler R, Weber R, Rosenthal DI, Nguyen-Tân PF. et al. Human Papillomavirus and Survival of Patients with Oropharyngeal Cancer. New England Journal of Medicine. 2010;363:24–35.
98. Pignon JP, le Maitre A, Maillard E, Bourhis J. Meta-analysis of chemotherapy in head and neck cancer (MACH-NC): an update on 93 randomised trials and 17,346 patients. Radiotherapy and oncology: journal of the European Society for Therapeutic Radiology and Oncology. 2009;92:4–14.
99. Gillison ML, Koch WM, Capone RB, Spafford M, Westra WH, Wu L. et al. Evidence for a causal association between human papillomavirus and a subset of head and neck cancers. Journal of the National Cancer Institute. 2000;92:709–20.
100. Rice AE, Latchman YE, Balint JP, Lee JH, Gabitzsch ES, Jones FR. An HPV-E6/E7 immunotherapy plus PD-1 checkpoint inhibition results in tumor regression and reduction in PD-L1 expression. Cancer Gene Ther. 2015;22:454–62.
101. de Jong A, van Poelgeest MI, van der Hulst JM, Drijfhout JW, Fleuren GJ, Melief CJ. et al. Human papillomavirus type 16-positive cervical cancer is associated with impaired CD4+ T-cell immunity against early antigens E2 and E6. Cancer Res. 2004;64:5449–55.
102. Spanos WC, Hoover A, Harris GF, Wu S, Strand GL, Anderson ME. et al. The PDZ binding motif of human papillomavirus type 16 E6 induces PTPN13 loss, which allows anchorage-independent growth and synergizes with ras for invasive growth. Journal of virology. 2008;82:2493–500.

103. Brehm A, Nielsen SJ, Miska EA, McCance DJ, Reid JL, Bannister AJ. et al. The E7 oncoprotein associates with Mi2 and histone deacetylase activity to promote cell growth. The EMBO journal. 1999;18:2449–58.
104. Blackford A, Parmigiani G, Kensler TW, Wolfgang C, Jones S, Zhang X. et al. Genetic Mutations Associated With Cigarette Smoking in Pancreatic Cancer. Cancer research. 2009;69:3681–8.
105. Rizvi NA, Hellmann MD, Snyder A, Kvistborg P, Makarov V, Havel JJ. et al. Mutational landscape determines sensitivity to PD-1 blockade in non-small cell lung cancer. Science. 2015;348:124.
106. Powles T, Eder JP, Fine GD, Braiteh FS, Loriot Y, Cruz C. et al. MPDL3280A (anti-PD-L1) treatment leads to clinical activity in metastatic bladder cancer. Nature. 2014;515:558–62.
107. Tumeh PC, Harview CL, Yearley JH, Shintaku IP, Taylor EJM, Robert L. et al. PD-1 blockade induces responses by inhibiting adaptive immune resistance. Nature. 2014;515:568–71.
108. Lim JY, Gerber SA, Murphy SP, Lord EM. Type I interferons induced by radiation therapy mediate recruitment and effector function of CD8(+) T cells. Cancer immunology, immunotherapy: CII. 2014;63:259–71.
109. Dewan MZ, Galloway AE, Kawashima N, Dewyngaert JK, Babb JS, Formenti SC. et al. Fractionated but Not Single-Dose Radiotherapy Induces an Immune-Mediated Abscopal Effect when Combined with Anti-CTLA-4 Antibody. Clinical Cancer Research. 2009;15:5379–88.
110. Postow MA, Callahan MK, Barker CA, Yamada Y, Yuan J, Kitano S. et al. Immunologic Correlates of the Abscopal Effect in a Patient with Melanoma. New England Journal of Medicine. 2012;366:925–31.
111. Stamell EF, Wolchok JD, Gnjatic S, Lee NY, Brownell I. The Abscopal Effect Associated With a Systemic Anti-melanoma Immune Response. International Journal of Radiation Oncology*Biology*Physics. 2013;85:293–5.
112. al Ce. The cBio Cancer Genomics Portal: An Open Platform for Exploring Multidimensional Cancer Genomics Data. Cancer Discovery; 2012. p. 2.

Chapter 2 Features of larynx squamous cell carcinomas

Chapter Summary In this chapter we present a retrospective analysis of CD103+, CD4+, and CD8+ tumor infiltrating lymphocytes (TILs) in recurrent laryngeal squamous cell carcinoma tumor specimens by tissue microarray. We demonstrate an association between specific TIL populations and improved outcomes in this cohort. To improve future modeling of this disease subtype, we also profiled a panel of LSCC cell lines derived at the University of Michigan (UM-SCC-) that will serve as a resource for contextualizing preclinical studies in terms of the heterogeneous characteristics of LSCCs.

2.1 Analysis of tumor-infiltrating CD103 resident memory T-cell content in recurrent laryngeal squamous cell carcinoma.[2]

Abstract

Background: Recurrent laryngeal squamous cell carcinomas (LSCCs) are associated with poor outcomes, without reliable biomarkers to identify patients who may benefit from adjuvant therapies. Given the emergence of tumor-infiltrating lymphocytes (TIL) as a biomarker in head

[2] This section was published in *Cancer Immunology, Immunotherapy* in collaboration with the following authors: Joshua Smith, Andrew Birkeland, Emily Bellile, Paul Swicicki, Michelle Mierzwa, Steven Chinn, Andrew Shuman, Kelly Malloy, Keith Casper, Scott McLean, Jeffrey Moyer, Gregory Wolf, Carol Bradford, Mark Prince, Thomas Carey, Jonathan McHugh, Matthew Spector, and Chad Brenner.

and neck squamous cell carcinoma, we generated predictive models to understand the utility of CD4+, CD8+ and/or CD103+ TIL status in patients with advanced LSCC.

Methods: Tissue microarrays were constructed from salvage laryngectomy specimens of 183 patients with recurrent/persistent LSCC and independently stained for CD4+, CD8+, and CD103+ TIL content. Cox proportional hazards regression analysis was employed to assess combinations of CD4+, CD8+, and CD103+ TIL levels for prediction of overall survival (OS), disease-specific survival (DSS), and disease-free survival (DFS) in patients with recurrent/persistent LSCC.

Results: High tumor CD103+ TIL content was associated with significantly improved OS, DSS, and DFS and was a stronger predictor of survival in recurrent/persistent LSCC than either high CD8+ or CD4+ TIL content. On multivariate analysis, an "immune-rich" phenotype, in which tumors were enriched for both CD103+ and CD4+ TILs, conferred a survival benefit (OS hazard ratio: 0.28, $p = 0.0014$; DSS hazard ratio: 0.09, $p = 0.0015$; DFS hazard ratio: 0.18, $p = 0.0018$) in recurrent/persistent LSCC.

Conclusions: An immune profile driven by CD103+ TIL content, alone and in combination with CD4+ TIL content, is a prognostic biomarker of survival in patients with recurrent/persistent LSCC. Predictive models described herein may thus prove valuable in prognostic stratification and lead to personalized treatment paradigms for this patient population.

Introduction

Advanced stage laryngeal squamous cell carcinoma (LSCC) remains a clinical challenge, with recurrence rates of up to 50% after primary radiation (RT) or chemoradiation (CRT) [1]. For patients with recurrent disease after RT/CRT, salvage surgery is often the only established curative option [2, 3]. However, operative morbidity is significant and survival rates after

salvage laryngectomy are poor [4, 5]. The significant proportion of patients who develop recurrence after RT/CRT and the poor prognosis for patients with recurrent LSCC provide the rationale for new biomarker studies to improve prognostication and treatment selection in this vulnerable cohort. Although a variety of biomarkers ranging from genetic alterations [6], to protein expression [7], to tumor-infiltrating cells [8, 9, 10, 11, 12, 13] have been evaluated in this population, no prognostic model has demonstrated sufficient sensitivity and specificity to warrant further evaluation in prospective cohorts or to dictate clinical decisions.

Despite the dearth of prognostic data within this population, the role of the adaptive immune system in tumor surveillance has emerged as an area of increasing interest for development of predictive assays of oncologic outcomes in patients with LSCC [14]. Certain immunologic signatures, including number of $CD4^+$ and $CD8^+$ tumor-infiltrating lymphocytes (TILs), portend improved survival and response to therapy in head and neck cancer [8, 9]. For example, we have recently shown that a higher proportion of $CD4^+$ and $CD8^+$ TILs correlates with improved disease-specific and disease-free survival (DFS) in patients with recurrent/persistent LSCC [9]. Subsequently, in order to further enhance the sensitivity and specificity of our model, we questioned whether prognostication in this cohort could be improved by considering immunologic biomarkers of cytotoxic TIL activity and tumor-cell kill, in addition to TIL number itself.

CD103, or $\alpha_E\beta_7$ integrin, localizes antigen-specific cytotoxic T lymphocytes to epithelial tissues and is an indicator of enhanced cytotoxicity and proliferative ability of these cells [14]. In recent studies of non-small cell lung cancer [15] and serous ovarian cancer [16, 17], the survival benefit conferred by $CD8^+$ TILs was shown to be dependent upon co-expression of CD103. Thus, we sought to address whether CD103 expression may better define the most beneficial

subsets of TILs with important prognostic and immunotherapeutic implications in patients with recurrent/persistent LSCC.

Herein, we evaluated the potential of $CD103^+$ TIL density to act as a robust predictor of improved survival in patients with recurrent/persistent LSCC. Further, we hypothesize that there are patients with distinct immunologic phenotypes of "immune-rich" and "immune-poor" tumors that predict survival in recurrent/persistent LSCC.

Materials and methods

Patient population

We performed a single-institution, retrospective analysis of patients with recurrent/persistent LSCC using a clinical epidemiology and tissue database. Inclusion criteria stipulated: (1) adults with biopsy-proven LSCC; (2) recurrent/persistent disease at the primary site after RT or CRT; (3) laryngectomy for surgical salvage; between 1997 and 2014 and (4) tumor tissue available for creation of tissue microarray, as previously described [9]. In total, 183 patients met inclusion criteria, and demographics and clinical characteristics are shown in Table 2.1. Patients were staged in accordance with the 7th edition American Joint Committee on Cancer (AJCC) Staging System [18].

Immunohistology

Formalin-fixed paraffin-embedded (FFPE) tissue blocks from salvage surgery and representative hematoxylin and eosin-stained slides were assessed for ≥ 70% tumor cellularity by a head and neck pathologist (Jonathan B. McHugh). A tissue microarray (TMA) was subsequently constructed with triplicate 0.7-mm-diameter cores from each patient [19]. TMAs were stained for $CD4^+$, $CD8^+$, and $CD103^+$ TILs on arrays constructed as previously described [9]. Briefly, 5-micron tissue sections were incubated overnight in a 65 °C oven, then

deparaffinized and rehydrated with stepwise xylene, graded alcohols, and buffer immersion. Heat-induced epitope retrieval was then performed, followed by incubation of the slides in a preheated pressure cooker with citrate buffer (pH 6) or Tris–EDTA buffer (Ph 9) and horse serum. Immunohistochemical staining was done with a DAKO autostainer using liquid streptavidin-biotinylated horseradish peroxidase complex and DBA (DAKO labeled avidin-biotin-peroxidase kits, Thermo Fisher Scientific) as chromogens, as previously described [9]. Deparaffinized sections were stained with monoclonal antibodies at the following titrations: CD103-1:500 (Abcam Ab129202); CD4-1:250 (Abcam Ab846); CD8-1:40 (Novocastra VP-C320). TMA slides were digitally imaged, scanned, and retrieved with Aperio ImageScope v.12 software (Leica Biosystems).

TIL scoring and statistical analysis

Cores consisting of < 50% tumor parenchyma, partial cores, and those with significant tumor necrosis were excluded from the analysis. The positively stained cells in each included core were manually counted at 200× magnification (20× objective lens) by two independent blinded reviewers (Jacqueline E. Mann and Joshua D. Smith). Inter-rater reliability was determined by calculation of the intraclass correlation coefficient (ICC) using R. Only intratumoral TILs were quantified, consistent with the biological function of the CD103 antigen and previous studies demonstrating reliability and reproducibility of this measurement parameter [14, 16, 17]. Mean TIL counts per core of triplicate samples for each patient were calculated, averaged between the two reviewers, and used in subsequent statistical analysis.

$CD4^+$, $CD8^+$, and $CD103^+$ TIL counts were first input as continuous variables into univariate and multivariate models to document that each marker was a significant predictor of OS, DSS, and DFS. Next, optimal cutpoints for each TIL marker were determined from the data

to maximize survival differences based on Cox proportional hazards regression of DSS using the survMisc v0.5.4 package in R [20]. Subsequently, combinations of the markers CD4, CD8 and CD103 were explored with multivariable Cox model and ROC analysis.

Deaths were confirmed through the electronic medical record and the Social Security Death Index. Primary outcome measures were overall survival (OS; time from salvage laryngectomy to death from any cause), disease-specific survival (DSS; time from salvage laryngectomy to death from any disease recurrence/persistence), and disease-free survival (DFS; time from salvage laryngectomy to any disease recurrence/persistence).

Results

CD103 staining patterns and TIL cutpoints

For our entire cohort, the mean (range) $CD103^+$ TIL count per tumor was 32.1 (0–298) and the median count was 16 (**Figure 2.1**). Inter-rater reliability for TIL counts between the two blinded reviewers was excellent (ICC: 0.919, 95% CI 0.906–0.930). As continuous variables, $CD4^+$, $CD8^+$, and $CD103^+$ TIL counts were each predictive of OS, DSS, and DFS (data not shown).

We then determined the optimal cutpoint for CD103+ TIL counts to allow for stratification of recurrent/persistent LSCC into CD103+ low (< 11 TILs) and CD103+ high groups (≥ 11 TILs) optimized for DSS [20]. Of our entire cohort (n = 183), ten (5.5%) tumors were excluded due to partial or absent tumor cores, yielding 69 (40%) CD103+ low tumors and 104 (60%) CD103+ high tumors. In a similar fashion, we determined optimal cutpoints for CD4+ and CD8+ TIL counts to stratify low and high groups with respect to these T-cell markers. CD4+ high tumors were defined as having greater than or equal to 3 TILs, yielding 36 (26%) CD4+ high and 101 (74%) CD4+ low tumors in our cohort after excluding 46 due to partial or

absent tumor cores. Finally, the CD8+ cutpoint was determined to be greater than or equal to 12 TILs, yielding 63 (41%) CD8+ high and 92 (59%) CD8+ low tumors in our cohort after excluding 28 due to partial or absent tumor cores. Each of the three dichotomized T-cell markers alone was correlated strongly with DSS (**Figure 2.2**). We had previously noted this for CD4+ and CD8+ TILs [9], but identified a new stronger association with CD103 status and DSS ($p < 0.0001$). Importantly, we noted significant correlation between CD8+ and CD103+ TIL content, confirming a unique population of cytotoxic T-cells that co-express these markers in recurrent/persistent LSCC (Pearson rho = 0.62, $p < 0.0001$). There was no similar overlap between CD4 and CD103 expression (**Figure 2.3**).

Univariate analysis of CD103$^+$ TILs on survival

We next performed univariate analysis to assess the prognostic value of CD103$^+$ TILs with respect to all three survival outcomes in patients with recurrent/persistent LSCC. Cox proportional hazards models found that patients with CD103$^+$ high TILs had a better OS ($p = 0.003$), DSS ($p < 0.0001$), and DFS ($p = 0.001$) in comparison to patients with CD103$^+$ low TILs (**Figure 2.4)**. In comparing CD103 with CD8 on prognostication of survival, CD103 status more strongly predicted survival. Thus, we continued forward with CD103 in multivariate analysis.

Multivariate analysis of CD103 and other predictors of survival

Next, we performed multivariate analysis in order to account for additional variables that have a prognostic survival value. We included variables previously validated in our cohort to be predictive of survival, namely CD4+ TILs, ACE-27 comorbidity status and node positivity [5, 9].

We found an interrelated effect between CD103+ and CD4+ TIL content, such that these variables combined were more predictive of survival parameters than either CD103+ or CD4+ TILs alone. Using the TIL cutpoint modeling described above, tumors were stratified into three groups: CD103+/4+ low (neither CD103+ or CD4+ high), CD103+/4+ mixed (either CD103+ or CD4+ high), and CD103+/4+ high staining (both CD103+ and CD4+ high). In univariate and multivariate modeling, high and mixed CD103+/4+ status were strong predictors of improved OS, DSS, and DFS in a dose-dependent fashion (**Figure 2.5**; **Table 2.2**). These models with combined CD103+/4+ status had good predictive value with c-indices of 0.75, 0.71, and 0.76, respectively, for DSS, OS, and DFS.

Discussion

An immunologic statistical profile informed by CD103+ TIL content appears to be a valuable predictive marker for survival in recurrent LSCC after RT/CRT. This adds to our previous findings that an immune-rich tumor-infiltrating phenotype carries a better prognosis in head and neck cancers [8, 9]. Greater TIL content in tumor specimens, whether CD103+, CD4+ or CD8+, portends a better prognosis. CD103+ TILs, in particular, were highly correlated with a favorable prognosis in our cohort. Moreover, combined high CD103+ and CD4+ TIL status had the best prognosis, suggesting an interrelated role of unique adaptive immune cells in controlling tumor progression and metastasis. Conversely, patients with “immune depleted” tumors relatively devoid of CD103+ and CD4+ TILs had significantly worse observed outcomes. These findings support previous studies in suggesting that “immune depleted” tumor status may be a key prognostic factor in many malignancies [21, 22, 23].

In our cohort, CD103+ and CD8+ TIL content overlapped significantly, supporting the presence of a distinct subtype of activated, epithelial-localized, cytotoxic T-cells capable of

malignant cell kill and tumor control. While a similar, albeit moderate, overlap of CD103 and CD8 expression was recently reported in TILs of non-small cell lung cancers [15], ours is the first study to confirm specialized TIL expression patterns in squamous cell carcinomas of the head and neck with translational implications. Further investigations into TIL expression patterns of CD4, CD8 and CD103 across a variety of head and neck cancers, both primary and recurrent, may lead to the discovery and functional characterization of further T-cell subpopulations vital to the adaptive immune response to malignancy.

Given our findings, it is quite likely that CD103+ TIL content may also prove to be a clinically useful biomarker for predicting response to induction chemotherapy, successful larynx preservation, and survival in primary laryngeal cancers treated with organ preservation protocols. To this aim, we are currently analyzing CD103+, CD8+ and CD4+ TIL content in our extensive repository of primary LSCC specimens treated with organ preservation protocols and hope to publish these data soon.

Of note, the pathogenesis of LSCC is not associated with human papillomavirus (HPV), and this is reflected in our LSCC cohort [5, 24]. Other HNSCC subsites, specifically oropharyngeal tumors, are more commonly associated with HPV, and these cancers are marked by a distinct immune phenotype with high levels of CD8+ T-cell infiltration and activation [25, 26]. HPV infection represents a favorable prognostic factor in HNSCC and it has been postulated that the associated immune response may play a role in this relationship. Thus, it is of great interest that an immune-rich tumor microenvironment was still associated with an improved prognosis in this cancer traditionally not associated with HPV and immune activation. Further studies investigating HPV + oropharyngeal cancers in the primary and salvage setting will be

important in determining the importance of CD103 status and other immune markers in disease prognosis for these head and neck cancer subsites.

While “immune depleted” tumors carry a worse prognosis, it remains to be seen whether they may respond differently to immunotherapeutics. Given that the anti-PD-1 antibodies pembrolizumab and nivolumab are dependent on T-cell activity, there is theoretical concern that these “immune depleted” tumors may also be more resistant to immunotherapies, given their relative depletion of TILs [27, 28]. Nevertheless, there remains significant room for further characterization of TIL status and “immune depletion” status in head and neck cancers, both in vitro and in the clinic. This will be crucial to validate our initial findings and to generate algorithms with which to prognosticate patients and potentially stratify treatments.

The importance of immune signatures in cancer prognosis and the related response of immunotherapy in cancer treatment is becoming increasingly apparent. Thus, further elucidation of prognostic biomarkers will be a watershed in predicting patient outcomes, and potentially selecting patients who may benefit from adjuvant immunotherapy. Accordingly, as future genetic studies are completed, it is possible that molecular variables ranging from the status of genomic alterations to gene expression may further improve these immune signature-driven predictive models. The present study describes for the first time the value of the TIL marker CD103 in survival prognostication in head and neck cancer (specifically recurrent LSCC). Our findings suggest that CD103 status may be the most significant immune biomarker for disease prognostication and thus warrants further investigation in prospective studies and in consideration of treatment stratification paradigms.

Figures

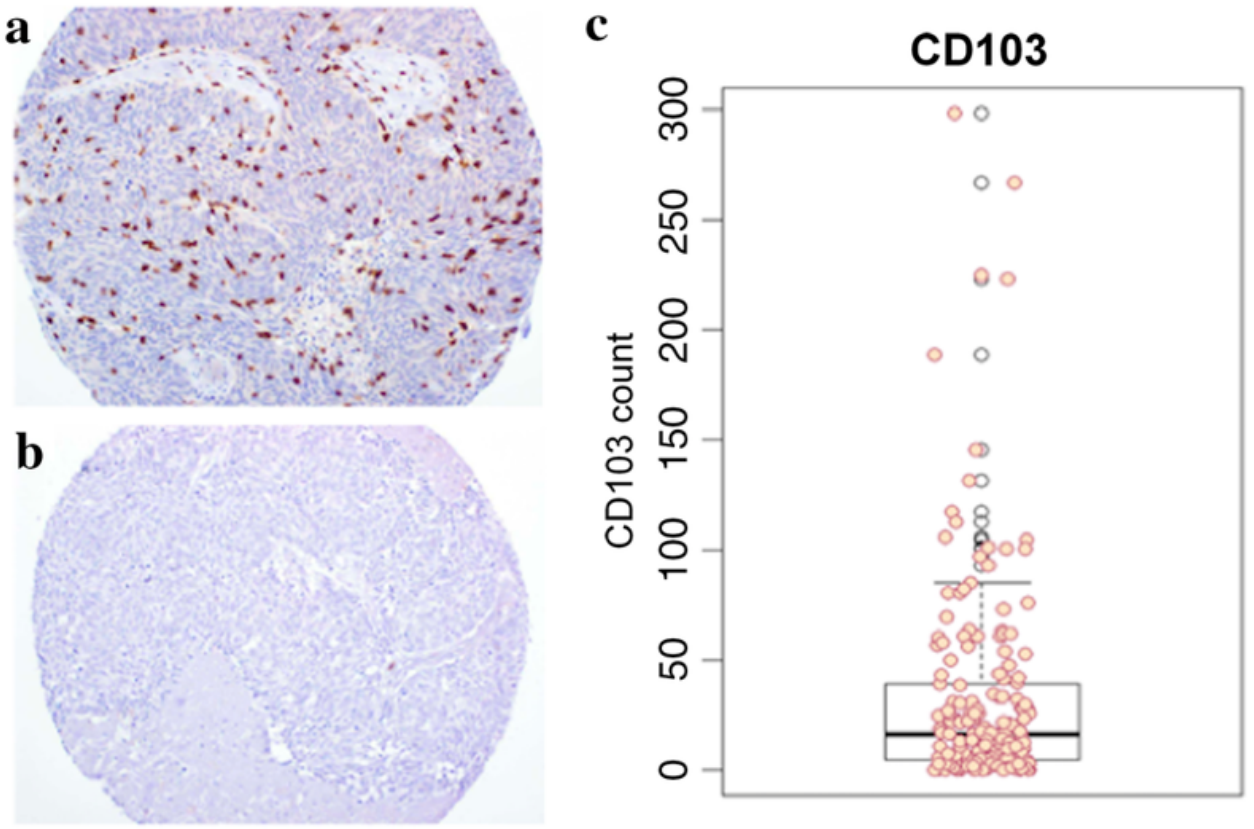

Figure 2-1. CD103 staining patterns and TIL counts.

Representative stains from $CD103^+$ high (**a**) and low (**b**) TIL tumor specimens from our TMA (magnification ×20). A box and whisker plot of TIL counts was constructed (**c**) with mean $CD103^+$ TIL count of 32.1 and median count of 16

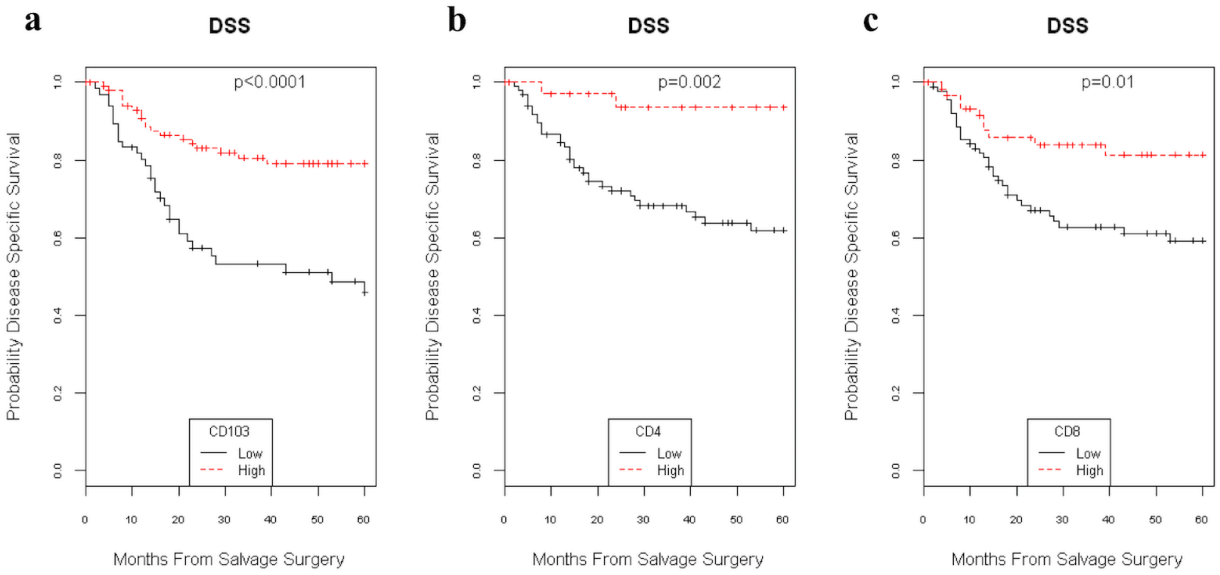

Figure 2-2. Disease specific survival correlation with TIL count.

We analyzed DSS stratified by CD103+, CD4+, and CD8+ TIL status. On univariate analysis, high expression of CD103+ (a), CD4+ (b), and CD8+ (c) TILs correlated with improved DSS.

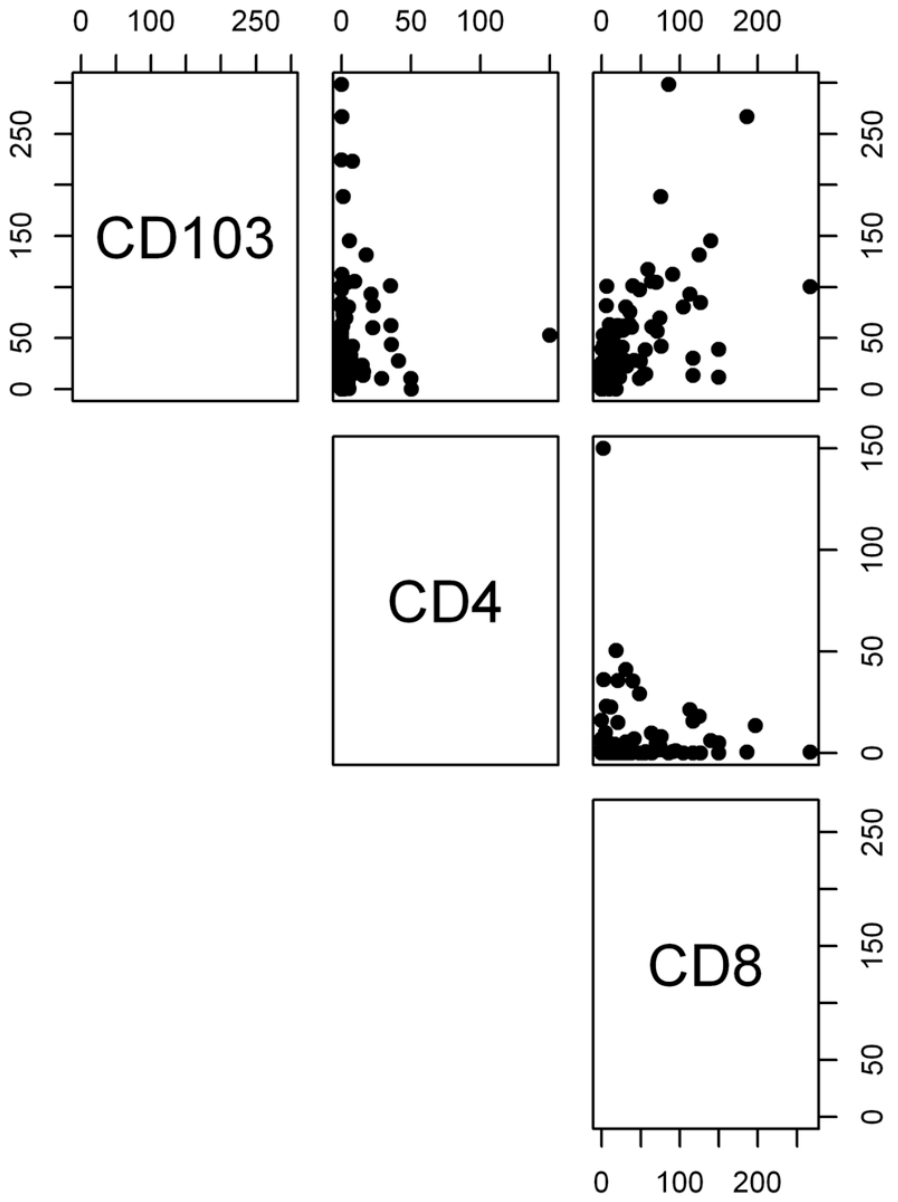

Figure 2-3. Analysis of co-expression of TIL markers in tumors.

Comparing $CD103^+$, $CD4^+$, and $CD8^+$ TIL counts for each tumor specimen, we identified a strong overlap between $CD103^+$ and $CD8^+$ TIL expression status (Pearson rho = 0.62, $p < 0.0001$). There was no correlation between $CD4^+$ expression status and $CD103^+/CD8^+$ TIL expression status.

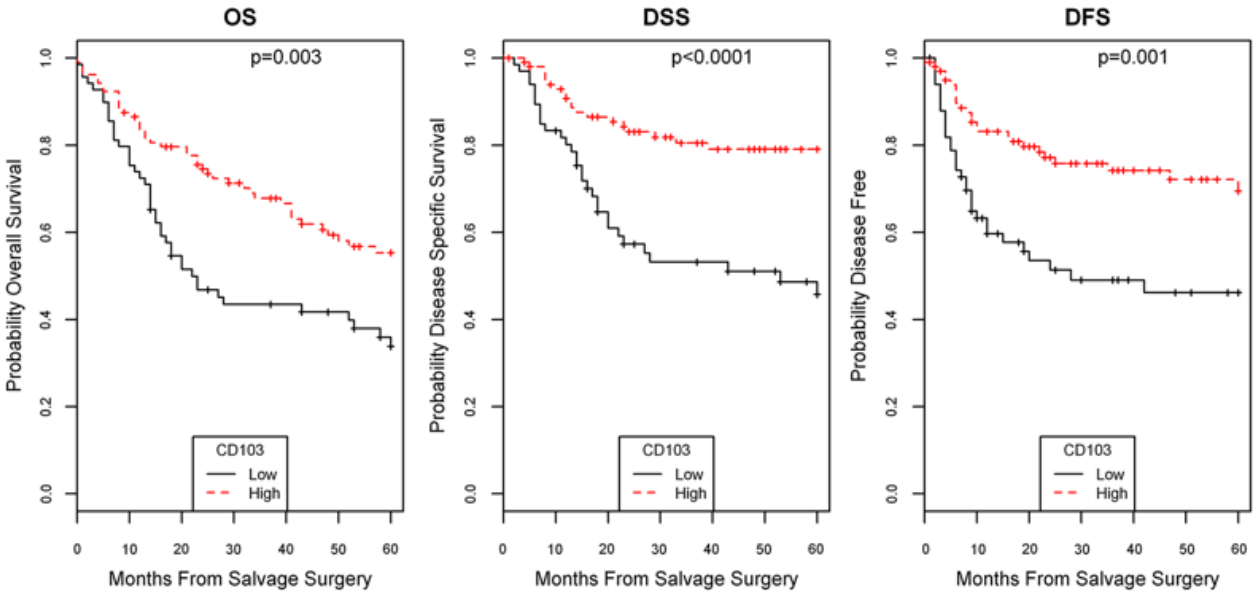

Figure 2-4. Association of CD103 status with survival.

On univariate analysis, $CD103^+$ high TIL status was strongly predictive of improved OS ($p = 0.003$), DSS ($p < 0.0001$), and DFS ($p = 0.001$)

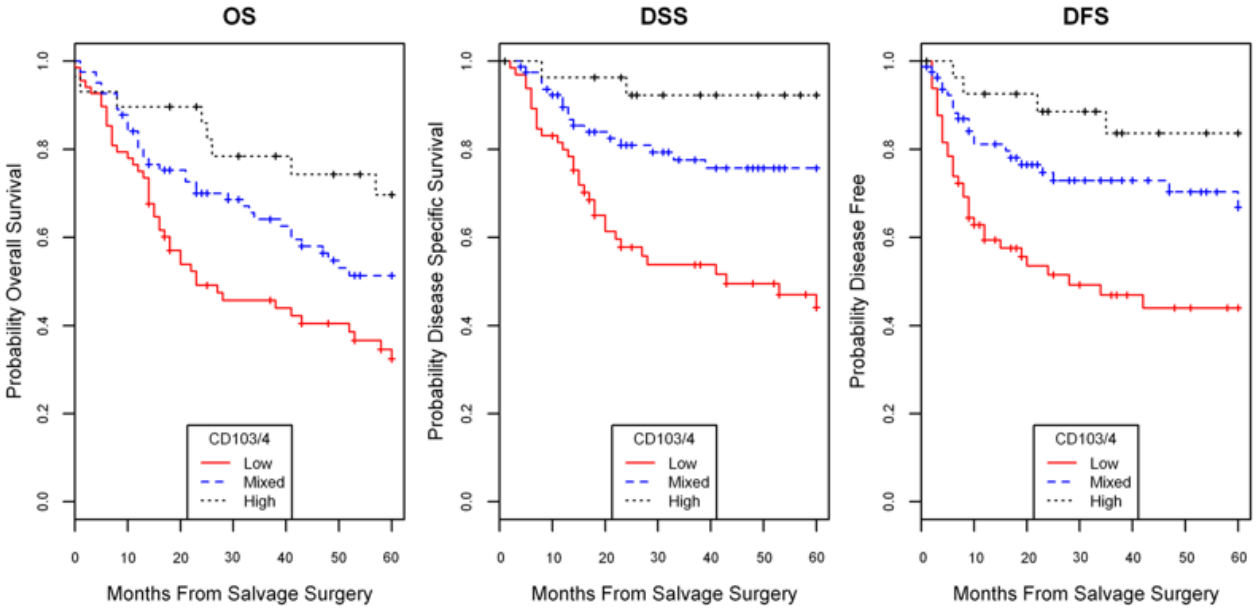

Figure 2-5. CD103/4 status association with survival.

CD103 and CD4 status stratified into high (both $CD103^+$ and $CD4^+$ high TIL status), mixed (either $CD103^+$ or $CD4^+$ high TIL status), or low (both $CD103^+$ and $CD4^+$ low TIL status) demonstrated significant association with OS, DSS, and DFS, with high the best prognosis, mixed with moderate prognosis, and low with poor prognosis

Tables

(N = 183)	
GENDER	
MALE	153 (83.6)
FEMALE	30 (16.4)
ETHNICITY	
WHITE	161 (88.0)
BLACK/OTHER/UNKNOWN	22 (12.0)
MEAN AGE AT INITIAL TUMOR (YEARS)	58.63
INITIAL CLINICAL STAGE	
I	46 (25.1)
II	54 (29.5)
III	44 (24.0)
IV	25 (13.7)
UNKNOWN	14 (7.7)
INITIAL TREATMENT	
RT	112 (61.2)
CRT	71 (38.8)
MEAN AGE AT RECURRENCE (YEARS)	60.87
TIME TO RECURRENCE (MONTHS)	23.48
RECURRENT PATHOLOGIC STAGE	
I	6 (3.3)
II	53 (29.0)
III	48 (26.2)
IV	76 (41.5)

Table 2-1. Characteristics of recurrent/persistent LSCC patient cohort.

Variable	OS		DSS		DFS	
	Hazard ratio (95% CI)	***p* value**	**Hazard ratio (95% CI)**	***p* value**	**Hazard ratio (95% CI)**	***p* value**
pN0 status	0.31 (0.20–0.49)	< 0.0001	0.24 (0.14–0.43)	< 0.0001	0.22 (0.13–0.38)	< 0.0001
pN+	Ref.		Ref.		Ref.	
ACE27 Grade 0	0.20 (0.09–0.49)	#####	0.30 (0.08–1.10)	0.07	0.44 (0.14–1.37)	0.16
ACE27 Grade 1	0.23 (0.10–0.50)	#####	0.27 (0.08–0.95)	0.04	0.29 (0.10–0.84)	0.02
ACE27 Grade 2	0.24 (0.10–0.58)	0.0014	0.26 (0.07–1.01)	0.05	0.24 (0.07–0.79)	0.02
ACE27 Grade 3	Ref.		Ref.		Ref.	
CD103/4 mixed	0.51 (0.33–0.80)	0.0036	0.32 (0.18–0.59)	0.0002	0.39 (0.23–0.69)	0.0009
CD103/4 high	0.28 (0.13–0.61)	0.0014	0.09 (0.02–0.41)	0.0015	0.18 (0.06–0.53)	0.0018
CD103/4 low	Ref.		Ref.		Ref.	
c-index	0.71		0.75		0.76	

Table 2-2. Multivariate analysis of CD103/4 status and survival.

Multivariable modeling with established variables for survival along with CD103/4 status demonstrates a significant survival benefit for CD103/4 mixed status and further greater survival for CD103/4 high status.

Bibliography

1. Forastiere AA, Zhang Q, Weber RS, Maor MH, Goepfert H, Pajak TF et al (2013) Long-term results of RTOG 91–11: a comparison of three nonsurgical treatment strategies to preserve the larynx in patients with locally advanced larynx cancer. J Clin Oncol 31:845–852
2. Forastiere AA, Weber RS, Trotti A (2015) Organ preservation for advanced larynx cancer: issues and outcomes. J Clin Oncol 33:3262–3268
3. Wolf GT, Fisher SG, Hong WK, Hillman R, Spaulding M, Laramore GE et al (1991) Induction chemotherapy plus radiation compared with surgery plus radiation in patients with advanced laryngeal cancer. N Engl J Med 324:1685–1690
4. van der Putten L, de Bree R, Kuik DJ, Rietveld DH, Buter J, Eerenstein SE et al (2011) Salvage laryngectomy: oncological and functional outcome. Oral Oncol 47:296–301
5. Birkeland AC, Beesley L, Bellile E, Rosko AJ, Hoesli R, Chinn SB et al (2017) Predictors of survival after total laryngectomy for recurrent/persistent laryngeal squamous cell carcinoma. Head Neck 39:2512–2518
6. Morris LG, Chandramohan R, West L, Zehir A, Chakravarty D, Pfister DG et al (2017) The molecular landscape of recurrent and metastatic head and neck cancers: insights from a precision oncology sequencing platform. JAMA Oncol 3:244–255
7. Mann JE, Hoesli R, Michmerhuizen NL, Devenport SN, Ludwig M, Vandenberg TR et al (2017) Surveilling the potential for precision medicine-driven PD-1/PD-L1-targeted therapy in HNSCC. J Cancer 8:332–344
8. Lei Y, Xie Y, Tan YS, Prince ME, Moyer JS, Nor J et al (2016) Telltale tumor infiltrating lymphocytes (TIL) in oral, head & neck cancer. Oral Oncol 61:159–165
9. Hoesli R, Birkeland AC, Rosko AJ, Issa M, Chow KL, Michmerhuizen NL et al (2018) Proportion of CD4 and CD8 tumor infiltrating lymphocytes predicts survival in persistent/recurrent laryngeal squamous cell carcinoma. Oral Oncol 77:83–89
10. Wolf GT, Hudson JL, Peterson KA, Miller HL, McClatchey KN (1986) Lymphocyte subpopulations infiltrating squamous carcinomas of the head and neck: correlations with extent of tumor and prognosis. Otolaryngol Head Neck Surg 95:142–152
11. Wansom D, Light E, Thomas D, Worden F, Prince M, Urba S et al (2012) Infiltrating lymphocytes and human papillomavirus-16 associated oropharynx cancer. Laryngoscope 122:121–127
12. Wolf GT, Chepeha DB, Bellile E, Nguyen A, Thomas D, McHugh J, The University of Michigan Head and Neck SPORE Program (2015) Tumor infiltrating lymphocytes (TIL) and prognosis in oral cavity squamous carcinoma: a preliminary study. Oral Oncol 51:90–95
13. Nguyen N, Bellile E, Thomas D, McHugh J, Rozek L, Virani S et al (2016) Tumor infiltrating lymphocytes and survival in patients with head and neck squamous cell carcinoma. Head Neck 38:1074–1084
14. Anz D, Mueller W, Golic M, Kunz WG, Rapp M, Koelzer VH et al (2011) CD103 is a hallmark of tumor-infiltrating regulatory T cells. Int J Cancer 129:2417–2426

15. Ganesan A, Clarke J, Wood O, Garrido-Martin EM, Chee SJ, Mellows T et al (2017) Tissue-resident memory features are linked to the magnitude of cytotoxic T cell responses in human lung cancer. Nature Immunol 18:940–950
16. Webb JR, Milne K, Watson P, deLeeuw RJ, Nelson BH (2014) Tumor-infiltrating lymphocytes expressing the tissue resident memory marker CD103 are associated with increased survival in high-grade serous ovarian cancer. Clin Cancer Res 20:434–444
17. Webb JR, Milne K, Nelson BH (2015) PD-1 and CD103 are widely coexpressed on prognostically favorable intraepithelial CD8 T cells in human ovarian cancer. Cancer Immunol Res 3:926–935
18. American Joint Committee on Cancer (2010) AJCC Cancer Staging Manual. 7th. Springer Press, Chicago
19. Keck MK, Zuo Z, Khattri A, Stricker TP, Brown CD, Imanguli M et al (2015) Integrative analysis of head and neck cancer identifies two biologically distinct HPV and three non-HPV subtypes. Clin Cancer Res 21:870–881
20. Mandrekar JN, Mandrekar SJ, Cha SS (2003) Cutpoint determination methods in survival analysis using SAS. In: Proceedings of the 28th SAS users group international conference (SUGI) 261-28
21. Galon J, Costes A, Sanchez-Cabo F, Kirilovsky A, Mlecnik B, Lagorce-Pages C et al (2006) Type, density, and location of immune cells within human colorectal tumors predict clinical outcome. Science 313:1960–1964
22. Brambilla E, Le Teuff G, Marguet S, Lantuejoul S, Dunant A et al (2016) Prognostic effect of tumor lymphocytic infiltration in resectable non-small-cell lung cancer. J Clin Oncol 34:1123–1130
23. Jiang D, Liu Y, Wang H, Wang H, Song Q, Sujie A et al (2017) Tumour infiltrating lymphocytes correlate with improved survival in patients with esophageal squamous cell carcinoma. Sci Rep7:44823
24. Chen X, Gao L, Sturgis EM, Liang Z, Zhu Y, Xia X et al (2017) HPV16 DNA and integration in normal and malignant epithelium: implications for the etiology of laryngeal squamous cell carcinoma. Ann Oncol 28:1105–1110
25. Zhang Y, Koneva LA, Virani S, Arthur AE, Virani A, Hall PB et al (2016) Subtypes of HPV-positive head and neck cancers are associated with HPV characteristics, copy number alterations, PIK3CA mutation, and pathway signatures. Clin Cancer Res 22:4735–4745
26. Solomon B, Young RJ, Bressel M, Urban D, Hendry S, Thai A et al (2018) Prognostic significance of PD-L1+ and CD8+ immune cells in HPV+ oropharyngeal squamous cell carcinoma. Cancer Immunol Res 6:295–304
27. Mandal R, Senbabaoglu Y, Desrichard A, Havel JJ, Dalin MG, Riaz N et al (2016) The head and neck cancer immune landscape and its immunotherapeutic implications. JCI Insight 1:e89829
28. Moskovitz J, Moy J, Ferris RL (2018) Immunotherapy for head and neck squamous cell carcinoma. Curr Oncol Rep 20:22.

2.2 The molecular landscape of the University of Michigan laryngeal squamous cell carcinoma cell line panel.[3]

Abstract

Background: Laryngeal squamous cell carcinomas (LSCCs) have a high risk of recurrence and poor prognosis. Patient-derived cancer cell lines remain important preclinical models for advancement of new therapeutic strategies, and comprehensive characterization of these models is vital in the precision medicine era.

Methods: We performed exome and transcriptome sequencing as well as copy number analysis of a panel of LSCC-derived cell lines that were established at the University of Michigan and are used in laboratories worldwide.

Results: We observed a complex array of alterations consistent with those reported in The Cancer Genome Atlas head and neck squamous cell carcinoma project, including aberrations in PIK3CA, EGFR, CDKN2A, TP53, and NOTCH family and FAT1 genes. A detailed analysis of FAT family genes and associated pathways showed disruptions to these genes in most cell lines.

Conclusions: The molecular profiles we have generated indicate that as a whole, this panel recapitulates the molecular diversity observed in patients and will serve as useful guides in selecting cell lines for preclinical modeling.

[3] This section was published in *Head & Neck* in collaboration with the following authors: Aditi Kulkarni, Andrew Birkeland, Judy Kafelghazal, Julia Eisenberg, Brittany Jewell, Megan Ludwig, Matthew Spector, Hui Jiang, Thomas Carey, and Chad Brenner.

INTRODUCTION

Head and neck squamous cell carcinoma (HNSCC) is the sixth most common cancer worldwide and can arise in the oral cavity, oropharynx, hypopharynx, or larynx (1). The 5-year survival rates for patients with HNSCC range from 40% to 80%, varying by anatomic site, tumor stage, and human papillomavirus (HPV) status (2). Laryngeal squamous cell carcinomas (LSCCs), which comprise 20% of all HNSCCs, are typically HPV negative and have a 5-year survival rate of 80% to 90% for stage I/II disease (3), but up to 50% of advanced patients with LSCC experience recurrence following frontline therapy, at which point disease progression often occurs rapidly with significant regression in quality of life metrics (4). Thus, robust models of LSCC are important for identification of biomarkers distinguishing patients most likely to fail therapy, as well as to develop novel treatments for aggressive disease. We believe LSCC cell line models representing the range of cancer stages and genetic composition in both primary and recurrent/metastatic settings will aid in better understanding individual disease processes and responses to treatment and in developing therapies that improve outcomes for LSCC.

From The Cancer Genome Atlas (TCGA) project, a molecular landscape of primary untreated LSCC is beginning to emerge (5). Alterations to *TP53*, *NOTCH1*, *CDKN2A*, and *PIK3CA* are common, whereas the presence of HPV is relatively rare. Meanwhile, studies of recurrent and/or metastatic LSCC suggest that with progression, the molecular landscape shifts to contain more oncogenic lesions (6), although this relationship has not been confirmed in large cohorts of matched primary and metastatic tumors. Regardless, it is clear that distribution of genetic lesions varies among tumors, and as new questions emerge, it will be important to interrogate them using appropriate models within the context of genetic status. Tissue type and

genetic background will likely impact the efficacy of targeted therapies, emphasizing the need for improved understanding of the unique complexity of individual cancers (7,8).

Cell lines serve as valuable tools for assessing the impact of genetic alterations (9-12). The University of Michigan previously created a repository of HNSCC cell lines (UM-SCC) that were characterized by short tandem repeat typing (13), and although many of these have been utilized extensively throughout the world, thorough genetic characterization has not yet been performed for cell lines derived specifically from laryngeal carcinomas (8). This limitation prevents researchers from interpreting phenotypic and therapeutic results in the context of tumor genetics. Thus, we aimed to profile the genetic and transcriptomic landscape of laryngeal UM-SCC cell lines in order to provide a molecular basis for future studies that leverage this panel.

MATERIALS AND METHODS

UM-SCC models

LSCC cell lines were established and characterized in the Head and Neck Oncology laboratory at the University of Michigan with written informed consent from patient donors with LSCC, who were treated for LSCC between 1980 and 2011. Cell lines were maintained in exponential growth phase in Dulbecco's modified eagle medium with 10% fetal bovine serum, 5% penicillin/streptomycin, and 5 mM nonessential amino acids in a 5% CO_2 incubator.
In all cases except UM-SCC-105, due to the age of the cell lines, donor tissue from either tumor or normal tissue was unavailable for further testing.

Exome sequencing

Exome capture library construction was performed using the NimbleGen V2 (44.1 Mbp) Exome Enrichment kit (Roche, Basel, Switzerland) for UM-SCC-10A, 10B, 11A, 13, 17B, 23, 25, 28,

41, 46, 76, and 81B, and paired-end sequencing (2 × 100 bp) was performed on an Illumina Genome Analyzer IIx Platform, with an average coverage of ×50. Library construction for UM-SCC-12 and 105 was performed using the Roche NimbleGen V3 and paired-end sequencing (2 × 150 bp) was performed on an Illumina HiSeq 4000 platform with average coverage of ×100. All sequencing was carried out at the University of Michigan DNA sequencing core according to standard protocol. Whole exomes are available through the Sequence Read Archive (**https://www-ncbi-nlm-nih-gov.proxy.lib.umich.edu/sra**) accession # PRJNA525437.

Variant Calling

Quality control checks were performed on the raw sequencing data using FastQC v.0.11.5 (14). Reads were aligned to hg19 reference genome using BWA v0.7.8 (15). Duplicates were marked using PicardTools v1.79 (Broad Institute, Cambridge, Massachusetts). BAM files were created by following the GATK best practices workflow (16). Variants were called on each cell line using the HaplotypeCaller producing a VCF file for each sample. These VCFs were then combined using the GenotypeGVCFs tool and a single VCF file was obtained for all the samples. Variant Quality Score Recalibration was applied to this joint VCF file to filter out low quality variants. To annotate and filter the variants of interest, the commercially available tool Goldex Helix Varseq v1.4.0 (Golden Helix, Inc., Bozeman, Montana) was used. Filters were set as previously described (17).

Variant pathogenicity analysis

The cancer-related analysis of variants toolkit (CRAVAT; **http://www.cravat.us**) was used to evaluate missense and indel mutations to predict pathogenicity via the variant effect scoring tool

(VEST) and driver/passenger status via the cancer-specific high-throughput annotation of somatic mutations (CHASM) tool. Missense mutations were scored with both VEST and CHASM; indels were scored with VEST only. The scores are used to generate *P* values, and a cutoff of $P < .05$ was used to designate highly pathogenic (VEST) or probable driver (CHASM) mutations.

Sanger sequencing validation

Genomic DNA isolation was performed using the Gentra PureGene kit (Qiagen, Hilden, Germany). DNA was then polymerase chain reaction (PCR) amplified with Platinum Taq DNA Polymerase High Fidelity (Invitrogen, Carlsbad, California) following manufacturer's instructions. PCR products were cloned into the pCR8 TOPO vector (Invitrogen) and subjected to Sanger sequencing on a 3730XL DNA Sequencer (Applied Biosystems, Foster City, California) at the University of Michigan DNA Sequencing Core. Sequence alignment was performed using the DNASTAR Lasergene software suite.

Copy number analysis

The Affymetrix OncoScan Assay kit was used to analyze copy number alterations in the cell lines. The CEL files produced by the kit were merged to produce OSCHP files using the OncoScan Console v1.3 software. These OSCHP files were then analyzed by applying the TuScan algorithm, which is a part of the Nexus Express for OncoScan software package. From our analysis, we found a disparity between the B-Allele Frequency plot and the copy number estimate made by the TuScan algorithm in case of some homozygous deletion calls (copy number = 0). To improve the accuracy of copy number calls in these cases, we used the presence

or absence of exome sequencing reads to confirm complete loss of the gene locus. Thus, we corrected copy number calls that were assigned a copy number call of zero by the TuScan software, but had exome sequencing reads, in **Table 2-3** to indicate a single copy of the gene. Each of these corrections was annotated with an asterisk to denote the change. Copy number data have been deposited in the National Center for Biotechnology Information Gene Expression Omnibus (NCBI GEO; **http://www-ncbi-nlm-nih-gov.proxy.lib.umich.edu/geo/**) and are available through GEO Series accession #GSE127231.

Transcriptome analysis

RNA sequencing was performed for UM-SCC-10A, 10B, 12, 17B, 23, 25, 28, 46, 81A, 81B, and 105 using Illumina stranded transcriptome library preparation kits with 75 nucleotide paired end sequencing to >×100 depth on an Illumina HiSEQ4000. Fragments per kilobase of transcript per million mapped read were calculated as previously described (16), and values for specific genes are listed in Table 2-4. Gene expression data from RNA-seq experiments have been deposited in the NCBI GEO and are available through GEO Series accession # GSE126975.

RESULTS

We performed exome sequencing and high-density arrays on a panel of UM-SCC cell lines generated from patients with LSCC. We analyzed 16 cell lines total, generated from 14 patients. Our panel represented a range of disease states (stage I through stage IV LSCC) and included cell lines from eight primary untreated, three recurrent, and four metastatic LSCCs (Table **2-5**). Smoking/alcohol use was reported in all except the patient from whom UM-SCC-105 was derived, who was HPV-18 positive (18). Two matched pairs of cell lines were included in certain analyses: UM-SCC-10A and 10B, derived from primary tumor and lymph node

metastasis, respectively, and UM-SCC-81A and 81B, derived from two masses resected in separate procedures.

Comprehensive capture-based exome sequencing was performed on 14 cell lines. Our analysis showed a large mutational load, with approximately 30-50 nonsynonymous mutations identified per Mb (Figure **2-6**). To annotate the cell line panel, we assessed common genetic aberrations previously reported by the HNSCC TCGA consortium (5). We identified nonsynonymous mutations affecting several of these genes, including *TP53* in 11 of 14 (79%) and *FAT* atypical cadherin 1 (*FAT1)* in 6 of 14 (43%) of cell lines (Figure 2-7A). Table 2-6 lists the specific mutations observed. Mutation rates for each gene are provided as compared to TCGA HNSCC data (5,19). Importantly, our study lacks matched normal samples and therefore cannot account for germline variants, although most genes were mutated with similar frequencies in the LSCC cell line panel as in the TCGA tumors. Notable exceptions included *FAT* and *NOTCH* family genes and *BRCA1*/2, which are mutated at higher rates in our models than in TCGA specimens.

The FAT family mutations identified in our LSCC cell line panel are depicted in Figure 2-7B and were validated by Sanger sequencing (Figure 2-8). For each FAT mutation identified in our panel, we used the VEST420-22 to predict pathogenic impact. Variant score P values are reported for each mutation in Figure 2-7B and support a pathogenic impact on FAT1 function of 5 of 7 of the identified alterations ($P < .05$). Interestingly, FAT4 mutations were also especially prevalent, and VEST4 scores predicted a pathogenic impact in 5 of 8 cases. For missense mutations, the CHASM-3.1 tool was used to predict driver mutations (Table 2-7). Similar analysis was completed for the NOTCH family genes, and BRCA1/2 alterations identified in our panel as these genes were altered at slightly higher than expected rates. Although VEST

pathogenicity scores for BRCA1/2 were not significant, the CHASM predictor of tumorigenic impact classified the mutations reported in both genes as likely driver mutations (Table 2-7).

After annotating molecular alterations found in the panel, we assessed copy number alterations in 12 LSCC cell lines via high-density single nucleotide polymorphism (SNP) arrays to provide additional molecular detail. We first performed a combined analysis of all 12 lines by summing copy number alterations at each probe site (Figure 2-9A). Our analysis revealed common copy number alterations in the cell line panel consistent with those reported in previous HNSCC studies, including broad amplifications of chromosome 3q, 5p, 7p, 8q, and 20q arms and deep deletions in the chromosome 3p, 8p, 9p, 11q, and 18q arms.5, 23-25 Importantly, the 3q amplicon includes transcription factors TP63 and SOX2, as well as the oncogene PIK3CA. As 35% of HNSCCs in the TCGA study harbor an alteration in PIK3CA, it is widely considered a potential therapeutic target, with several clinical trials investigating PI3K inhibitors in patients with HNSCC (26). Additionally, both broad and focal deletions were observed in the 4q35 region containing the FAT1 gene. Thus, our analysis suggests that this panel as a whole recapitulates the landscape of major chromosomal aberrations found in HNSCC tissues.

Next, we further interrogated our panel to characterize key genes and pathways. Genes chosen for analysis were previously identified as commonly altered in the TCGA HNSCC cohort,5 are otherwise implicated in HNSCC pathogenesis (SRC, BCL6, and JAK2), or are reportedly linked to FAT1 signaling (SCRIB, STK3, WWTR1, WWC1, MTNR1A, and FAT3). Copy number calls are reported in Table 2-3. Median copy numbers are depicted in a heat map (Figure 2-9B, upper panel). We refer to median values ≥ 0.5 as amplifications and values ≤ -0.5 as copy losses. Consistent with TCGA findings, we observed amplifications of EGFR in 8 of 12

cell lines and amplifications of PIK3CA in 5 of 12. Copy losses at the CDKN2A-CDKN2B locus were especially prevalent (10 of 12 cell lines). We observed broad 9p deletions in 6 of 12 cell lines, with an additional 4 cell lines exhibiting focal deletions at the CDKN2A-CDKN2B locus (Figure 2-9C). We also performed RNAseq for a subset of UM-SCC larynx cell lines (Figure 2-9B, lower panel). As expected, EGFR was highly expressed in all cell lines. In many cases, copy number alterations corresponded with variations in gene expression (Figure 2-10). For example, we report deletion and low expression of CDKN2A/B in UM-SCC-12 and 81A, as well as amplification and high expression of YAP1 in UM-SCC-81B. We also asked whether cell lines harboring nonsense mutations likely to confer loss of function might exhibit altered gene expression, but in this small sample size, we observed no trends with regard to RNA expression and mutation status (Figure 2-10).

FAT1 copy loss was observed in 4 of 12 cell lines in this analysis, with focal deletions in UM-SCC-10B and 12 (Figure 2-9D). Notably, FAT1 was also a commonly mutated gene in our panel (Figure 2-7A). Interestingly, of those cell lines that lacked a point mutation, some (UM-SCC 10A, 10B, and 46) did exhibit FAT1 deletions, for a total of nine cell lines with potential loss of FAT1 function. Some cell lines exhibited loss of multiple FAT family genes: FAT1 and FAT2 losses were both observed in the UM-SCC-10A/B pair and losses of all four FAT genes were observed in UM-SCC-46 (Figure 2-9B). However, RNA-seq indicated high expression of FAT1 in most cell lines, with the exception of UM-SCC-10A/B.

Given the high rate of FAT1 alterations with predicted functional impact in our panel, we sought to summarize alterations in FAT family genes. FAT1 alterations occurred in 35% of the 110 LSCCs in the TCGA cohort and 29% of the overall cohort (Figure 2-11A) (19), and of the 9 UM-SCC cell lines with both copy number and single nucleotide variant data available, 7

exhibited loss of function alterations in FAT1, consistent with its purported role as a tumor suppressor. About 55% of LSCCs and 44% of all HNSCCs in the TCGA study harbored at least one FAT family gene alteration. Among these samples, the majority of 110 of 143 (77%) of FAT1 mutations are reported as truncating mutations (Figure 2-11A), which was consistent with our observation of missense mutations, a frameshift, and a stopgain among UM-SCC lines (Figure 2-7). Figure 2-11B summarizes FAT family alterations observed in the cell line panel. Although most FAT1 mutations were truncating or deep deletions, mutations in other FAT family members were predominantly missense mutations in TCGA samples and UM-SCC cell lines.

Our data support a model in which functionally recurrent alterations to multiple genes within a pathway contribute to overall pathway disruption. To further understand functional recurrence of alterations to FAT signaling, we next examined alterations to genes linked to FAT1 signaling in both the TCGA dataset and our cell line panel. FAT1 has been shown to inhibit Hippo/YAP1 pathway-induced proliferation and survival through its interactions with Scribble (SCRIB) and serine/threonine kinase 3 (STK3) (28-30). Figure 2-11C summarizes the prevalence of genetic alterations in these genes identified in TCGA primary larynx tumors27 and all TCGA HNSCC tumors (black). From this summary, it appears that alterations to FAT signaling are more common in LSCC than other HNSCC disease sites; in particular, we noted that alterations affecting WWTR1, a YAP1 paralog, were especially prevalent in larynx tumors, with 31 of 110 (28%) larynx tumors harboring a WWTR1 amplification, compared with 39 of 394 (10%) at other subsites. Unfortunately, the relatively low number of tumors from each subsite limits the ability to test this association statistically.

In the UM-SCC panel, we observed broad copy gains to 11q22, which contains the YAP1 gene, in 2 of 12 cell lines, further implicating Hippo/YAP1 activation in promoting growth and survival in these models (Figure 2B). WWTR1 is also frequently amplified, with copy gains occurring in 6 of 12 cell lines. This is consistent with frequent WWTR1 amplifications observed in the TCGA HNSCC dataset. Figure 2-11D summarizes alterations to Hippo/YAP1 pathway genes in UM-SCC cell lines. Interestingly, contrary to their documented tumor suppressive functions, amplifications of both STK3 and SCRIB were observed in 2 of 14 and 6 of 14 cell lines, respectively (Figure 2B), with modest copy gains observed in several additional cell lines. This is consistent with the broad 8q copy gains observed in the UM-SCC panel and TCGA data.5

Also linked to this pathway is the KIBRA protein, encoded by WWC1, which is thought to promote the phosphorylation and inhibition of YAP1 and WWTR1 (31). We observed WWC1 loss in 3 of 12 cell lines, consistent with a role in dampening Hippo/YAP1 signaling, although UM-SCC-81A exhibits a modest copy gain. Furthermore, NOTCH3, mutated in 5 of 14 cell lines in our mutation analysis, was recently shown to act as a tumor suppressor in breast cancer cells by inducing KIBRA upregulation (32). Overall, the prevalence of alterations in FAT1-related genes supports a role for Hippo/YAP1 and FAT family signaling in these models, warranting further investigation of this network in LSCC.

DISCUSSION

As precision medicine protocols are developed, comprehensive genetic stratification of tumors becomes increasingly crucial to correlate with disease prognosis and to target known driver mutations (33). Large-scale, integrated analyses have recently provided unparalleled molecular detail toward stratification of tumors, paving the way for precision medicine protocols based upon comprehensive molecular profiles (5,25). To advance novel targets and

combinations, an array of well-characterized models representative of the diversity of disease observed in the clinic must also develop in tandem, as preliminary studies using these tools are critical to predict therapeutic response. The UM-SCC cell line panel is widely used to model HNSCC, but genetic characterization of these cell lines has been limited. Furthermore, LSCC is a challenging clinical entity, with limited response to current treatment modalities and poor survival rates, especially in recurrent disease (34). We therefore sought to create a profile of UM-SCC cell lines derived from patients with LSCC to better understand these models and determine how accurately they reflect genetic characteristics of patients.

Overall, our analysis indicates that many aberrations recurrently identified in the HNSCC TCGA study are well represented in the UM-SCC larynx cell line panel. *EGFR*, *PIK3CA*, and *CCND1* copy gain, *CDKN2A* copy loss, and *TP53* and *FAT1* mutation are among the most common aberrations observed in our panel, consistent with reports of clinical specimens. Thus, this panel appears to adequately represent many well-studied, targetable alterations in HNSCC and should serve as an important tool in advancing combination therapies targeting these pathways. Importantly, there were some genes (*FBXW7*, *BRCA1*, *NOTCH2*, and *NOTCH3*) for which our analysis indicated considerably higher mutation rates than those observed in the TCGA dataset. Such discrepancies may be attributed to our small sample size, differences in variant calling pipelines, or to the fact that the TCGA report includes only somatic mutations, whereas our analysis cannot distinguish somatic mutations from germline. It is also possible that certain alterations have been selected for during cell line derivation and culture.

Notably, significant variation in molecular profiles exists within tumor sets and across the UM-SCC panel. For example, UM-SCC-17B is strikingly devoid of point mutations and copy number alterations, but harbors a *PIK3CA* hotspot mutation at the *3:178938934* position (Table **2-6**)

(35). Likewise, UM-SCC-105, an HPV-18 positive cell line, appears similarly genomically stable but harbors a pathogenic nonsense mutation in *BRCA2*. Identification and stratification of such molecular subsets will benefit research applications and could aid in selection of appropriate models based on patient characteristics.

Our data show an unexpectedly high prevalence of *FAT1* inactivating mutations or genetic deletions and support a deeper analysis of the pathway. Although *FAT1* alterations are well documented in HNSCC, few reports address *FAT2*, *FAT3*, and *FAT4*, which have lower alteration rates than *FAT1* in the TCGA dataset (Figure 2-11A). In our cell line panel, we found that *FAT* family alterations were prevalent and UM-SCC-10A, 10B, and 46 harbored alterations in multiple *FAT* genes. We observed *FAT1* and *FAT2* copy loss in the UM-SCC-10A/10B pair, along with both copy loss and mutation in *FAT4* in UM-SCC-10A. Furthermore, a *FAT2* mutation with high predicted pathogenic impact was identified in both cell lines, further supporting a prominent pathogenic role for *FAT* genes in these particular models. Although *FAT3* is considered paralogous to *FAT1* and exhibits similar functions (30), fewer *FAT3* alterations were discovered in the TCGA cohort, and these appeared less likely to confer loss of function, consisting of a mix of amplifications, deletions, missense mutations, and truncating mutations (Figure **2-11**A). Similarly, in the 12 cell lines subjected to copy number analysis, we observed one loss and one gain in *FAT3* (in UM-SCC-46 and -25, respectively; Figures 2-9B and 2-11B). Only three *FAT3* mutations were observed in our cell line panel and all were missense mutations (Figure **2-7**). However, UM-SCC-11A and 17B both harbored mutations classified as pathogenic by the VEST tool, and the mutation in 11A is a predicted driver according to the CHASM score. Interestingly, expression of FAT3 was very low in most cell lines in our panel (Figure 2-9B). This suggests that further dissection of *FAT3* genetic

alterations may be required to understand how each type of alteration affects *FAT3* pathway activity.

When we expanded our analysis to additional genes linked to FAT signaling, we noted frequent copy number alterations consistent with dysregulated Hippo/YAP1 signaling, both in our cell lines and in the TCGA dataset, particularly affecting *WWTR1*. Although amplifications of purported tumor suppressors *STK3* and *SCRIB* were also observed, this may be due to the fact that both genes are located in a broadly amplified region of 8q. Although a mechanistic role for *STK3* and *SCRIB* in promoting tumorigenesis has not been clearly defined, the seemingly paradoxical overexpression of these proteins is commonly reported in human cancers (36). *FAT1* is in the cadherin class of membrane-bound proteins, with functions that remain to be fully characterized. Notably, *FAT1* mutations may have context-dependent effects depending on the tissue source. In HNSCC and esophageal squamous cell carcinomas, it appears to act as a tumor suppressor gene, inhibiting epithelial-mesenchymal transition and cell proliferation (37), whereas in other tumors, it may have oncogenic function (38,39). There is limited understanding of the role of *FAT1* in HNSCC in general, apart from the high mutational rate reported in the recent TCGA study. Interestingly, *FAT1* mutant HNSCCs may have better overall survival (40), suggesting that it may portend a better prognosis for which clinical treatment modification may be investigated. A prognostic role for *FAT1* will need to be investigated in confirmatory cohorts, and further characterization of tumors harboring *FAT1* alterations will be necessary. Recently, Martin et al showed that FAT1 participates in assembly of a Hippo signaling complex responsible for negatively regulating YAP1 in HNSCC cell lines, thus its loss may result in unrestrained YAP1 activity (27). Reintroduction of FAT1 intracellular domain into FAT1 deficient cell lines resulted in decreased YAP1 activity, reduced proliferation, and abrogated

tumorigenesis in vivo. These effects were rescued by YAP1 overexpression. A 2017 study by Pan et al assessed YAP1 protein by immunohistochemistry in 121 LSCC tumor samples and found positive YAP1 expression to be associated with clinical stage, TNM classification, lymph node metastasis, and poor overall survival (41). Taken together, these studies support YAP1 as a promising therapeutic target in the context of genetic alterations in FAT1 and the Hippo signaling pathway.

Another recent study identified a potential interaction between *FAT1* and *CASP8* in oral cavity squamous cell carcinomas (42), showing increased growth and migration in cell lines with FAT1 loss of function, further corroborating the functional role of *FAT1* as a tumor suppressor gene. FAT1 may function as a tumor suppressor by binding to β-catenin and blocking its nuclear translocation, thereby inhibiting Wnt signaling pathways fundamental to growth and proliferation.**38** As discussed above, FAT1 may inhibit the YAP1 pathway, which is critical for cell growth and survival. Thus, with FAT1 loss of function in LSCC, there may be unchecked tumor cell growth and proliferation through both Wnt/β-catenin and YAP1 pathways. In selecting targeted therapies in LSCC, consideration of *FAT1* status may be beneficial, as agents inhibiting the Wnt/β-catenin pathway, many of which are in development, may be particularly efficacious.

The UM-SCC larynx cell line panel has been in use in laboratories throughout the world for the past several decades. We now provide a comprehensive genetic characterization of these models that can be used to contextualize past and future studies in terms of the genetic diversity seen in patients. However, in utilizing cell lines as model systems, it is important to note the likelihood of variations between stocks of the same cell line. In support of the concept that genetic diversity exists between models cultured separately, cytogenetic analysis was originally

performed for UM-SCC-17A/B at several different passages by Carey et al in 1989 (43). There were no karyotypic differences between UM-SCC-17A cells analyzed at passages 8, 23, 28, and 37 nor between UM-SCC-17B cells at passages 13, 17, and 52. However, a UM-SCC-17A subline was also discovered, differing from the UM-SCC-17A stem line both at the cytogenetic level and by expression of various surface antigens, including the E7 and A9 antigens. This subline was believed to represent a distinct population present in the primary tumor, indicating that multiple heterogeneous populations existed initially. Furthermore, Ludwig et al performed comprehensive profiling of the UM-SCC oral cavity cell line panel and provided evidence of multiple clones through copy number analysis and fluorescence in situ hybridization (17).

The concept of cell line evolution in culture was highlighted more recently in a comprehensive characterization of 27 MCF7 strains in which the authors observed considerable variations in genetics, gene expression programs, morphology, and drug response (44). Many of the cell lines discussed here have been distributed to laboratories throughout the world, and genetic drift and divergence among lineages cultured in different laboratories is highly likely. As the purpose of the present study is to offer a baseline profile of the LSCC cell lines, a direct comparison between the genetics of our cell lines and lineages propagated in other laboratories is beyond the scope of this report. However, we do describe and reference many of the same genetic alterations reported by other laboratories. For example, a 2018 study by Cheng et al assessed mutations and copy number variations in a panel of 26 HNSCC cell lines, notably including UM-SCC-46 and UM-SC-105 (45). We recapitulate many of their findings in UM-SCC-46, such as 3q copy gain, *YAP1/BIRC2* deletion, a *TP53* nonsense mutation, and *KMT2D* frameshift. Cheng et al also report a 3q gain in UM-SCC-105, as well as *CASP8* deletion, and so forth, which our study did not detect further supporting the concept of

potential genetic drift between models cultured in different labs over time. Additionally, while Cheng et al report *FAT1* copy gain in nearly all cell lines, including UM-SCC-46 and 105, our data show copy loss in UM-SCC-46 and no alteration in UM-SCC-105.

Furthermore, Nisa et al analyzed alterations in several UM-SCC cell line pairs in 2018, including the UM-SCC-10A/B, 17A/B, and 81A/B pairs (46). They report several differences between the 10A (primary tumor) and 10B (lymph node metastasis) lines, including as a *FAT4* mutation only in 10A, an observation recapitulated in our study. We also reproduce their findings of *TP53* and *FAT2* mutations in both lines, but interestingly, Nisa et al also report *FAT1*, *2*, and *4* mutations in UM-SCC-17B, as well as a *PTEN* mutation in UM-SCC-81B, which we did not observe.

The present study emphasizes the utility of continuing to expand the available array of well-characterized HNSCC cell lines. Importantly, this report also highlights an underappreciated but broad range of molecular alterations to multiple genes associated with FAT signaling and supports a need to deeply dissect the function of this pathway in HNSCC pathogenesis. As we refine our understanding of molecular complexity and heterogeneity in HNSCC, our study provides a foundation for modeling therapeutic responses and advancing personalized medicine protocols.

Acknowledgements.

The authors would like to thank Apurva Bhangale for bioinformatics support.

Tables

Cell line (UM-SCC-)	10A	10B	12	17B	23	25	28	46	57	81A	81B	105
TP63	5	3	7	2,2.5	8.67, 5.33	4	2.33	2.67	6	2.33	6	2
PIK3CA	5	3	5	2	4.67	4	2.33	2.67	6	2.33	6	2
PTEN	1	1.67	2	2,1.5	3.33	4	1.67	1.67	2	2	3	3
PIK3R1	0	1.33	2	2	2.33	3	2	2	2	2	4	3
CDK6	2	1.67	7	2	4.33	4	2.67	3	3	1.67	4	2
CDKN2A	0	1.33	1	0,2	0*	4	1	1	0	0*	1.5	3
CDKN2B	0	1.33	0	2	2.33	4	1	1	0	0*	1.5	3
TP53	1	1.67	5	2	3.33	3	2.33, 2	1.67	2	1.67	1.5	2
NF1	1	2	4	2	4	0	2.67	2	3	2.67	4	2
CASP8	1	2.33	1.5	2	3.33	4	1.67	1	5	1.67	3	2
NOTCH1	1.5	2	5	3	4.67	2	3.33, 3.67	2.33	3	2.33	5	3
MYC	3	3	15	2	3.33	4	2.67	2	5	3	4	3
HRAS	1.5	1.67	3	3	2.33	4	1.33	1.67	2	2	3	2
CCND1	1.5	2	2	3	3.67	6	2	7.33	2	2.33	4	1.5
SRC	3	2.67	5	2	4	4	1.67	2	3	3	4	3
BCL6	5	3	4	2	6.33	4	2.33	2.67	6	2.33	6	2
EGFR	5	3.33	6	3	5, 2.33	8	3	2.33	5,2,4	2.67	4	4
FGFR1	3	2.67	4	2	2	1.5	2.67	2	5,2.5	1.67	3,2.5	3
FGFR3	1	2	2.5	1	2	2	1.33	1.67	2	2	2.5	2
IGF1R	1	1.33	6	2	3.33	2	1.67	2	4	2	4,3	3
ERBB2	1	2	4	2	3.67	3	2.33, 2.67	2.33	4	2.67	4	2
EPHA2	2.5	2.67	2	2	3	3	2	2	3	2	2.5	2

DDR2	2	2.33	3	2	4	4	2	1.67	3	2.67	2.5	2
MET	2.5	2.33	14, 4	1	6.67, 4	5, 4	2.33	2	3	1.67	4	2
JAK2	0	1.33	7	2	2	4	1	1.67	2	1.67	1,1.5	3
TRAF3	0	2	4	3	3	1	1	2	4	2.33	4	2
KEAP1	0	2	3	2	1.67	1	1.33	1.67	2.5	1.67	2.5	1.5
MYH9	1	2	0	1	3.67	2	1.67	2	2.5	1.67	4	2
BIRC2	2	2	2	3	3.33	6	1.67	1	3	2.67	21	2
YAP1	2	2	2	3	3.33	6	1.67	1	3	2.67	21	2
SCRIB	2.5	2	3	2	3.33	4	2.67	2	4	2.33	4	3
STK3	3	2.67	4	2	3.33	4	2.67	2	4	3	4	3
WWTR1	4	3	5	3	6	5	2.33	2.67	2	2.33	6	2
WWC1	1	1.67	5	2	2	4	2	1.67	2	2	4	2
FAT4	1	2	2	2	4.33	2	1.67	1	3	1.67	2	2.5
FAT3	2	2	2	3	2.33	6	1.67	1	3	2.67	1.5	2
FAT2	1	1.67	4	2	2	4	2	2	2	2.33	4	2
FAT1	0	1	0	2	2	2, 8	0.67, 2	1	2	1.67	1.5	2
AJUBA	2.5	2	3	2	3.33	5	1	2	2	2.67	4	2

Table 2-3. Estimated copy numbers for gene list as noted by the TuScan algorithm for the indicated UM-SCC-cell lines.

For entries containing multiple copy numbers separated by a comma, multiple values were reported over the length of the gene. Where a copy number of 1* is reported, the TuScan algorithm estimated a complete deletion (CN=0), however, we observed those genes had exome sequencing reads. Thus, we determined it more accurate to report a single copy loss rather than a complete deletion in those cases.

	10A	10B	12	17B	23	25	28	46	81A	81B	105
TP63	*7.6623*	*8.1646*	*6.7623*	*8.3993*	*6.1935*	*2.5379*	*6.4389*	*6.9031*	*0.3340*	*6.0780*	*5.9351*
PIK3CA	4.8020	3.6584	3.4539	2.9023	3.5593	3.1881	2.9400	3.6907	3.5514	4.4735	2.5713
PTEN	3.4256	4.6801	4.4520	5.0443	4.2966	4.0593	4.0263	4.9740	4.3265	4.2996	4.8531
PIK3R1	2.1450	2.5989	3.4658	3.4931	2.5063	2.5891	2.4788	2.2305	2.6461	3.2411	2.5006
CDK6	6.2933	6.4345	5.1640	4.7098	5.3604	4.7772	6.5492	5.6388	5.1648	4.4781	4.9268
CDKN2A	6.8201	6.3759	0.0393	3.8224	0.0603	5.9065	4.3914	3.9035	0.0000	5.2869	7.0785
CDKN2B	3.2566	4.5155	0.0000	2.8831	3.3877	4.5271	4.9087	3.8782	0.0070	3.2560	4.8319
TP53	5.4030	4.8597	2.1541	4.3951	5.6513	1.9003	4.9494	4.7691	4.1666	4.6973	4.9388
NF1	4.5408	4.5404	5.3128	4.9547	5.1048	3.6482	5.4243	4.9164	4.9959	5.1343	4.1364
CASP8	3.7236	2.9777	3.3700	3.9183	4.0217	3.7642	3.3313	2.6991	2.4962	2.8335	3.5611
NOTCH1	3.3731	3.6975	4.2125	5.1377	3.3959	0.9943	2.6231	3.7287	3.6116	4.1226	5.1034
MYC	4.3881	4.9783	5.4592	5.7721	6.2044	3.3831	4.1588	5.2268	4.7677	5.8586	7.1268
HRAS	4.5701	3.5060	5.0894	5.2871	4.4427	3.0434	5.3468	4.5178	3.8444	4.0430	4.6768
CCND1	7.8498	7.1665	5.0656	5.9039	7.2620	5.1855	7.3009	8.1828	6.7250	6.5615	5.6538
SRC	4.3635	4.5835	4.8736	4.6138	4.0139	4.6236	3.8402	3.1397	4.2211	4.7096	4.8396
BCL6	3.3161	4.6113	2.5132	2.9562	3.5186	3.0358	3.0722	4.0914	2.4507	4.8402	3.9008
EGFR	7.8369	7.1857	6.4553	6.9589	5.6047	5.2484	6.4214	6.2852	6.2873	6.2430	6.9608
FGFR1	1.6183	2.4480	2.3312	3.1269	0.0499	0.7250	2.1736	3.5468	3.9369	0.8622	1.7425
FGFR3	4.3248	5.6194	2.6482	2.4520	4.5837	1.3600	4.2373	4.6962	2.2620	4.4536	5.3393
IGF1R	6.3115	5.5859	4.8908	5.3333	5.1304	4.1813	5.3536	4.6125	5.0596	5.8664	5.5535

ERBB2	4.9432	4.6229	3.4282	4.7632	4.6750	4.6946	4.6523	4.4665	5.3251	4.1712	4.6199
EPHA2	6.1029	6.0810	3.9771	4.0648	5.6189	4.6384	5.3724	5.1853	4.8663	5.0718	5.4191
DDR2	0.0633	0.1773	0.1324	0.1555	2.1455	0.6135	0.3841	0.0989	3.7724	0.3785	0.4390
MET	6.7031	6.2867	4.5971	3.6581	6.2914	5.8806	6.5183	4.2425	6.0979	6.3115	5.7766
JAK2	1.2706	1.6025	1.6964	1.6806	1.0809	1.6428	1.1048	1.9090	1.3916	1.1277	2.2140
TRAF3	2.5141	2.5284	3.6473	3.4388	3.3495	3.0201	2.3404	3.1884	3.2421	4.2148	3.4136
KEAP1	3.9783	3.8006	5.7343	4.0167	4.0860	3.6292	4.1860	4.7475	4.2453	4.0303	4.4340
MYH9	7.2056	6.9068	5.8622	5.5756	8.1863	7.3177	6.8321	6.5500	8.4220	7.7824	7.1305
BIRC2	4.5467	5.2006	3.5243	4.0231	3.2013	4.1267	4.1765	3.3233	4.5288	7.4342	3.4313
YAP1	6.1855	6.0123	5.3423	6.2335	5.3618	6.2527	5.7629	4.8658	6.0854	9.1912	5.4303
SCRIB	5.2346	4.2303	3.7906	2.2627	4.3241	3.7329	5.2019	4.1153	5.0544	4.4928	5.4409
STK3	3.8531	4.7517	3.1143	3.7440	4.5267	4.9563	4.4056	3.5592	6.0992	4.1279	4.2794
WWTR1	4.0481	3.5084	5.0286	4.8644	5.9052	3.3997	2.9458	3.2259	3.5284	4.7621	2.6416
WWC1	3.7137	4.5820	3.2929	3.0437	3.4207	5.6651	4.0195	4.5026	5.7884	4.6707	4.1991
FAT4	2.3774	2.0248	1.3965	2.4367	2.1770	2.4085	0.5321	0.0548	3.2649	0.2501	1.1720
FAT3	0.2546	2.0054	0.5291	0.2707	0.0082	2.7879	0.0620	0.7411	0.4098	0.8205	0.0000
FAT2	4.9577	4.7640	5.9967	6.1288	1.1908	2.7020	6.2136	6.1634	0.6397	5.9187	5.5510
FAT1	0.2184	0.8399	5.8568	7.0253	5.8733	3.7984	6.1790	6.2621	5.9881	6.0268	7.3524
AJUBA	7.3530	7.1279	5.9213	5.8679	6.0761	6.0936	6.2687	6.2640	6.7508	6.2323	6.6578

Table 2-4. Fragments Per Kilobase of transcript per Million mapped reads (FPKM) values for selected genes in UM-SCC laryngeal cell lines.

Cell line	Age	Sex	Clinical TNM	Stage	Specimen site	Type of lesion	Previous therapy	HPV status	Smoking (pack-years)	Alcohol
UMSCC-10A	57	M	T3N0M0	III	True cord	P	None		20	Heavy
UMSCC-10B	58	M	rT3N1M0	III	Lymph node	Met	S		20	Heavy
UMSCC-11A	65	M	T2N2aM0	IV	Epiglottis	P	ICX		35	Heavy
UMSCC-12	71	M	T2N1M0	III	Larynx	R	S, RT		—	—
UMSCC-13	60	M	T3N0M0	III	Stoma	R	RT,S		90	Heavy
UMSCC-17B	47	W	T1N1M0	III	Soft tissue-neck	Met	RT		40	None
UMSCC-23	36	W	T2N0M0	II	Supraglottis	P	None		48	Heavy
UMSCC-25	50	M	rT3N2bM0	III	Lymph Node	Met	RT,S,S		Heavy	Heavy
UMSCC-28	61	W	T1N0M0	I	True cord	P	None		40	—
UMSCC-41	78	M	T2N1M0	III	Arytenoid	P	None		50	Moderate
UMSCC-46	58	W	T2N2M0	IV	Supraglottis	R	RT,S		60	Heavy
UMSCC-57	69	M	—	—	Supraglottis	—	—		—	—
UMSCC-76	66	M	T3N2cM0	IV	Lymph node	Met	ICX		40	Heavy
UMSCC-81A	53	M	T2N0M0	II	Anterior commisure	P	None		100	Heavy
UMSCC-81B	58	M	T2N0M0	II	True cord	P	None		100	Heavy
UMSCC-105	51	M	T4N0M0	IV	True cord	P	None	HPV-18	0	None

Table 2-5. Clinical characteristics of patients with LSCC from whom UM-SCC cell lines were derived.

Note: UM-SCC-10A and 10B were derived from samples taken from the same patient at different times and sites. UM-SCC-81A and 81B were derived from two vocal cord masses resected in separate procedures. HPV-18 was detected in UM-SCC-105 by HPV-PCR mass array. HPV was not detected in other cell lines. Categories for which no data were available are marked with a dash.
Abbreviations: HPV, human papillomavirus; ICX, induction chemotherapy; LSCC, laryngeal squamous cell carcinomas; M, men; Met, metastasis; P, primary; R, recurrence; RT, radiation therapy; S, surgery; UM-SCC, University of Michigan squamous cell carcinoma; W, women.

Gene	UM-SCC-													
	10A	10B	11A	12	13	17B	23	25	28	41	46	76	81B	105
TP53	17:7577548	17:7577548	17:7577556	17:7579377	17:7578442		17:7578403	*17:7578291*	17:7577046, 17:7577120		17:7574012, 17:7577106	17:7579320*	17:7578271	
FAT1			4:187518878					4:187629411*, 4:187630099	4:187541379	4:187518255		4:187630240	4:187540040	
FAT2	5:150943061	5:150943061		5:150945830							5:150942985	5:150924968		
FAT3			11:92086828			11:92533622						11:92533495		
FAT4	4:126337669					4:126369804, 4:126412106	4:126355547	4:126370896	4:126319964, 4:126372555	4:126241248				4:12641398**
RB1					13:48934219									
CDKN2A								9:21971124*			9:21971096			
PIK3CA				3:178936094		3:178938934, 3:178942545						3:178916924		
PIK3R1												5:67584513**	5:67584513**	
AJUBA													14:23450548	
NOTCH1			*9:139396366, 9:139401091, 9:139410173,* 9:139405111					9:139411814*, 9:139411816	9:139411794*			9:139409082, *9:139393448, 9:139396541, 9:139396544, 9:139396546, 9:139396548, 9:139401091, 9:139396366 9:139407991, 9:139407992, 9:139409852, 9:139417644 9:139412391, 9:139412392,*		

											9:139417398, 9:139399557^		
NOTCH2							1:120572572, 1:120491153	1:120572572		1:120572572	1:120484306, 1:120572572	1:120572572	
NOTCH3							19:15302584	*19:15295265*		19:15273335		19:15289850, 19:15299051	19:15289850
KMT2D		12:49433848, 12:49426283		12:49435240				12:49447384		12:4943187*			
NSD1		5:176722417			5:176637471, 5:176638506, 5:176710840	5:176709524							
TGFBR2										3:30691872*	3:30732942, 3:30733052		
FBXW7	*4:153268228*	4:153249384, *4:153253874, 4:153253876*									*4:153268228*		
TRAF3						14:103342015					14:103342060		
NFE2L2			2:178098810										
CUL3								2:225449767**					
BRCA1			17:41243509, *17:41256877*	17:41243509		17:41246812		17:41244429	17:41244429				
BRCA2										13:32893369		13:32954265	13:32972626

Table 2-6. Locations of all mutations identified in the indicated cell lines by capture based exome sequencing.

All mutations were missense mutations unless otherwise indicated. Those listed in italics represent splice donor or acceptor regions. Red text indicates a stop gain (nonsense) mutation; *Frameshift; **UTR variant; ^In-frame indel.

Gene	Cell Line	Locus	CHASM p value	VEST p value
BRCA1	UMSCC13	17:41243509	0.0006	0.1821
BRCA1	UMSCC28, 41	17:41244429	0	0.4463
BRCA1	UMSCC23	17:41246812	0.0006	0.2527
BRCA1	UMSCC12	17:41243509	0.0006	0.1821
BRCA2	UMSCC46	13:32893369	0.0214	0.1092
BRCA2	UMSCC81B	13:32954265	0.0206	0.1789
BRCA2	UMSCC105	13:32972626	*stopgain*	0.1821
NOTCH1	UMSCC28	9:139411794	*frameshift*	0.0217
NOTCH1	UMSCC25	9:139411814	*frameshift*	0.0127
NOTCH1	UMSCC25	9:139411816	0.1854	0.0534
NOTCH1	UMSCC11A	9:139405111	0.3448	0.2049
NOTCH1	UMSCC76	9:139417398	*stopgain*	0.1222
NOTCH1	UMSCC76	9:139409082	0.061	0.0827
NOTCH2	UMSCC76	1:120484306	0.5182	0.6263
NOTCH2	UMSCC25	1:120491153	0.2608	0.2178
NOTCH2	UMSCC25, 28,76,23,46,81B	1:120572572	0.0064	0.8694
NOTCH3	UM46	19:15273335	0.3292	0.1253
NOTCH3	UM81B		0.2398	0.4617
NOTCH3	UM11A	19:15299051	0.157	0.3026
NOTCH3	UM81B	19:15299051	0.157	0.3026
NOTCH3	UM25	19:15302584	*stopgain*	0.0245
NOTCH3	UM105	19:15289850	0.2398	0.4617
FAT4	UM10A	4:126337669	0.267	0.0908
FAT4	UM23	4:126355547	0.088	0.0054
FAT4	UM17B	4:126369804	0.1516	0.722

FAT4	UM25	4:126370896	0.094	0.0025
FAT4	UM28	4:126372555	0.2948	0.6406
FAT4	UM17B	4:126412106	0.1928	0.1877
FAT4	UM28	4:126319964	0.0152	0.0035
FAT4	UM41	4:126241248	0.2948	0.0229
FAT3	UM11A	11:92086828	0.014	0.0091
FAT3	UM17B	11:92533622	0.102	0.0136
FAT3	UM76	11:92533495	0.291	0.1849
FAT2	UM76	5:150924968	0.0884	0.0201
FAT2	UM46	5:150942985	0.6368	0.1877
FAT2	UM10A,B	5:150943061	0.1382	0.0147
FAT2	UM12	5:150945830	0.6464	0.9886
FAT1	UM25	187629411	*frameshift*	0.0954
FAT1	UM41	187518255	0.0582	0.0025
FAT1	UM28	187541379	*stopgain*	0.0225
FAT1	UM25	187630099	0.2398	0.0417
FAT1	UM76	187630240	0.1536	0.0298
FAT1	UM81B	187540040	0.8576	0.2982
FAT1	UM11A	187518878	0.0436	0.0109

Table 2-7. Supplemental Table 4. CHASM and VEST p-values for BRCA, NOTCH, and FAT family mutations.

The Cancer-Related Analysis of Variants Toolkit (CRAVAT; http://www.cravat.us) was used to predict pathogenicity via the VEST-4 and CHASM-3.1 tools. Missense mutations were scored with both VEST and CHASM; Indels were scored with VEST only. A p-value was generated for each score and a cutoff of $p<0.05$ was used to designate highly pathogenic (VEST) or probably driver (CHASM) mutations, highlighted in red.

Figures

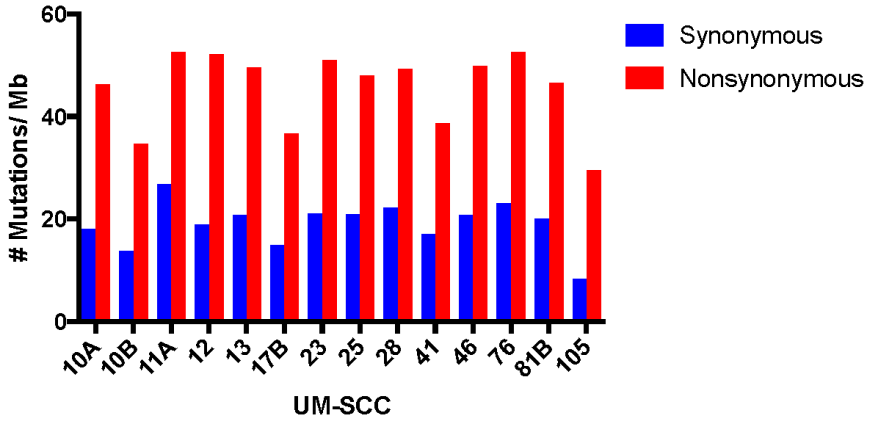

Figure 2-6. Mutation rates in laryngeal UM-SCC cell lines.

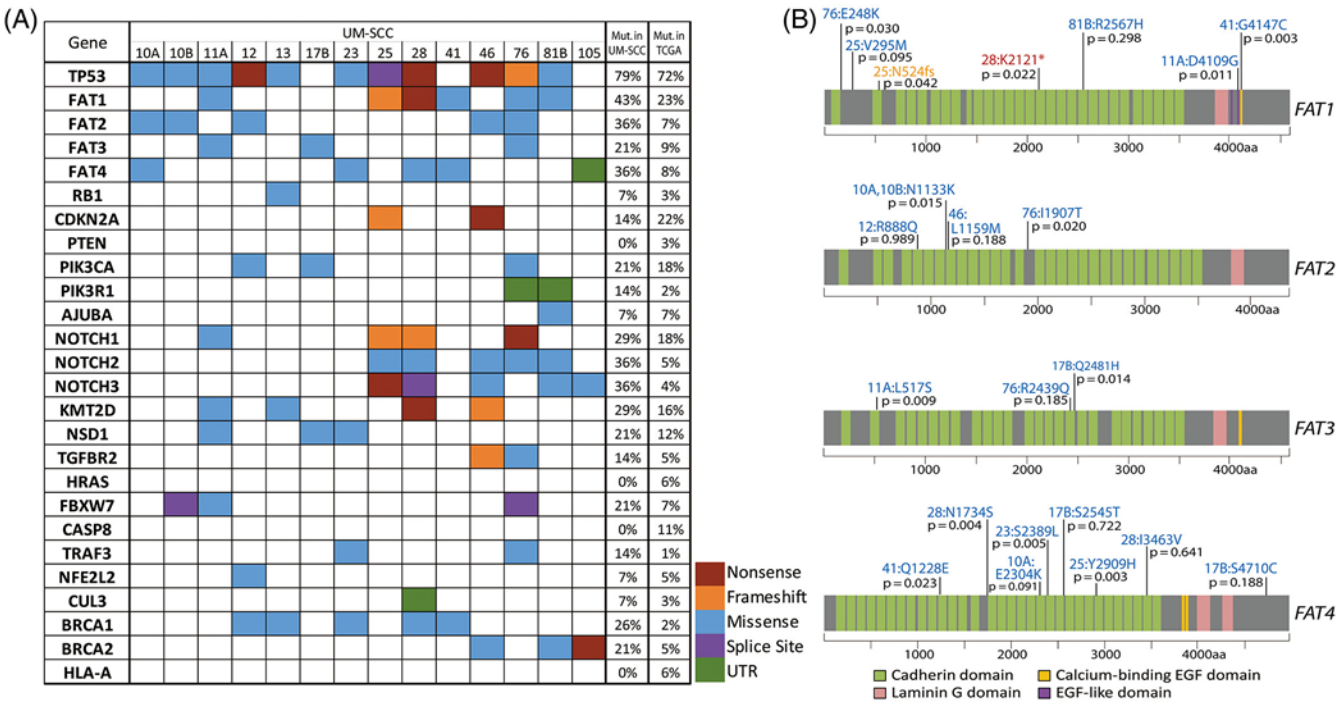

Figure 2-7Genetic characterization of laryngeal UM-SCC cell lines by copy number analysis.

Genomic DNA was harvested from low passage UM-SCC cell lines and analyzed using high-density SNP arrays (Affymetrix OncoScan Assay) and compared to a commercially available pooled control. Affymetrix software was used to call copy number alterations. A, Copy number alterations were summed across UM-SCC-10A, 10B, 12, 17B, 23, 25, 28, 46, 57, 76, 81A, 81B, and 105. Alterations for individual cell lines are shown below with gains indicated in blue and losses indicated in red. B, Heat maps displaying median copy numbers (upper panel) and RNA expression (lower panel) for selected genes. Key functions and relevant chromosomal regions are noted below each column. C, Focal deletions (arrow) at the CDKN2A-CDKN2B (9p21) locus occurring in UM-SCC 12, 23, 57, and 17B. The CDKN2A gene is indicated by a bracket in the row labeled “Genes.” *, CDKN2A;**, CDKN2B. D, Focal deletions (arrow) at the FAT1 locus (4q35) occurring in UM-SCC-10B and 12. The FAT1 locus is indicated by a bracket and an asterisk in the row labeled “Genes.” UM-SCC, University of Michigan squamous cell carcinoma.

		Primers (5'-3')	Chromatogram
UM-SCC-76 4:187630240 G>A	F	CCAAGCTCTATGAGATGGAAA	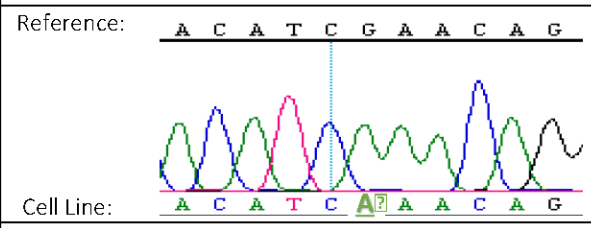
	R	CACAATTGCATATGCTGGG	
UM-SCC-25 4:187630099 G>A	F	GACATTGTCACCATCAGAAC	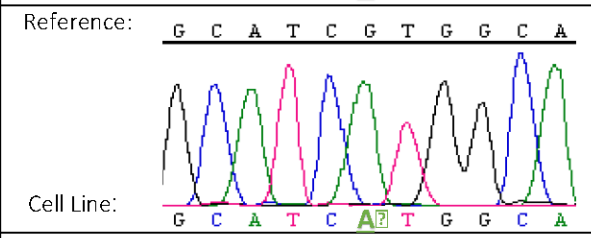
	R	TGTGAGATTGTAGCCGAAAG	
UM-SCC-25 4:187629411 A>DEL	F	CGTTTGCGATTGACCATTT	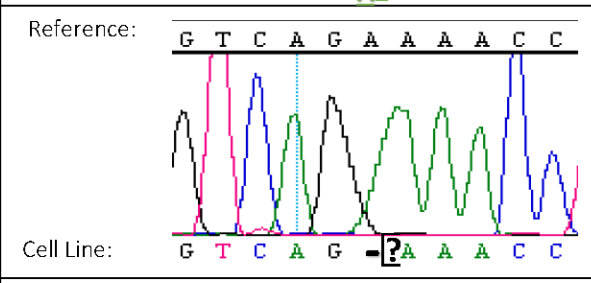
	R	GCACGAATCCTCAGAGTATAA	
UM-SCC-28 4:187541379 A>T	F	TTAAAGTGGACACTGAGGTG	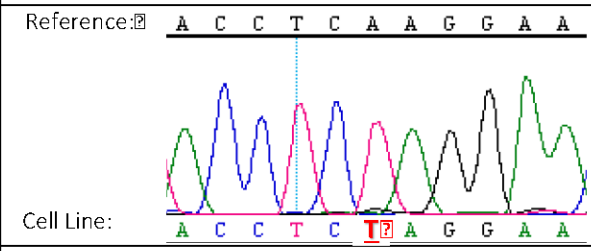
	R	GTGTCAAGCTCAAATTGCTT	
UM-SCC-81B 4:187540040 G>A	F	AAAACTTGATCGAGAAACCC	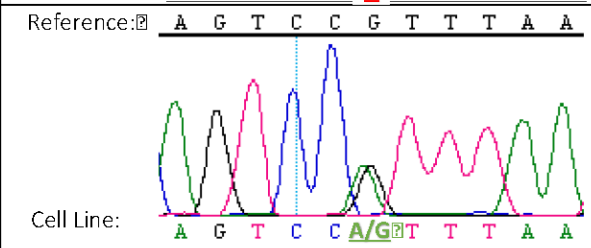
	R	GTAAGGATGACATTCACGGT	

Figure 2-8. Primer sequences and chromatograms for point mutations validated by sanger sequencing in the FAT1 gene.

Cell line and mutation (identified via exome sequencing) are shown in left column. Forward (F) and Reverse (R) sequences are shown for each product. Sections of the chromatogram are shown for each PCR product with the product sequence aligned with wild-type FAT1. Altered bases are underlined.

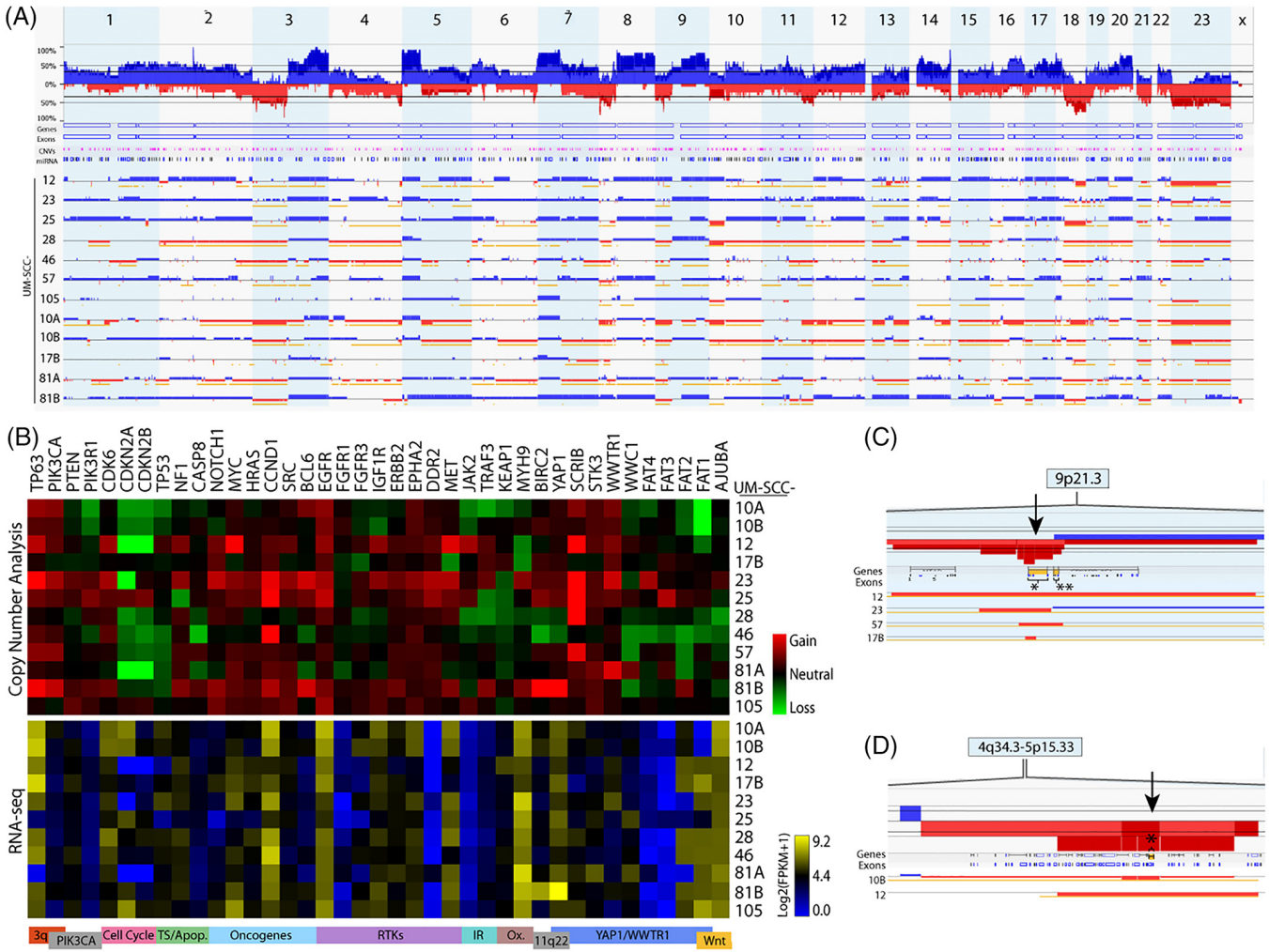

Figure 2-9. Genetic characterization of laryngeal UM-SCC cell lines by copy number analysis

Genomic DNA was harvested from low passage UM-SCC cell lines and analyzed using high-density SNP arrays (Affymetrix OncoScan Assay) and compared to a commercially available pooled control. Affymetrix software was used to call copy number

alterations. A, Copy number alterations were summed across UM-SCC-10A, 10B, 12, 17B, 23, 25, 28, 46, 57, 76, 81A, 81B, and 105. Alterations for individual cell lines are shown below with gains indicated in blue and losses indicated in red. B, Heat maps displaying median copy numbers (upper panel) and RNA expression (lower panel) for selected genes. Key functions and relevant chromosomal regions are noted below each column. C, Focal deletions (arrow) at the *CDKN2A-CDKN2B* (9p21) locus occurring in UM-SCC 12, 23, 57, and 17B. The *CDKN2A* gene is indicated by a bracket in the row labeled "Genes." *, *CDKN2A*;**, *CDKN2B*. D, Focal deletions (arrow) at the *FAT1* locus (4q35) occurring in UM-SCC-10B and 12. The *FAT1* locus is indicated by a bracket and an asterisk in the row labeled "Genes." UM-SCC, University of Michigan squamous cell carcinoma.

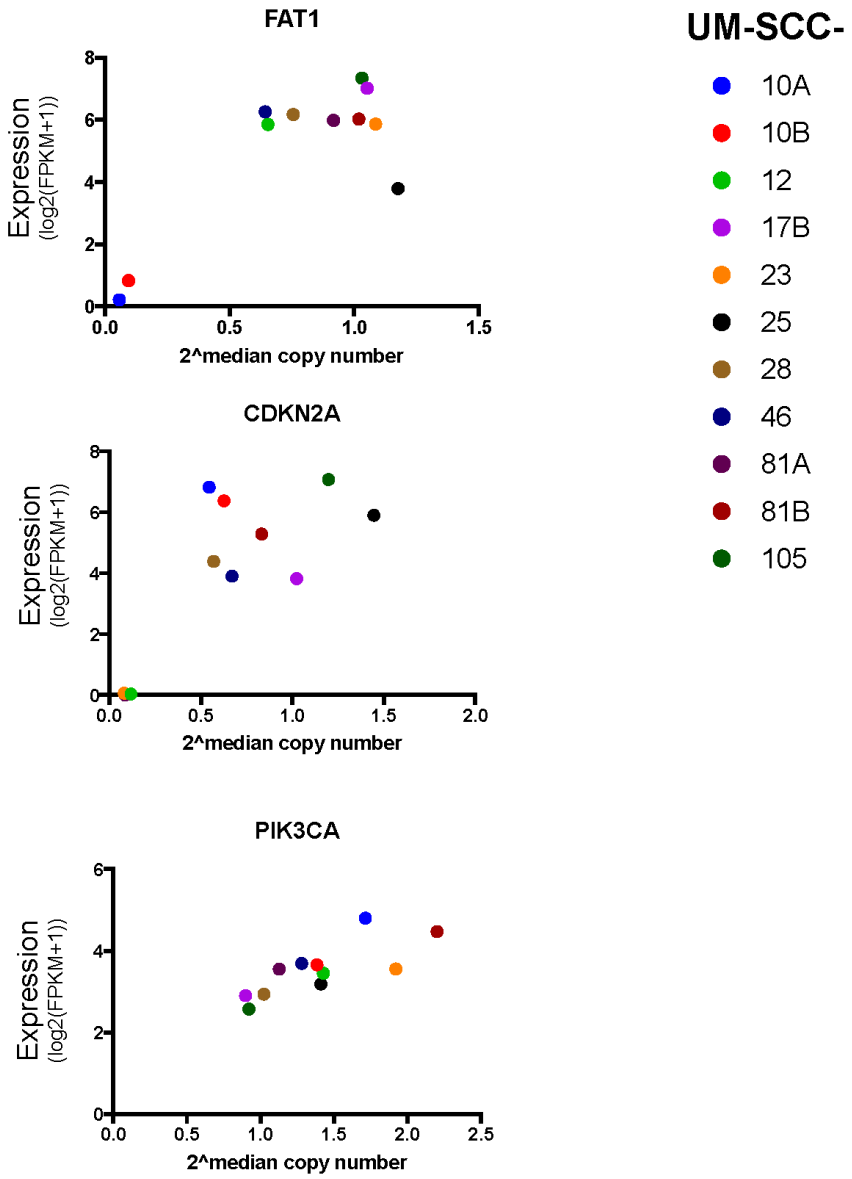

Figure 2-10. Relationship between median copy number (x-axis) and RNA expression (y-axis) of indicated genes in 11 UM-SCC laryngeal cell lines.

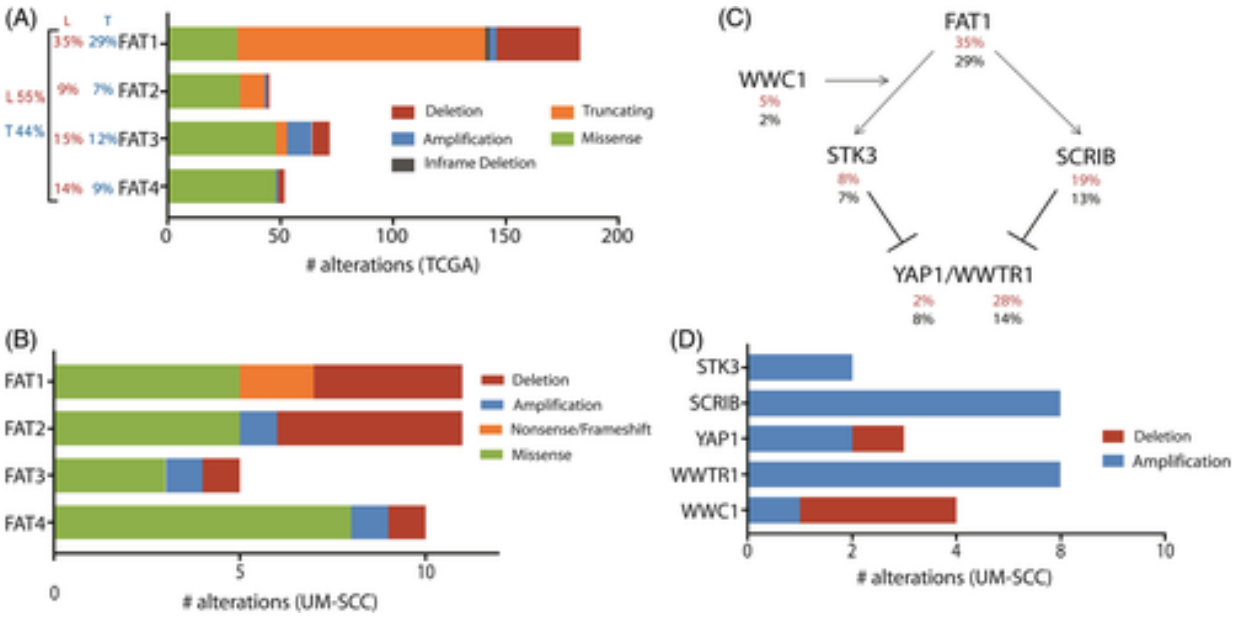

Figure 2-11 Summary of aberrations in FAT-related genes in TCGA tumors and laryngeal UM-SCC cell lines.

Summary of aberrations in *FAT*-related genes in TCGA tumors and laryngeal UM-SCC cell lines. A, Alterations reported in TCGA provisional dataset (cbioportal.org; http://cancergenome.nih.gov) for FAT1-4. Total numbers observed for each category of mutation or copy number variation are displayed. For each gene, the percentage of 510 tumors in the total HNSCC dataset with an alteration is reported to the left in blue (T). The percentage of the 110 laryngeal primary tumors in this dataset harboring an alteration in each gene is reported in red (L). The percentage of all HNSCC (blue) and LSCC (red) tumors harboring one or more mutations in any FAT gene are reported to the far left.27 B, Alterations identified in the laryngeal UM-SCC cell line panel for FAT1-4. This analysis considers available data for all 16 cell lines in this study, although exome sequencing was not performed for UM-SCC-57 or 81A, and copy number data are not available for UM-SCC-11A, 13, 41, or 76. C, Schematic diagram describing proposed signaling interactions involving the FAT1 protein. Percentages of HNSCC tumors bearing alterations (amplifications, deletions, and mutations) in each gene are displayed below the gene name for LSCC only27 and the overall cohort (black). D, Alterations identified in the laryngeal UM-SCC cell line panel for Hippo/YAP1 pathway genes.

Bibliography

1. Jemal A, Bray F, Center MM, Ferlay J, Ward E, Forman D. Global cancer statistics. *CA Cancer J Clin*. 2011; **61**: 69- 90.
2. Gillison ML, D'Souza G, Westra W, et al. Distinct risk factor profiles for human papillomavirus type 16-positive and human papillomavirus type 16-negative head and neck cancers. *J Natl Cancer Inst*. 2008; **100**: 407- 420.
3. Mendenhall WM, Werning JW, Hinerman RW, Amdur RJ, Villaret DB. Management of T1-T2 glottic carcinomas. *Cancer*. 2004; **100**: 1786- 1792.
4. Forastiere AA, Weber RS, Trotti A. Organ preservation for advanced larynx cancer: issues and outcomes. *J Clin Oncol Off J Am Soc Clin Oncol*. 2015; **33**: 3262- 3268
5. The Cancer Genome Atlas N. Comprehensive genomic characterization of head and neck squamous cell carcinomas. *Nature*. 2015; **517**: 576- 582.
6. Morris LG, Chandramohan R, West L, Zehir A, Chakravarty D, et al. The molecular landscape of recurrent and metastatic head and neck cancers: insights from a precision oncology sequencing platform. *JAMA Oncol*. 2016; **3**: 244- 255.
7. Birkeland AC, Ludwig ML, Meraj TS, Brenner JC, Prince ME. The tip of the iceberg: clinical implications of genomic sequencing projects in head and neck cancer. *Cancer*. 2015; **7**: 2094- 2109.
8. Ludwig ML, Birkeland AC, Hoesli R, Swiecicki P, Spector ME, Brenner JC. Changing the paradigm: the potential for targeted therapy in laryngeal squamous cell carcinoma. *Cancer Biol Med*. 2016; **13**: 87- 100.
9. Grenman R, Carey TE, McClatchey KD, Wagner JG, Pekkola-Heino K, et al. In vitro radiation resistance among cell lines established from patients with squamous cell carcinoma of the head and neck. *Cancer*. 1991; **67**: 2741- 2747.
10. Bradford CR, Zhu S, Ogawa H, et al. P53 mutation correlates with cisplatin sensitivity in head and neck squamous cell carcinoma lines. *Head Neck*. 2003; **25**: 654- 661.
11. Liu J, Pan S, Hsieh MH, et al. Targeting Wnt-driven cancer through the inhibition of porcupine by LGK974. *Proc Natl Acad Sci U S A*. 2013; **110**: 20224- 20229.
12. Akervall J, Guo X, Qian CN, et al. Genetic and expression profiles of squamous cell carcinoma of the head and neck correlate with cisplatin sensitivity and resistance in cell lines and patients. *Clin Cancer Res*. 2004; **10**: 8204- 8213.
13. Brenner JC, Graham MP, Kumar B, et al. Genotyping of 73 UM-SCC head and neck squamous cell carcinoma cell lines. *Head Neck*. 2010; **32**: 417- 426.
14. Andrews S. FastQC A Quality Control tool for High Throughput Sequence Data. http://www.bioinformatics.babraham.ac.uk/projects/fastqc/. Published 2014; Last accessed November 1, 2017.
15. Li H, Durbin R. Fast and accurate short read alignment with burrows-wheeler transform. *Bioinformatics (Oxford, England)*. 2009; **25**: 1754- 1760.
16. DePristo MA, Banks E, Poplin R, Garimella KV, Maguire JR, et al. A framework for variation discovery and genotyping using next-generation DNA sequencing data. *Nat Genet*. 2011; **43**: 491- 498.
17. Ludwig ML, Kulkarni A, Birkeland AC, et al. The genomic landscape of UM-SCC oral cavity squamous cell carcinoma cell lines. *Oral Oncol*. 2018; **87**: 144- 151.
18. Walline HM, Goudsmit CM, McHugh JB, Tang AL, Owen JH, et al. Integration of high-risk human papillomavirus into cellular cancer-related genes in head and neck cancer cell lines. *Head Neck*. 2017; **39**: 840- 852.

19. Cerami E, Gao J, Dogrusoz U, et al. The cBio cancer genomics portal: an open platform for exploring multidimensional cancer genomics data. *Cancer Discov*. 2012; **2**: 401- 404.
20. Carter H, Douville C, Stenson PD, Cooper DN, Karchin R. Identifying Mendelian disease genes with the variant effect scoring tool. *BMC Genomics*. 2013; **14**(Suppl 3): S3.
21. Douville C, Carter H, Kim R, et al. CRAVAT: cancer-related analysis of variants toolkit. *Bioinformatics (Oxford, England)*. 2013; **29**: 647- 648.
22. Douville C, Masica DL, Stenson PD, et al. Assessing the pathogenicity of insertion and deletion variants with the variant effect scoring tool (VEST-Indel). *Hum Mutat*. 2016; **37**: 28- 35.
23. Liehr T, Ries J, Wolff E, et al. Gain of DNA copy number on chromosomes 3q26-qter and 5p14-pter is a frequent finding in head and neck squamous cell carcinomas. *Int J Mol Med*. 1998; **2**: 173- 179.
24. Carey TE, Frank CJ, Raval JR, et al. Identifying genetic changes associated with tumor progression in squamous cell carcinoma. *Acta Otolaryngol Suppl*. 1997; **529**: 229- 232.
25. Campbell JD, Yau C, Bowlby R, et al. Genomic, pathway network, and immunologic features distinguishing squamous carcinomas. *Cell Rep*. 2018; **23**: 194- 212.e6.
26. Cai Y, Dodhia S, Su GH. Dysregulations in the PI3K pathway and targeted therapies for head and neck squamous cell carcinoma. *Oncotarget*. 2017; **8**: 22203- 22217.
27. Martin D, Degese MS, Vitale-Cross L, et al. Assembly and activation of the Hippo signalome by FAT1 tumor suppressor. *Nat Commun*. 2018; **9**: 2372.
28. Ahmed AF, de Bock CE, Lincz LF, et al. FAT1 cadherin acts upstream of Hippo signalling through TAZ to regulate neuronal differentiation. *Cell Mol Life Sci*. 2015; **72**: 4653- 4669.
29. Zhao B, Li L, Lei Q, Guan KL. The Hippo-YAP pathway in organ size control and tumorigenesis: an updated version. *Genes Dev*. 2010; **24**: 862- 874.
30. Katoh M. Function and cancer genomics of FAT family genes. *Int J Oncol*. 2012; **41**: 1913- 1918.
31. Hill VK, Dunwell T, Catchpoole D, Krex D, Brini AT, et al. Frequent epigenetic inactivation of KIBRA, an upstream member of the Salvador/Warts/Hippo (SWH) tumor suppressor network, is associated with specific genetic event in B-cell acute lymphocytic leukemia. *Epigenetics*. 2011; **6**: 326- 332.
32. Zhang X, Liu X, Luo J, et al. Notch3 inhibits epithelial-mesenchymal transition by activating Kibra-mediated Hippo/YAP signaling in breast cancer epithelial cells. *Oncogene*. 2016; **5**:e269.
33. Giefing M, Wierzbicka M, Szyfter K, et al. Moving towards personalised therapy in head and neck squamous cell carcinoma through analysis of next generation sequencing data. *Eur J Cancer*. 2016; **55**: 147- 157.
34. Birkeland AC, Beesley L, Bellile E, et al. Predictors of survival after total laryngectomy for recurrent/persistent laryngeal squamous cell carcinoma. *Head Neck*. 2017; **39**: 2512- 2518.
35. Chang MT, Asthana S, Gao SP, et al. Identifying recurrent mutations in cancer reveals widespread lineage diversity and mutational specificity. *Nat Biotechnol*. 2016; **34**: 155- 163.
36. Vaira V, Faversani A, Dohi T, et al. Aberrant overexpression of the cell polarity module scribble in human cancer. *Am J Pathol*. 2011; **178**: 2478- 2483.
37. Hu X, Zhai Y, Kong P, et al. FAT1 prevents epithelial mesenchymal transition (EMT) via MAPK/ERK signaling pathway in esophageal squamous cell cancer. *Cancer Lett*. 2017; **397**: 83- 93.
38. Morris LG, Kaufman AM, Gong Y, Ramaswami D, Walsh LA, et al. Recurrent somatic mutation of FAT1 in multiple human cancers leads to aberrant Wnt activation. *Nat Genet*. 2013; **45**: 253- 261.
39. Valletta D, Czech B, Spruss T, et al. Regulation and function of the atypical cadherin FAT1 in hepatocellular carcinoma. *Carcinogenesis*. 2014; **35**: 1407- 1415.

40. Kim KT, Kim BS, Kim JH. Association between FAT1 mutation and overall survival in patients with human papillomavirus-negative head and neck squamous cell carcinoma. *Head Neck*. 2016; **38**(Suppl 1): E2021- E2029.
41. Pan C, Du Z, Cai Z, Liu Y, Sun Y, et al. Elevated expression of yesassociated protein is associated with the malignant status and prognosis of laryngeal squamous cell carcinoma. *Mol Med Rep*. 2017; **16**: 4934- 4940.
42. Hayes TF, Benaich N, Goldie SJ, Sipila K, Ames-Draycott A, et al. Integrative genomic and functional analysis of human oral squamous cell carcinoma cell lines reveals synergistic effects of FAT1 and CASP8 inactivation. *Cancer Lett*. 2016; **383**: 106- 114.
43. Carey TE, Van Dyke DL, Worsham MJ, Bradford CR, Babu VR, et al. Characterization of human laryngeal primary and metastatic squamous cell carcinoma cell lines UM-SCC-17A and UM-SCC-17B. *Cancer Res*. 1989; **49**: 6098.
44. Ben-David U, Siranosian B, Ha G, et al. Genetic and transcriptional evolution alters cancer cell line drug response. *Nature*. 2018; **560**: 325- 330.
45. Cheng H, Yang X, Si H, et al. Genomic and transcriptomic characterization links cell lines with aggressive head and neck cancers. *Cell Rep*. 2018; **25**: 1332- 1345. e5.
46. Nisa L, Barras D, Medová M, et al. Comprehensive genomic profiling of patient-matched head and neck cancer cells: a preclinical pipeline for metastatic and recurrent disease. *Mol Cancer Res*. 2018; **16**: 1912- 1926.

Chapter 3 Functional Profiling of 17,000 Open Reading Frames for Identification of Drivers of PDL1

Abstract

Head and Neck Squamous Cell Carcinoma (HNSCC) is the sixth most common cancer globally and is often rapidly lethal, especially in the recurrent and metastatic setting. Recently, inhibition of the PD1:PDL1 immune checkpoint has been modestly successful in advanced disease, but the proportion of patients that benefit from these strategies remains limited. We therefore sought a more comprehensive understanding of the signals modulating the PD1: PDL1 checkpoint in HNSCC in order to gain insight into factors that may impact response to therapy. Here, we used a genome-wide open reading frame (ORF) library of 17,000 transcript constructs corresponding to 14,000 unique genes, to screen for ORFs capable of driving high cell surface PDL1 expression. We identify 335 ORFs that were enriched following sorting for PDL1-high expressing cells and validated five of these ORFs, including *FGF6*, *IL17A*, *CD300C*, *KLR1C* and *NFKBIA*. Further, we show that FGF ligand is sufficient to induce PDL1 expression as well as glycosylation, even in the absence of induction by interferon gamma. Small molecule inhibition of FGFR signaling also blocked interferon-regulated PDL1 expression through a STAT1 independent pathway.

Introduction

HNSCC is an extremely aggressive disease with poor overall survival that has remained unchanged for several decades [1-4]. The disease is molecularly characterized by overexpression of several receptor tyrosine kinases, human papilloma virus (HPV) status, and a complex array of genomic alterations that comprise a high mutational burden relative to many other cancers [5, 6]. Importantly, in the recurrent and metastatic (R/M) setting, HNSCC patients have exceptionally poor quality of life and extremely short survival outcomes, and novel treatment strategies that improve outcomes are desperately needed. Recently, the PD1:PDL1 immune checkpoint inhibitors pembrolizumab and nivolumab have gained FDA approval for use in the R/M HNSCC setting with response rates of 13-18% [7-10].

Despite this advance, and the broad popularity of PD1 blockade across many cancer types, the complex molecular mechanisms that regulate PDL1 expression on tumor cells are only beginning to be understood. While interferon gamma (IFNγ), which may be released by T-lymphocytes, has long been known to induce cell surface expression of PDL1, other often cell-intrinsic signals have more recently been shown to induce PDL1 expression independently of IFNγ. For example, treatment of HNSCC cell lines with EGF induced PDL1 expression in a JAK2/STAT1 dependent manner, indicating that activation of EGFR, often overexpressed in HNSCC, may serve as an IFNγ- independent mechanism for PDL1 upregulation[11]. Furthermore, the EGFR effector STAT3 has been shown to be a potent driver of PDL1 expression in genetically engineered HNSCC mouse models [12]. However, the relationship between EGFR expression and PDL1 expression is unclear, as various reports have produced conflicting results with regard to this question [13]. Thus, it is likely that multiple different mechanisms drive PDL1 expression in different settings.

Recently, whole-genome screening techniques, such as pooled CRISPR-Cas9 screens, have been adapted for a variety of applications to identify mediators of particular phenotypes [14]. These strategies often entail lentiviral delivery of pooled shRNA or RNA guided Cas9 libraries to induce genome-wide disruption of gene expression. The cell population is then monitored for dropout of particular constructs, indicating the essentiality of their targets for cell viability. Here, we have modified this scheme to utilize a genome-scale open reading frame (ORF) library for overexpression of 17,000 genes in a pooled format, from which we can select individual cells in which PDL1 expression has been induced. Through this novel high throughput profiling approach, we sought to identify novel regulators of PDL1 expression such that we may begin to understand heretofore undiscovered mechanisms that regulate cell surface expression of PDL1 in HNSCC. We hypothesize that inhibition of PDL1 drivers may serve as an effective strategy to enhance the effects of immune checkpoint therapy for a subset of HNSCC patients.

Materials and Methods

Cell Lines and Reagents. All UM-SCC cell lines were derived and characterized in the Head and Neck Oncology laboratory at the University of Michigan after consent of the patient donors [15]. The oral cavity and larynx cell lines studied in this report were selected from models with comprehensive integrated SNP array, exome sequencing, and transcriptome sequencing data recently completed by our team [16]. All cell lines were grown in exponential growth g in DMEM containing 10% FBS, 7μg/mL penicillin/streptomycin and 1% Non-essential amino acids in a 5% CO_2 incubator. All cell lines were genotyped throughout the study to ensure identity as previously described [15].

Small molecule inhibitors were purchased from Selleck Chemicals and maintained in DMSO at -80C for a period of no more than 1 year. Interferon gamma (IFN-γ) was purchased from R&D and stored in PBS at -20C for no more than 2 months. FGF ligands were purchased from Thermo Fisher Scientific and stored in PBS containing 0.5% bovine serum albumin and stored at -20C for no more than 2 months.

ORF Library transduction. The genome-wide ORF library was purchased from Sigma Aldrich as transduction-ready pool. We first determined the appropriate multiplicity-of-infection [17] by transduction of UM-SCC-49 cells, puromycin selection and cell count assays. Using an MOI of 0.3-0.5, we then transduced the cell line, selected puromycin resistant clones and expanded the population. UM-SCC-49-ORF library cells were maintained and treated in groups of no less than 6 million. After selection, small subsets were cloned out from control and treated populations to ensure enrichment of PDL1 expression in individual clones

Flow Cytometry. Cells were stained for analysis by flow cytometry using the anti-PDL1 antibody #14-5983-82 against PDL1 or isotype control #14-4714-82 purchased from Thermo Fisher Scientific. Antibodies were diluted to 0.5ug/mL in PBS containing 1% FBS with 1 million cells per mL. Analysis and sorting were performed at the University of Michigan Flow Cytometry Core. For UM-SCC-49 ORF library selection, cells were sorted on a Moflo Astrios cell sorter to select the top 2.0% of *PDL1* expressing cells, expanded in culture, and sorted again to collect the top 11%.

Library preparation. Genomic DNA was harvested from control and sorted populations using the Gentra Puregene kit according to manufacturer's instructions. PCR amplification was performed for each of four primer sets in each sample. These were pooled and a second round of PCR amplification was performed. Primer sequences are listed in Table 3-1.

ORF Barcode Quantification. Adapter contamination in the samples was removed using Trim_galore (v 0.4.4). For mapping the reads to the ORF reference library, seqmap(v 1.0.13) was used. Since seqmap requires FASTA files as input, all the read FASTQ files were converted to FASTA by extracting only the sequence information from the FASTQ files. All the FASTA files were also mapped to the reverse complements of the barcodes in the ORF library. The barcode counts obtained by mapping the reads to the ORF library were normalized based on the total read counts for a sample and the log2 fold change was calculated between the conditions to be compared. Using the log-rank list of genes, we then uploaded the gene set into GSEA (MIT, Broad) to identify significant overlap with Hallmark, KEGG and GO biological process pathways with false discovery rate (FDR) q-value < 0.05 considered significant.

Expression of ORF constructs. We purchased cDNA clones for *CD300C*, *KLRC1, FGF6, IL17A,* and *NFKBIA* from Geneocopeia, which did not produce usable lentivirus. Therefore, we cloned the genes into the PCR8 vector, confirmed the correct orientation and sequence by Sanger sequencing, and transferred the expression cassettes to pLenti6.0 using Clonase according to manufacturer protocol. Sanger sequencing was again used to confirm the orientation and sequence of the inserts, all of which were cloned without a stop codon such that the ORF of each construct would contain a c-terminal V5 epitope tag. Lentivirus made from each of these constructs was then used to transduce UM-SCC-49 cells and blasticidin selection was used to create stable populations.

Western Blots. Western blot analysis was performed as described [18]. Briefly, UM-SCC cell lines in log-phase growth were treated as indicated, rinsed twice with PBS, and then lysed in mild detergent buffer containing protease and phosphatase inhibitors (150 mM NaCl, 10%

Glycerol, 1% NP40, 0.1% Triton X-100, 1 mM PIPES, 1 mM MgCl, 50 mM Tris; inhibitors: Thermo 186129, 1861277) as previously described [19].

TCGA transcriptome analysis. Log_2(RSEM+1) values from TCGA Head and Neck Cancer cohort (n=566) were retrieved from the UCSC cancer genomics browser (xenabrowser.net). Correlations were calculated using Pearson r test, and linear regressions and box and whisker plots were generated using GraphPad Prism 8 software.

HNSCC cell line transcriptome analysis. RNA sequencing was performed for 43 HNSCC cell lines using Illumina stranded transcriptome library kits as described in (Mann et al.) Heatmaps were generated using MeV software version 4.9 based on log_2(FPKM+1) values.

Quantitative PCR. For qPCR analysis, cells were lysed in QIAzol and RNA was isolated using the QIAgen RNeasy Mini Kit (Qiagen, Hilden, Germany) according to manufacturer's protocol. cDNA synthesis was performend using the Superscript™ VILO kit (Thermo Fisher Scientific, Waltham, MA, USA). RT-qPCR was then performed using the Quantitect SYBR Green RT-qPCR kit (QIAgen) and run using a QuantStudio™ 5 System (Applied Biosystems, Foster, CA, US). Primer sequences are listed in Table 3-2.

Results.

To begin our study, we first analyzed a panel of 6 UM-SCC cell lines to determine the relative level of total PDL1 induction driven by interferon gamma (IFNγ) by western blot analysis (**Figure 3-1A**). ImageJ intensity analysis of the bands demonstrated an average PDL1 induction of 6-fold across the 6 cell lines, with UM-92 exhibiting the smallest induction of PDL1 expression (2-fold) and UM-SCC-49 and 59 exhibiting the greatest (approximately 14-fold). For our screen, we chose to use the UM-SCC-49 cell line due to its ability to upregulate PDL1. Previously, several groups have characterized a JAK2- and STAT1-dependent mechanism by

which IFNγ drives increased *PDL1* transcription and expression [11]. Thus, we confirmed that IFNγ induces STAT1 phosphorylation on tyrosine 701, indicative of activation (**Figure 3-1B**). Similarly, inhibition of JAK2 activity with TG101348 blocked both IFNγ-mediated STAT1 phosphorylation and PDL1 expression in the UM-SCC-49, 92, and 14a models, supporting that the canonical IFNγ-regulated pathway is active in these models.

We next confirmed IFNγ-inducible cell surface expression of PDL1 in UM-SCC-49 cells by flow cytometry (**Figure 3-2A**). As depicted in **Figure 3-2B**, we then created stable pools of UM-SCC-49 cells transduced with the 17,000 different open reading frame (ORF) constructs, in which each ORF contained an in-frame C-terminal V5 epitope tag, by lentiviral transduction and puromycin selection. Sorting of the population for the 2% of cells with highest PDL1 expression by flow cytometry was followed by expansion in culture. A subsequent sort for the highest 11% was used to further enrich the population for ORFs that drove increased cell surface expression of PDL1 ($PDL1^{high}$) (**Figure 3-2C**). To confirm that the approach was successful, we expanded 2 clones from the unsorted population and 7 clones from the serially sorted population. Comparison of total and cell surface PDL1 expression between the clones and unsorted pooled ORF cells demonstrated a substantial increase in total PDL1 expression in all serially sorted clones relative to unsorted pools and clones, confirming that the overall strategy of enriching for this phenotype was successful (**Figure 3-2D,E**). Sanger sequencing of these clones revealed the ORF constructs listed in **Table 3-**3. We then isolated DNA and created Illumina MiSEQ compatible libraries from the unsorted ORF pool and $PDL1^{high}$ population and sequenced libraries to a depth of >1.5 million reads per library. Mapping barcodes to the reference identified a ≥2-fold enrichment in 335 genes (**Table 3-4**) including *IL17A*, which has previously

been shown to regulate PDL1 expression in a murine model of breast cancer [20], supporting that our overall strategy was successful.

Detailed analysis of the results using gene family annotation of the overrepresented genes demonstrated a large increase in cytokines, transcription factors, and kinases in the gene set (**Table 3-5**), suggesting that the enrichment process may have identified ORFs that regulate PDL1 expression on multiple levels from transcription to autocrine stimulation. We next performed gene set enrichment analysis on the rank list to identify potential over-represented pathways. This demonstrated a strongly significant 34 gene overlap with genes in the GO pathway: regulation of immune response (FDR q = 1.55 x 10^-7) demonstrating that the ORFs driving increased PDL1 expression in our model were also strongly associated with immune response in previously defined gene sets. Similarly, we observed enrichments within gene sets associated with "response to external stimulus," "regulation of response to stress," and "TNF alpha signaling driven by NFκB" (**Table 3-6**). Collectively, the gene set enrichment analysis supported the role of ORFs identified in our screen in the regulation of immune response pathways and also suggested that the ORFs drive PDL1 expression through mechanistically diverse pathways, some of which may be NFκB-dependent.

Validation of candidate PDL1 drivers. From the top overall hits, we selected a diverse set of ORFs for subsequent validation experiments. We opted to validate *IL17A* because it had recently been shown to modulate PDL1 expression in murine breast and lung tumors, but has not been studied in the context of HNSCC [20, 21]. We also interrogated TCGA HNSCC RNAseq data to examine expression of genes of interest nominated by the screen in relation to PDL1 (**Figure 3-3A**). We discovered a number of genes nominated by our screen for which expression

positively correlated with PDL1, including *CD300C* (Pearson r =0.41, p<0.0001) and *KLRC1* (Pearson r=0.44, p<0.0001). *CD300LB,* an uncharacterized gene related to *CD300C*, also weakly correlated with PDL1 expression in TCGA (Pearson r = 0.22, p<0.0001), and was enriched in the PDL1-sorted pool to a similar degree to *CD300C*, but we chose to first focus our analysis on *CD300C* due to its stronger correlation in TCGA. We also proceeded with validation of two additional genes of interest that did not correlate with PDL1 RNA expression in the TCGA dataset: *NFKBIA* and *FGF6*, although, notably, FGF6 was undetected in the majority of the TCGA specimens. We were intrigued by the finding of *FGF6* in our dataset due to the known tumorigenic role for FGFR signaling in HNSCC and other cancers [22], and because EGFR, which acts through similar downstream mechanisms to FGFRs, was previously shown to regulate PDL1 in HNSCC [11]. We were surprised that our screen identified *NFKBIA* as a potential driver of PDL1 expression, as this gene is known to inhibit NFκB activity by blocking translocation of p65 to the nucleus, and NFκB is a known transcriptional driver of PDL1. Thus, we hypothesized that this gene might represent a false positive result of our screen.

The ORFs of interest were each cloned into a lentiviral vector with a c-terminal V5 epitope tag and expressed in wild type UM-SCC-49 cells following lentiviral transduction. Western blot confirmed overexpression of the V5-tagged construct in each case (**Figure 3-3B**) and flow cytometry confirmed that each gene drove an increase in median fluorescence intensity of PDL1 cell surface expression in each case, which validated these genes as PDL1 drivers (**Figure 3-3C**). To then determine the effect of these constructs on total PDL1 expression, we cultured cells with or without IFNγ and characterized the changes to total PDL1 expression by Western blot (**Figure 3-3D**). All ORF constructs led to increases in IFNγ-regulated total PDL1 expression while only some increased baseline PDL1, suggesting that differences exist in the

mechanisms through which each gene regulates PDL1 expression. For example, some of these genes may modulate cell surface presentation of PDL1, while others modulate total PDL1 protein expression.

Given that JAK2/STAT1 signaling is implicated in mediating PDL1 induction in similar HNSCC models [11], we then assessed the expression and phosphorylation status of STAT1 in each of the UM-SCC-49-ORF-V5 cell lines. As shown in **Figure 3-3E**, STAT1 phosphorylation on Y701 in UM-SCC-49-FGF6-V5 is comparable to that in UM-SCC-49-LacZ-V5 in both untreated and IFNγ treated conditions. Further, JAK2 inhibition using TG101348, a selective ATP-competitive inhibitor [23], blocked IFNγ-induced PDL1 expression in both cell lines, and reduced baseline PDL1 levels of UM-SCC-49-FGF6-V5, indicating that the JAK2/STAT1 pathway may modulate FGF6-V5-induced PDL1 expression as well.

Analysis of FGF/FGFR signaling in UM-SCC cell lines. Given the immediate potential to advance FGFR inhibitors clinically, especially with genetic role of *FGFR1* and *FGFR3* in HNSCC pathogenesis [24], we next focused our study on the relationship of FGF/FGFR activity with PDL1 expression in HNSCC models. RNAseq analysis of 40 HNSCC cell lines revealed high expression of *FGFR2*, *FGFR3*, and *FGF11* across nearly all cell lines, with many also exhibiting high levels of *FGF2*, *FGFR1*, and *FGFR4* (**Figure 3-4A**). UM-SCC-17B showed remarkably high expression of nearly all FGF ligands and receptors, with two interesting exceptions: UM-SCC17B had the lowest *FGF11* expression of all cell lines assessed, and also did not have detectable *FGFR1* reads. Notably, *FGF6* was not highly expressed in any of the 40 cell lines; and, to ensure that we studied clinically relevant secreted ligands of the FGF/FGFR pathway, we next characterized publicly available HNSCC tissue expression data. Importantly,

the expression of FGF ligands and receptors in the RNAseq HNSCC cell line data set was similar to the expression pattern observed in the TCGA HNSCC RNAseq data (**Figure 3-4B**). This analysis demonstrated that FGF receptors *FGFR1*, *FGFR2*, and *FGFR3* were highly expressed in HNSCC tumors, which is consistent with previous data [25], and that the FGF ligands *FGF2* and *FGF11* were the most highly expressed FGF family genes in both the HNSCC cell lines and the TCGA cohort. However, while *FGF11* is not known to be secreted or interact with any FGFRs [26], FGF2 has been reported to promote growth, angiogenesis, survival, motility, and cell proliferation in numerous *in vitro* and *in vivo* models of HNSCC and other cancers [27, 28]. We next asked whether expression of any FGF ligands or receptors correlated with PDL1 expression, but found no positive correlations and surprisingly, weak negative correlations for FGFR1 and 2 (**Figure 3-4C**). Thus, it was important to understand the role of activated FGF receptors in our models. Due to its stability in cell culture media and frequent expression in HNSCC tumors and cell lines, we focused our subsequent analysis on FGF2. We treated UM-SCC cells with recombinant FGF2 (rFGF2) to assess its effect on PDL1 expression, and to understand whether a role for FGFRs in regulating PDL1 could be recapitulated across multiple models. In UM-SCC-92 and UM-SCC-14A, rFGF2 induces total PDL1 expression, even in the absence of IFNγ stimulation, further supporting the ability of FGF/FGFR signaling to promote PDL1 expression in HNSCC (**Figure 3-4D**).

Modulation of FGFR alters PDL1 expression. To assess the role of FGFR signaling in UM-SCC-49-FGF6-V5 cells, we pretreated UM-SCC-49-FGF6-V5 or UM-SCC-49-LacZ-V5 with either BGJ398, an inhibitor of FGFR1, 2, and 3 [29], or PD173074, a specific inhibitor of FGFR1 [30], then added IFNγ to the cell culture media as indicated and incubated for 72 hours

(**Figure 3-5A**). BGJ398 reduced both baseline and IFNγ-induced expression in both UM-SCC-49-FGF6-V5 or UM-SCC-49-LacZ-V5. Likewise, PD173074, also reduced PDL1 expression, but had a greater impact on IFNγ-induced total PDL1 protein expression in UM-SCC-49-FGF6-V5 than UM-SCC-49-LacZ-V5 cells (**Figure 3-5B).** The ability of FGFR inhibitors to modulate IFNγ induced PDL1 expression was also recapitulated in certain other cell lines, including UM-SCC-14a (**Figure 3-5C).** These data suggested that baseline FGF/FGFR signaling through FGFR1 plays an important role in modulating IFNγ-induced total PDL1 protein expression, and that situations with accentuated FGF ligand in the microenvironment may further potentiate the effects of IFNγ on tumor cells.

To then better understand the interplay between the FGFR and IFNγ signaling pathways, we tested RNA expression of various downstream targets of FGFR and IFNGR activation by qPCR in UM-SCC-49 and -14a. At this time point, both IFNγ and rFGF2 induce an increase in *PDL1* RNA (2-fold and 1.3-fold, respectively). We observed that RNA expression of genes regulated by IFNγ in other model systems, such as *STAT1*, *IRF9*, *SOCS1*, and *SOCS3* [31], were indeed induced 2-4-fold by IFNγ treatment, but not by rFGF2 (**Figure 3-5D,E)**. Instead, rFGF2 appears to induce a separate transcriptional program that included 1-3-fold upregulation of *CXCL8* and *SPRY*. Jak2 inhibition by TG101348 reduces RNA expression of both the IFNγ- and rFGF2-regulated gene sets, while BGJ398 reduced RNA expression of only the rFGF2-regulated gene set. *PDL1* RNA expression, however, is induced 2-fold by IFNγ and this induction is diminished in cells pre-treated with BGJ398, consistent with protein-level data above. Also of interest, despite the known ability of FGF signaling to activate the Jak/Stat pathway, only IFNγ, not rFGF2, induces *STAT1* RNA expression in this setting.

Finally, because glycosylation of PDL1 is known to prevent its degradation in other model systems [32], we asked whether the rFGF2-induced increase in PDL1 may be due to glycosylation, and therefore stabilization, of the protein. When we treated UM-SCC-14a with tunicamycin, an inhibitor of N-linked glycosylation [33], we observed a dramatic decrease in the ability of rFGF2 to drive PDL1 expression, and an accumulation of 33kD PDL1, which represents the non-glycosylated form (**Figure 3-5F**) [32]. Two recent studies in breast cancer cells describe a dual role for EGFR in stabilizing PDL1 protein. EGFR activity and can induce upregulation of B3GNT3, an enzyme that catalyzes PDL1 glycosylation, and may promote inactivation of GSK3β, a kinase responsible for targeting PDL1 for E3 ligase mediated degradation [32, 34]. We therefore speculated that FGFR signaling may act through analogous mechanisms to stabilize PDL1. To understand whether the EGFR-induced mechanisms described in breast cancer cells might also be at play in our system, we assessed expression of several glycosyltransferases reported to be upregulated by EGFR to determine whether FGFR signaling could regulate a similar program in HNSCC. While we noted very modest increases in some of the N-acetylglucosaminyltransferase family genes that we tested, including *B3GNT3*, *MGAT5*, and *GNPTAB* following IFNγ or rFGF2 stimulation relative to a vehicle control, it was unclear from these data (n=2) whether FGFR inhibition could modulate this effect due to high error among technical and biological replicates (**Figure 3-5G**).

We next monitored PDL1 expression and inhibitory phosphorylation of GSK3β on serine 9 following either stimulation with EGF or pharmacological inhibition of EGFR with gefitinib. Interestingly, we were able to recapitulate the effects reported by Li et al [32], demonstrating that EGF indeed increased PDL1 protein levels and that gefitinib treatment led to a reduction in phospho- GSK3β at 6h (**Figure 3-5H**). However, neither pan-FGFR inhibition

nor stimulation with rFGF2 affected GSK3β phosphorylation, suggesting a different mechanism may mediate the effects of FGFR signaling on PDL1 expression.

Discussion

HNSCC is a strongly immunosuppressive disease for a majority of patients, and understanding the molecular mechanisms that guide immune escape are critical to developing therapeutic strategies that create a more favorable tumor niche. Here, we are the first to perform a genome-wide ORF screen as an approach to identify novel PDL1 regulatory mechanisms. Importantly, our data identified several genes previously known to regulate adaptive PDL1 expression in other models, including *IL17A*, which supported the accuracy of the overall discovery approach. For example, inhibition of IL17A in ER-negative breast cancer models has been shown to inhibit PDL1 expression [20]. HNSCC has previously been associated with high TIL infiltrates [35-37], and specifically serval reports have documented significant increases in TH17-cells, which express high levels of IL17A, in both pre-malignant oral lesions [38] and HNSCC tumor microenvironment [39, 40], supporting a critical role for IL17A-mediated PDL1 expression in these settings.

Similar to the known regulators, our experiment also identified several novel genes closely linked to pathways known to regulate adaptive PDL1 expression in other cancer settings including the NFKB pathway (NFKBIA) and FGF/FGFR signaling pathways (FGF6). In fact, while NFKB signaling is one of the most well recognized regulators of adaptive PDL1 expression discovered thus far [41-46], *NFKBIA* has not previously been linked with the regulation of PDL1. In the HNSCC TCGA project, *NFKBIA* is amplified in 8/517 (1.5%) cases, and a recent independent report also demonstrated a significant enrichment of *NFKBIA*

alterations in HPV+ squamous cell carcinomas with 12/149 (8%) harboring either mutations or CNV alterations to the gene [47]. Hence, given our validation of NFKBIA as a driver of IFNγ-induced PDL1 expression in HNSCC models, the overall data supports a pivotal role for this gene in modulation of immune reactivity in HPV+ HNSCC.

Further, we and others have also previously identified FGFR signaling as a driver pathway of some HNSCCs [24, 48-51], and FGFR1 protein has been observed to be overexpressed in >80% of HPV+ HNSCCs and 75% of HPV- HNSCCs [51] suggesting an important role for the pathway in a large subset of the disease. Similarly, FGFR signaling has been shown to be upregulated in HNSCC cancer stem cell (CSC) populations in response to platinum-based therapy *in vitro* [52]. When considering our data showing the strong regulation of PDL1 expression by activated FGF/FGFR signaling, the data support the hypothesis that cisplatin-mediated adaptive FGFR1 expression may activate the PDL1 checkpoint in the CSC population in some tumors, thereby preventing immune-mediated killing of the CSC population. Indeed, while we show a strong dependence of PDL1 expression on FGF/FGFR signaling in some cell line models, and the CSC data suggest that other common HNSCC therapies such as platinum-based regimens, may also induce FGF/FGFR-dependent activation of the PDL1 immune checkpoint. As such, our finding may have implications for a larger subset of HNSCC patients. To understand the link between FGFR and PDL1, a more comprehensive study of these pathways will be necessary. Proteomic and transcriptomic analysis following FGF/FGFR modulation, and comparison of these data to IFNγ stimulation, will be valuable, especially in clarifying a potential node of crosstalk between IFNγ and FGFR signaling cascades. Further, it will be of interest to examine the posttranslational modification status and stability of PDL1 under these conditions in more detail.

Overall, the approach discovered 335 enriched genes that potentially drive PDL1 expression in HNSCC, of which we validated a few genes as novel drivers including two which are genetically linked to subsets of HNSCC patients. The data support the use of ORF profiling as discovery technique to complement the previously published functional approach of CRISPR profiling that also successfully discovered novel PDL1 regulators. Indeed, we are in an exciting time when multiple complementary discovery approaches can be used to help understand to combat the immunosuppressive tumor microenvironment of HNSCC and other tumors and hopefully develop rational combination approaches to improve survival outcomes.

Acknowledgements.

Thank you to Samantha Devenport, Rebecca Hoesli, and Susan Foltin for assistance in generation of the UM-SCC-49-ORF pool and stable cell lines. Thank you to Aditi Kulkarni for bioinformatics analysis. Thank you to Judy Kafelghazal, Julia Eisenberg, Erin Scheftz, Isabel Murray, and Tala Al-Saghir for technical support.

Figures

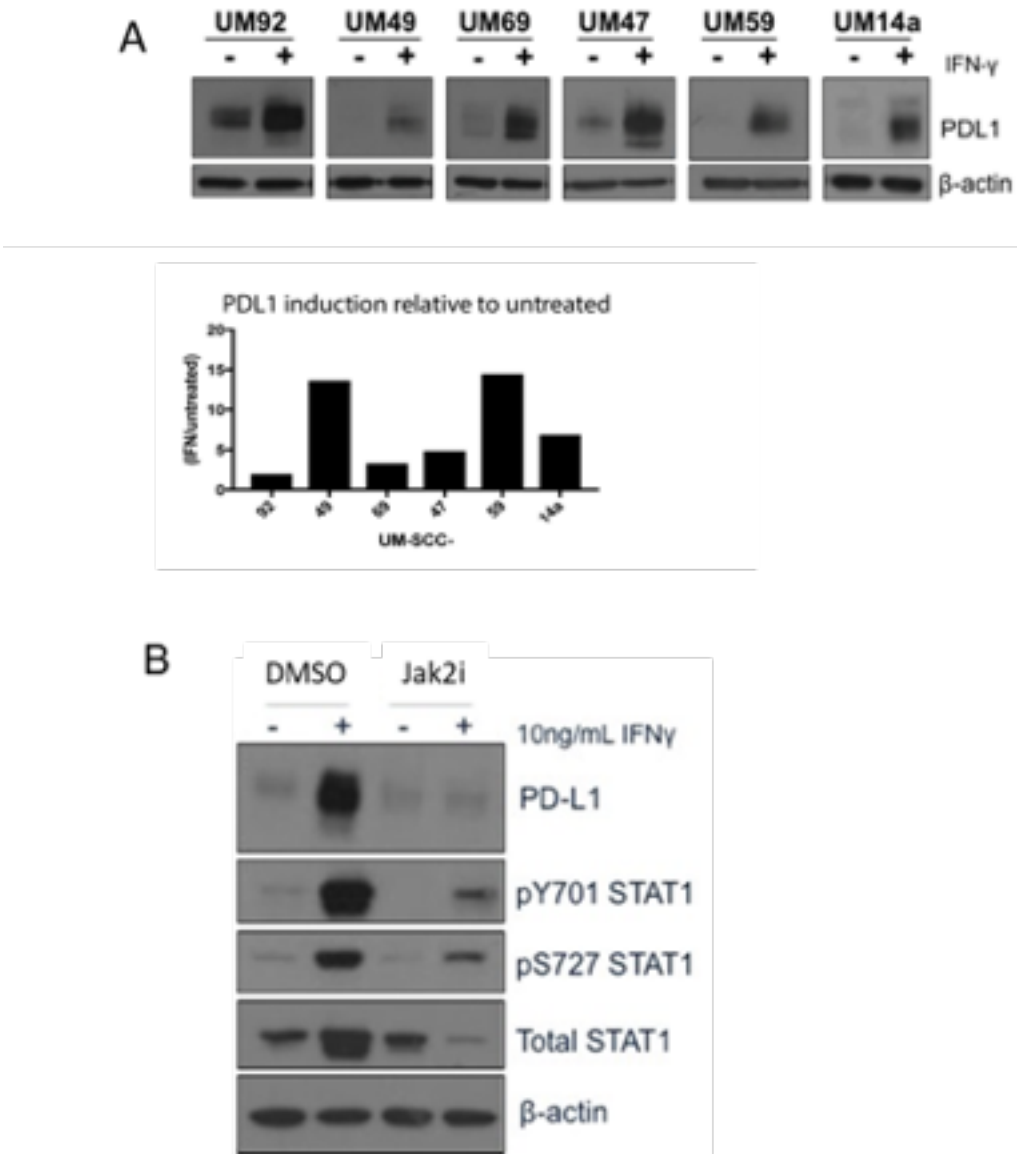

Figure 3-1. Characterization of UM-SCC HNSCC cell line models.

A) Cell lines were treated with 10ng/mL IFNγ for 72 hours and total PDL1 expression was assessed by immunoblot (upper). Densitometry analysis was performed in ImageJ with PDL1 bands normalized to corresponding beta actin bands. Relative expression was then calculated by dividing IFNγ treatment by untreated (lower). B) PDL1 and STAT1 were assessed by immunoblot after 72h treatment with 10ng/mL IFNγ with 6h DMSO or TG101348 (2uM) pretreatment.

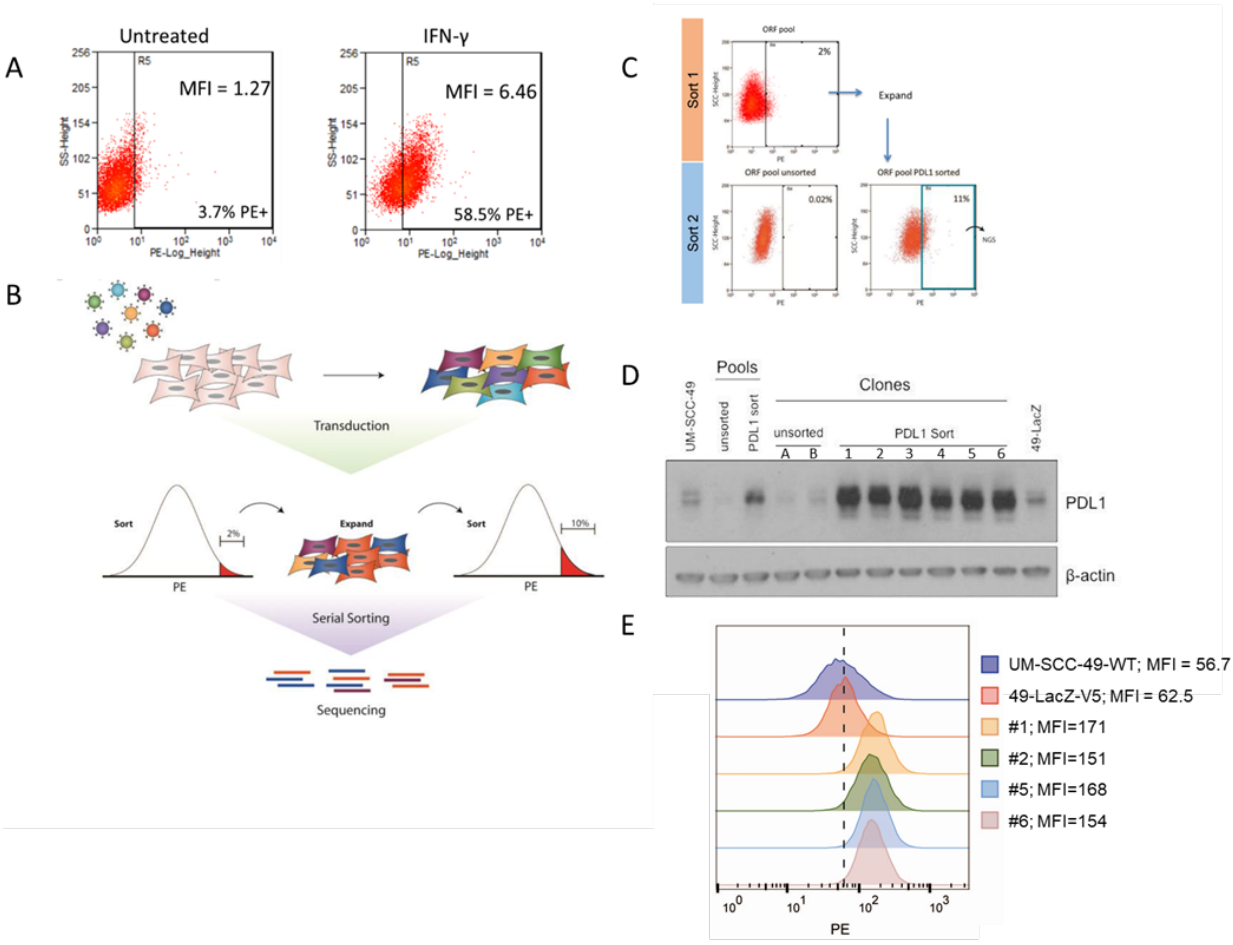

Figure 3-2. Discovery of ORFs that drive PDL1 cell surface presentation in HNSCC.

A) Cell surface expression of PDL1 in UM-SCC-49. UM-SCC-49 cells were treated -/+10ng/mL IFNg for 72h, trypsinized, and stained for cell surface expression of PDL1. **B)** Schematic of overall project workflow. UM-SCC-49 cells were transduced with the 17,000 gene ORF library at an MOI of 0.3 and selected with puromycin. Cells were then serially sorted for the top 2% of PDL1 expressing cells in the population. PCR amplified barcodes from the genomic DNA of PDL1 enriched or control populations was then sequenced on an Illumina MiSEQ for quantification. **C)** Sorting UM-SCC-49 ORF library for high PDL1 expressing cells. The UM-SCC-ORF library cells were stained for cell surface expression of PDL1 and the 2% of cells with highest PE positivity were selected and expanded in culture (top). The select population was then subjected to staining and sorting again, this time with the top 11% collected for sequencing (bottom right). The initial ORF pool was also analyzed for PDL1 expression for comparison (bottom left). **D)** Clones from the PDL1 enriched population were expanded and used to confirm high total PDL1 expression in each clone by Western blot. **E**) A subset of the clones from (E) were immunostained for PDL1 and analyzed by flow cytometry. Dashed line represents MFI for UM-SCC-49-LacZ-V5.

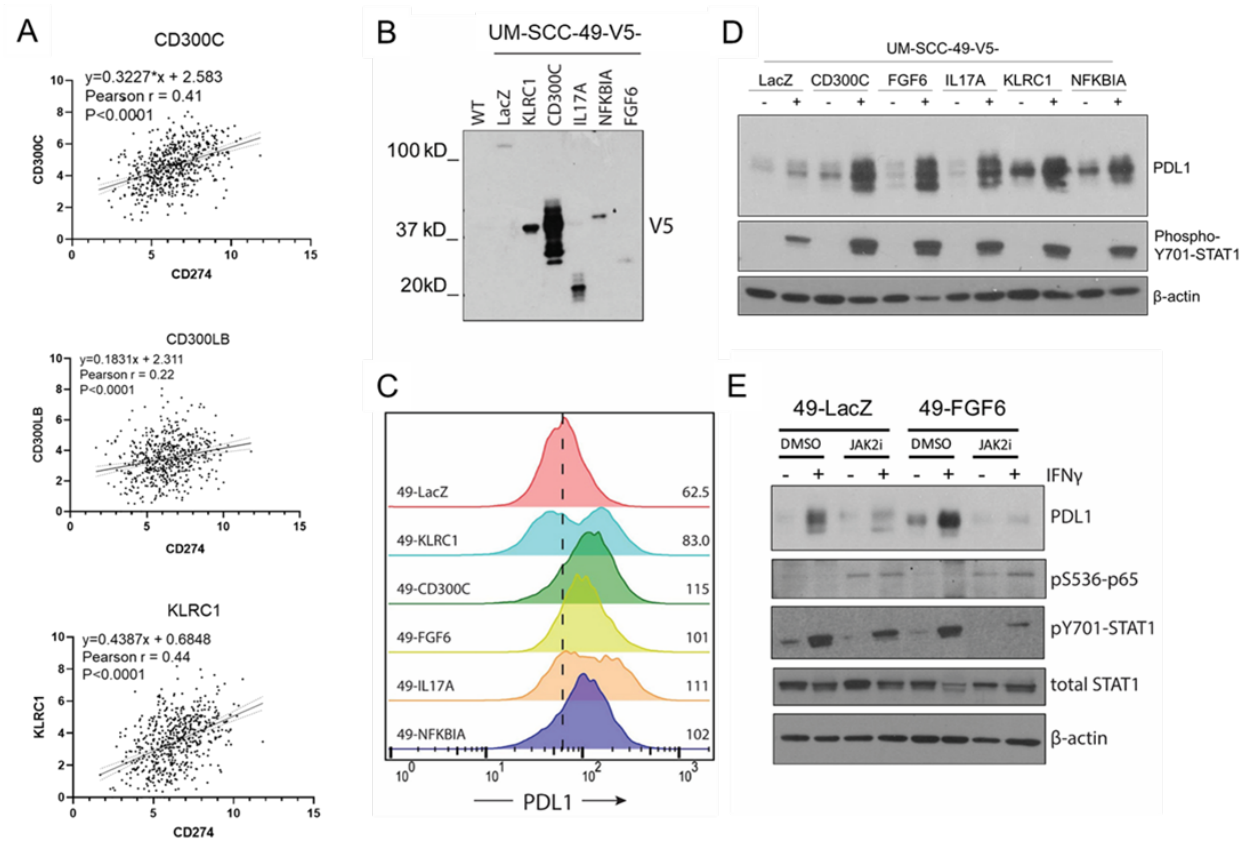

Figure 3-3. Validation of FGF6, IL17A, CD300C, KLR1C and NFKBIA as drivers of PDL1 expression in HNSCC.

A) Linear regression analysis reveals correlations with PDL1 expression in TCGA HNSCC RNAseq data. B) Lentiviral ORF-V5 tagged expression vectors were cloned and used to overexpress each of five candidate genes and one control (LacZ) in UM-SCC-49 cells. Expression of V5 tag was confirmed in each cell line by anti-V5 immunoblot. Expected molecular weights of protein products are as follows: LacZ. 121kD; KLRC1, 31kD; CD300C, 29kD; IL17A, 22kD; NFKBIA, 40kD; FGF6, 28kD. C) Quantitative PCR was used to assess mRNA expression for target ORFs in each cell line as well as PDL1 transcript levels. D) Flow cytometry was used to determine changes to cell surface presentation of PDL1. Median fluorescence intensity was quantified from each histogram. E) Changes to total PDL1 and phosphorylated STAT1 were analyzed by western blot in each 49-ORF cell line. E) 49-LacZ and 49-FGF6 were pretreated with DMSO or JAK1/2 inhibitor TG101348 (2uM) for 6h, followed by addition of IFNγ (10ng/mL) as indicated. Cells were harvested 72h after IFNγ treatment. PDL1 expression, p65 activation, and STAT1 activation were assessed by immunoblot.

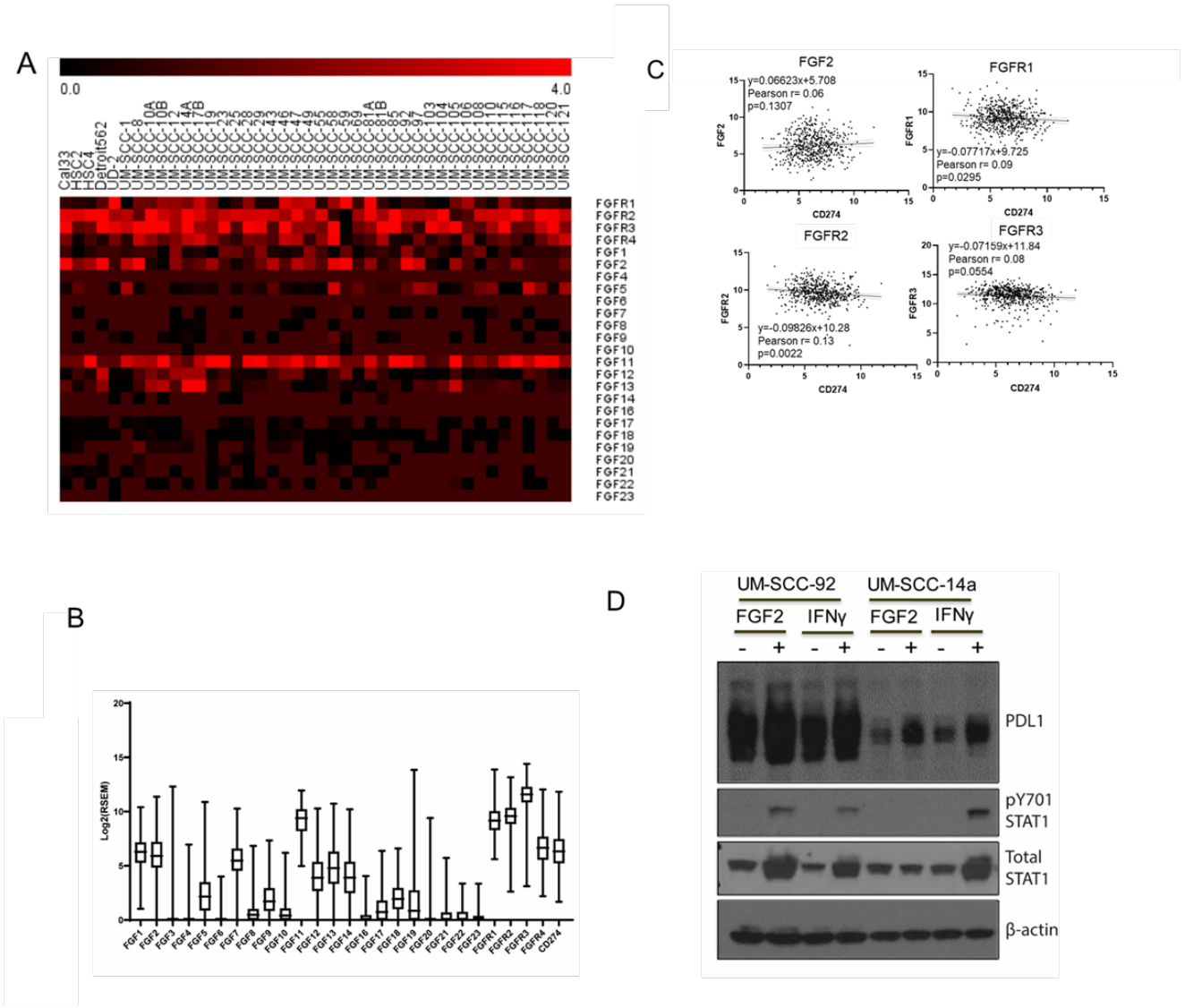

Figure 3-4. The FGF/FGFR pathway in HNSCC.

A) Log2(FPKM+1) for FGF and FGFR family genes in 40 HNSCC cell lines. B) Log2(RSEM+1) for FGF and FGFR family genes in the TCGA Head and Neck PanCancer Atlas dataset accessed via cbioportal.org. C) Protein isolate from UM-SCC- cell lines in log-phase growth was immunoblotted using an antibody directed against FGF2. D) UM-SCC-14a and UM-SCC-92 were treated -/+ 30ng/mL FGF2 or 10ng/mL IFNγ for 72h. PDL1 expression was assessed by immunoblot.

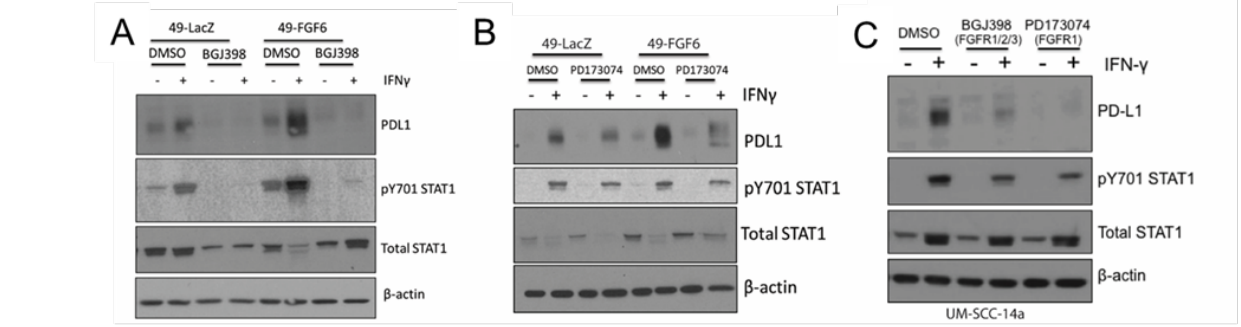
A
49-LacZ
49-FGF6
DMSO
BGJ398
DMSO
BGJ398
IFNγ
PDL1
pY701 STAT1
Total STAT1
β-actin
B
49-LacZ
49-FGF6
DMSO
PD173074
DMSO
PD173074
IFNγ
PDL1
pY701 STAT1
Total STAT1
β-actin
C
DMSO
BGJ398 (FGFR1/2/3)
PD173074 (FGFR1)
IFN-γ
PD-L1
pY701 STAT1
Total STAT1
β-actin
UM-SCC-14a

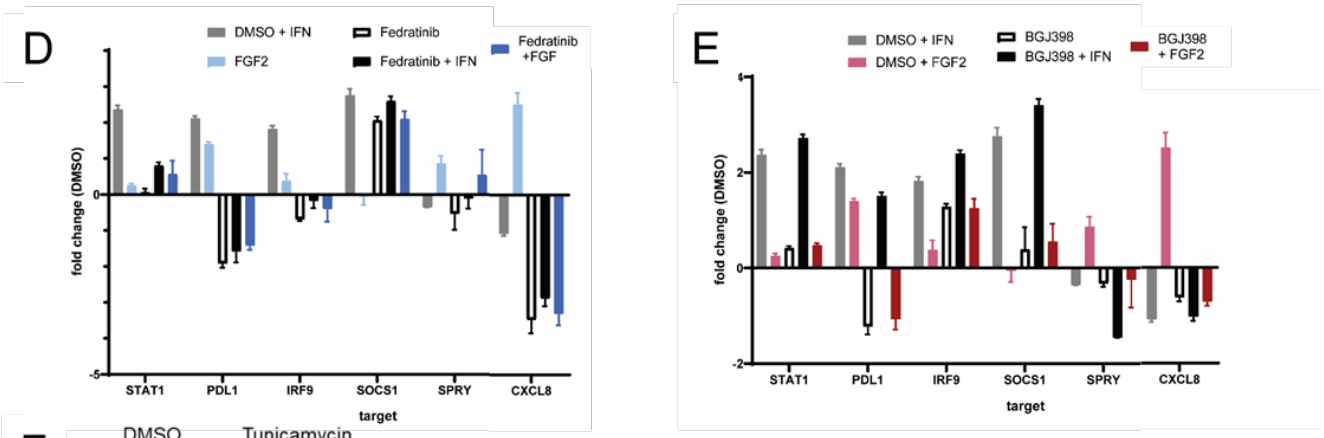
D
DMSO + IFN
FGF2
Fedratinib
Fedratinib + IFN
Fedratinib +FGF
fold change (DMSO)
STAT1
PDL1
IRF9
SOCS1
SPRY
CXCL8
target
E
DMSO + IFN
DMSO + FGF2
BGJ398
BGJ398 + IFN
BGJ398 + FGF2
fold change (DMSO)
STAT1
PDL1
IRF9
SOCS1
SPRY
CXCL8
target

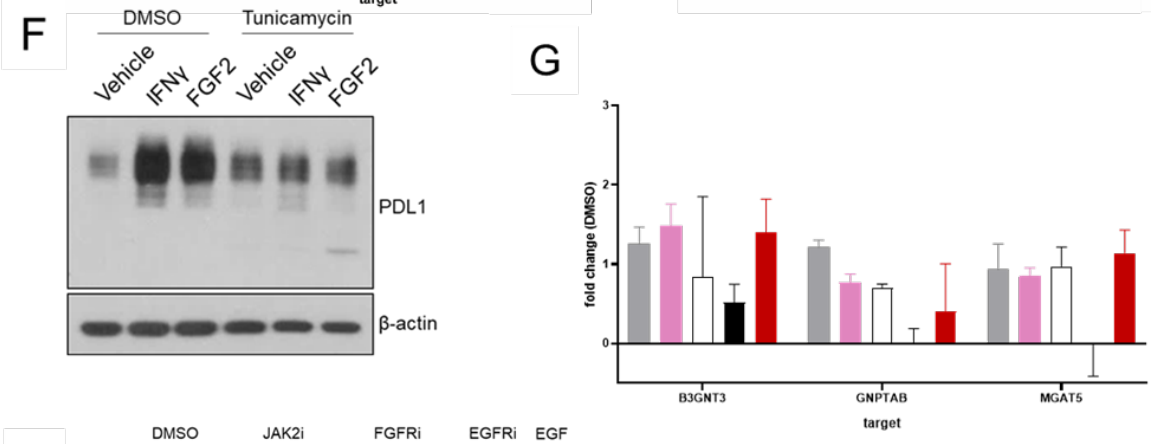
F
DMSO
Tunicamycin
Vehicle
IFNγ
FGF2
Vehicle
IFNγ
FGF2
PDL1
β-actin
G
fold change (DMSO)
B3GNT3
GNPTAB
MGAT5
target

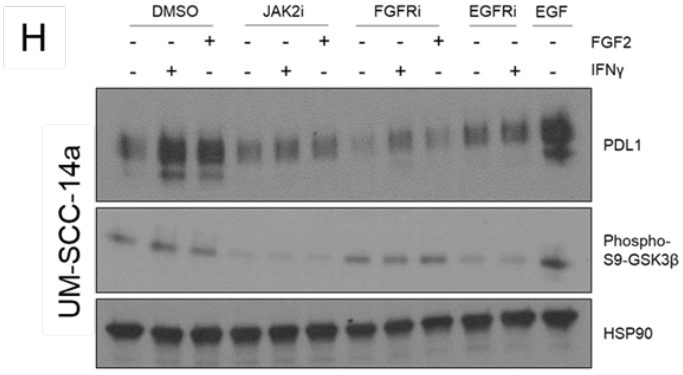
H
DMSO
JAK2i
FGFRi
EGFRi
EGF
FGF2
IFNγ
UM-SCC-14a
PDL1
Phospho-S9-GSK3β
HSP90

Figure 3-5. Effects of FGFR modulation.

UM-SCC-49-LacZ-V5 and -FG6-V5 were pretreated with DMSO or 3uM BGJ398 (A) or 3uM PD173074 (B) for 6h, then 10ng/mL IFNg was added to the cell culture media. Protein expression was assessed after 72h by immunoblot. C) UM-SCC-14a-WT cells were pretreated with 3uM BGJ398 or PD173074 for 6h, then stimulated with IFNg for 72h prior to immunoblotting. D,E) UM-SCC-14a cells were pretreated with DMSO, Fedratinib or BGJ398 for 3h as indicated, then 10ng/mL IFNg or 30 ng/mL FGF2 was added for an additional 3h. F) UM-SCC-14a cells were pretreated overnight with 50ng/mL tunicamycin or DMSO control for 6h, then 10ng/mL, 30ng/mL IFNg or rFGF2 was added as indicated. PDL1 expression was assessed by immunoblot. Arrow points to 33kD band. G) UM-SCC-14a cells were treated for 3h with 3uM BGJ398, then IFNg or FGF2 was added. RNA expression of candidate glycosyltransferases was assessed. H) Cells were pretreated with inhibitors as indicated at 3uM (TG101348, FGFR1; BGJ398, pan).

Tables

		Sequence
First Round	ORF_F1	actgGCTTTATATATCTTGTGGAAAGG
	ORF_F2	cagtGCTTTATATATCTTGTGGAAAGG
	ORF_F3	tgacGCTTTATATATCTTGTGGAAAGG
	ORF_F4	gtcaGCTTTATATATCTTGTGGAAAGG
	ORF_R1	actgGTAATCCAGAGGTTGATTGTC
	ORF_R2	cagtGTAATCCAGAGGTTGATTGTC
	ORF_R3	tgacGTAATCCAGAGGTTGATTGTC
	ORF_R4	gtcaGTAATCCAGAGGTTGATTGTC
Second Round	AmpFW_	5'-TCGTCGGCAGCGTCAGATGTGTATAAGAGACAGGCTTTATATATC-3'
	AmpRV_	5'-GTCTCGTGGGCTCGGAGATGTGTATAAGAGACAGGTAATCCAGAGG-3'

Table 3-1. PCR primer sequences for amplification of ORF library.

Gene	Forward	Reverse
TLR2	AGCAGGATCCAAAGGAGACC	ACCAAGGTGGTTTGCTGAGT
GAPDH	AATGGGCAGCCGTTAGGAAA	GCCCAATACGACCAAATCAGA
PDL1	AGTCAATGCCCCATACAACAA	CGTCACTGCTTGTCCAGATGA
MYD88	GACTGCTCGAGCTGCTTACC	ACATTCCTTGCTCTGCAGGT
IRF7	GCCTGGCCACCATAAAAGCG	TGTTGAACCAGTGTCCAGGC
STAT1	AAAATGCTGGCACCAGAACG	AGAGGTCGTCTCGAGGTCAA
B3GNT3	GCAACGCCTGTCCTCCTTTG	AAGGTGTCGCCCCTTCCTAT
GNPTAB	CCAGTTCGGAGAGGTGGTTC	ATCTGTGCCATTCACCCAGG
MGAT5	CATGGTATCCTCAGTGGACGG	TGGGATGTCAGCTCTCTCAG

Table 3-2 qPCR primer sequences 3' to 5'

Clone #	ORF
A	SLC10A7
B	CTH
1	SENP8
2	SENP8
3	PPIAL4G
4	CNR2
5	DPF3
6	TMEM25
7	ZNF550

Table 3-3. Open reading frames identified by Sanger sequencing in cell lines derived from sorted ORF pool.

ENRICHED ORFS IN PDL1 SORTED POPULATION

	Barcode	Gene	Control #	PDL1 #	Total Read Count Normalized Ratio	Log2 (N. Ratio)
1	ACTTCATCAGCAGTGAGAATTCCA	ERO1L	7	10889	1208	10.2
2	CACGACGACATGGGTTATATCGAA	NUP85	3	4378	1134	10.1
3	AGATCAACGCGCCCATACGCACAT	OR2L2	15	19065	987	9.9
4	GCAGGATATTGGTTACATCGACCT	TDP2	120	111075	719	9.5
5	CCGAACACCCTCTAACTCGGCCTC	ATF7	352	290057	640	9.3
6	AAGAATATGTGGTAGTGCTTGATG	AMT	48	29441	476	8.9
7	TGTACACTCGGTGTGATTTGTAGT	GSTO1	245	146097	463	8.9
8	GATCGTATTAACTAGGCTAATGGC	SPACA3	5	2513	390	8.6
9	AATTCCCATTGTGATTGGGCCTGC	ZNF101	52	19317	289	8.2
10	ACCACTAAGGGACAGCAAACCTTC	HNF4G	158	53187	261	8.0
11	TGGCTCATAGCACCATACCCTCCT	PPP1R2	99	31497	247	7.9
12	CTTAGTCTTCATCCTCGTCTTATT	FAM209A	1	293	228	7.8
13	ATGAGCCTTATTGGAGGCTGAAAT	LINC00242	129	33748	203	7.7
14	CCACCTTCCCACCCTCACGAACGA	ENOSF1	9	2159	186	7.5
15	AGAAGGCACGCTTCAGCCGCGCCG	ZFHX2	216	48351	174	7.4
16	ATTATGTTTAGAACTAATATCTAG	ZNF581	132	28361	167	7.4
17	AACCGATGCCTTAAAGGGTAGTCC	TALDO1	29	5796	155	7.3
18	TGTACCCGCGAGTCTCCACACCGT	HTR2C	1	178	138	7.1
19	TTTAAGATTTCTGGGCTTCCCCCT	ABHD12B	5	850	132	7.0
20	ACTAAATTCAGTGATGCCACATAC	C8G	93	15030	126	7.0
21	TAAGCGAATAGTACCAGGGGTTGA	DNASE1L1	88	13212	117	6.9
22	CAGTGACTTATCGTATTTGTCTGA	DNM1	2	290	113	6.8
23	CTGATTCAGACAACGAGCATCAAC	CTSL1	125	16125	100	6.6
24	TCTCTTGGGAGGTGCATTCGATCA	PPIAL4G	122	15117	96	6.6
25	GCCCATCCAGCATGGCGGATTCCC	EFNA1	87	10319	92	6.5
26	ACAGCACTAGCAGGAACCTGGACT	TMED4	203	22053	84	6.4
27	CAACACGAGGCCATACATTGCTTA	PRKAA1	23	2471	83	6.4
28	TCATTGCTGTACATCTAGAGTTCG	S100A1	6	618	80	6.3
29	CTGTATAGACTGGCCGTCGAACTT	KRT23	12	1225	79	6.3
30	ATCGCTCCCTTCACAGTAAGCATA	C1ORF49	53	5353	78	6.3
31	TAGACGGTTTTATACGCTCAGCCA	EFHD1	100	9775	76	6.2
32	TAGAGGAAAGAATACAGGATCTAC	DLX6-AS1	397	38327	75	6.2
33	TAACTTGACGAAAGGACCCTGTGC	EIF4B	14	1328	74	6.2
34	CAAATCGCCTGACCCCAATAAAGA	BOD1P	12	1095	71	6.1
35	AACCCGCAACATGCCCGGTGGTCA	CPEB1	5	436	68	6.1
36	TAGTACCAAAAGCTTAACAGCGTT	ATCAY	26	2176	65	6.0
37	CTAGACATACATGATGCGGCACCT	ADORA2B	92	7575	64	6.0
38	CTATAAGAGCTCAATCACTGCGGA	TCN1	10	804	62	6.0

39	TTAGCTCCGTGCCGCGATATGAAA	BDNF	36	2867	62	6.0
40	AGAGTCCATTCTCCCACTATGCCC	REP15	227	17349	59	5.9
41	ACTTTTCCCGCTTGTCCTGCCCCC	GRK6	1	74	57	5.8
42	CCTGTTTCCCCCGACCCTGAGTCG	RASA3	2	138	54	5.7
43	AATTAACTGTTCATCCGAGTCTTT	ZCCHC9	1	68	53	5.7
44	GTGTTCCCCGCGGTCTGGCGAACG	TP73-AS1	81	5274	51	5.7
45	TTAACTTCAATTCTCTTTTTAATT	DIMT1	21	1294	48	5.6
46	CCTGGTTGCCCCTCTAGGGCTTGA	DPY19L2P1	151	8998	46	5.5
47	GCCACTTTGTAGGCGCCATTCGAC	CAPN1	1	59	46	5.5
48	CACTATATCAATGTTTCCATTCGT	FAM78A	8	462	45	5.5
49	TACCTGATAATGGCACCATGCAAA	DEFB129	259	13571	41	5.3
50	CCAATCAACCGGGCCCCGAAACTC	CDK16	10	522	41	5.3
51	CACCCTATCGTCGAGGTCGACTGC	PRAMEF5	63	3288	41	5.3
52	TCAGCCTACCATCAACTTCGTATT	SET	1	51	40	5.3
53	AAGCTGGGATTACTTCTGTACGGC	EEF1G	133	6536	38	5.3
54	AAGTGGGAGAGTAAGTGCCTGGTC	PRB4	371	18019	38	5.2
55	TTCGTACTCCGGTTCCTGTGCTTC	RHOG	213	10224	37	5.2
56	GGCATATGTCCTGACATCTGGCAG	CHIA	111	5244	37	5.2
57	CCGCATAAGGCCAGATCGGTGCTC	CAMLG	43	1997	36	5.2
58	GATACCATACGACATCCTGTTCAC	CCNL1	13	598	36	5.2
59	ACCTACCTCCTGACACATCAACTT	CNBP	216	9539	34	5.1
60	CCTCACAGTACTTGCCATCCTGAC	RBX1	278	11605	32	5.0
61	AGCAGAACCCTTAAAAGCTCGAGT	CST8	227	9049	31	5.0
62	TGTTGAATCGGTAACGATGACCTG	CDX4	24	942	30	4.9
63	TGCCCGTGTTCTCCATCAGGTTTA	TRIM72	1	39	30	4.9
64	AACTATTAGTGCCCGAGTCATCCC	CD82	57	2195	30	4.9
65	GTTTGTTCTAAACATTGCGACATC	ZNF578	9	339	29	4.9
66	TACACACCCTTCTTAGCCATTCAT	***NFKBIA***	242	9003	29	4.9
67	TCGGAAACCAGAACTATTAGTATA	RHPN1	3	111	29	4.8
68	CTACAATTTCTGTTCTGCACCTTA	ASIC1	18	659	28	4.8
69	TCCAACACAGCGAGCCTCTTGGCT	TNFSF11	79	2841	28	4.8
70	CACGCCCACCCGTGCCAGGACTAC	OR7E91P	45	1617	28	4.8
71	TCAAGATACCCTTGACCAAATGTT	ZNF550	25	883	27	4.8
72	ATTAACAACCATCCTGTCCTGGCC	C1QTNF2	255	8720	27	4.7
73	TTTAGACTGGTTTTGTAAGAGACC	UFSP1	152	5090	26	4.7
74	ACCGAGTCCGAATAGTTTATTCAG	HOOK1	23	764	26	4.7
75	GTCAACTGGGGCATCTGGCACCTC	ARHGEF26	222	7316	26	4.7
76	AGCTCAATCAACTCAACCTTACAA	KLRC1	101	3228	25	4.6
77	CCCTATGAAGGCCTGAAGCGGGCA	METTL21A	464	14778	25	4.6
78	GCACCGATACCGATCCCCCCAATC	GALNT10	147	4385	23	4.5
79	GTAGGTGCAAACGCGAGACAGACC	MAS1	168	4858	22	4.5
80	TTCAAAGAACAGGAACGGGCTCAT	FMN1	33	943	22	4.5
81	CTGGCATGCTAACCAAGTACACGC	CDH26	306	8694	22	4.5
82	CAAAGGCCTAAGAGGACAGAGAGT	ORAI1	185	5160	22	4.4
83	TCTTGCTACCGGTGACATTCTCCG	KCNJ15	51	1420	22	4.4

84	TGAATTGTCGCCCCCAGATACACC	ZCCHC10	208	5745	21	4.4
85	GCCTAATTCGTGACGTCCCCAAAT	DCLRE1B	10	276	21	4.4
86	TTGCCGAACCGCGCACTCAGAATC	PIAS4	15	385	20	4.3
87	ACGCGCCCGATCCCCACTTCCAAT	ANXA11	74	1865	20	4.3
88	ATAGAACGTGACCAATCGTTGTTT	PIPOX	20	491	19	4.3
89	GCTGTAGTGTGCCCGCTGAGGCCT	PRKCZ	9	218	19	4.2
90	ACCAGAATGATACCTTGATCTCAC	GPBAR1	8	191	19	4.2
91	GTGATACCTCCTTCTCCCGACCCA	ASPDH	65	1547	18	4.2
92	CCATTCCACCTAGAGAATTTATAC	P2RX2	1	23	18	4.2
93	CGTCATTATATTCCTCTCCAGGAT	KIAA0284	55	1233	17	4.1
94	ACTTCCTGGAGAGGGGCTAACAGT	WBP2NL	200	4481	17	4.1
95	CTTAATAAGTCGAAATCCGAGGAC	GPR139	13	290	17	4.1
96	TGGCCCATCAAACGAGCCTTATTT	AKR1B1	46	1011	17	4.1
97	GAGGATGTCACACCACGATATCAT	SLC22A11	27	581	17	4.1
98	CTTGCCCCCATCACCCATATTTCT	CMTM2	339	7270	17	4.1
99	ACACCGGTCTGCTCCCGATCGGGC	TNFAIP2	85	1805	16	4.0
100	TCGACGGACATGGGAAAGATCAAC	REEP5	142	2956	16	4.0
101	AACCTTACTAATAGCTTGGTTGCC	CCDC138	9	187	16	4.0
102	AGCAATCTTACCGGAGCAGTTACA	CEACAM8	18	373	16	4.0
103	TCAGAGCAATATCCCATAATCAGT	RUVBL1	109	2242	16	4.0
104	TTGATTTCCAGTGCGAGAAGACCG	HMX2	16	316	15	3.9
105	ATTGTCAATGGTTTGATCTCAGCA	FOS	99	1952	15	3.9
106	TTCCGCCCTGTATTCCGGTACGTC	ENTPD2	8	156	15	3.9
107	TATATGTCTGAATACTCCGATCAG	OR14J1	4	78	15	3.9
108	AAGCACATCCGTTGTGCGCACAGA	BAMBI	19	359	15	3.9
109	ATCGAGGGTCCACGTACCTGTACT	RABL2A	113	2132	15	3.9
110	CATCACATATAAATGAGGACATGG	STRN	10	184	14	3.8
111	ACCTTAGACGCTCCTTTTCGCTGA	TAC1	97	1764	14	3.8
112	TCTCATCTGTCCCTGGCCCCGTAA	TERF2IP	16	285	14	3.8
113	ACGCCGAGATCCGCATAAGCCGTA	GLO1	76	1350	14	3.8
114	CCATCCTTACCAGAAACAACTCCC	UBE2W	102	1800	14	3.8
115	ATCACAACTATCGTTATTTACCGC	KCNAB2	11	194	14	3.8
116	GGTCGAATGGTCGCATTAGATTCC	HIST2H2AA3	91	1592	14	3.8
117	CATCATTCGCCTCTATCAACAATA	ZNRD1	82	1424	13	3.8
118	ACTTGCATCCTGCCCCAGAGGCTG	OR56B1	8	132	13	3.7
119	TCTGAAAAACTCCGAAATAGCAGA	HINFP	47	768	13	3.7
120	AACTACTATGGGGCCTTGCACCTT	RHBDD2	160	2599	13	3.7
121	TCGACAGCACTCACGGGTTAGCAG	LINC00482	48	767	12	3.6
122	TAATTAACCGTTTGAACTGCAACT	SAMD10	44	690	12	3.6
123	ACTGAGCAAGTCCCCCTTCCTATA	C7ORF42	112	1755	12	3.6
124	GTTCGGAGAGGCTCTATGGTTGGG	DUSP10	61	953	12	3.6
125	CAGCCTTAAACAGACTTCATAAGC	HSPA8	56	865	12	3.6
126	CCGCAGGTCTTCTGTTTTTAGGAT	FAM71B	17	262	12	3.6
127	TTCTAACCCCTTTGTAGACCAATG	HIST2H2BA	443	6778	12	3.6
128	CTGAGGCAGCGTCGGCTATTCGCA	MST4	217	3280	12	3.6

129	AGCCAATTATCCTGTTGTGTCCCG	ANAPC16	222	3188	11	3.5
130	GTTCGCTAAATCCGTTCTCCCGGC	LRRC52	74	1061	11	3.5
131	ACGCTCAATGAGTGCACGCTCACC	PCSK9	94	1324	11	3.5
132	TTGTCTTCTATTATGAGTTGCGTA	CXCL5	43	596	11	3.4
133	GCTTCTCTAGTGAAAGTAATTTTG	FMR1	14	189	10	3.4
134	ATAACCAAGTTATGGAAACAGGCC	CPSF4	97	1305	10	3.4
135	GGGACCATAATGGCGATCCATTAG	AREG	6	80	10	3.4
136	TCCCGTGTGAATATTTTGGCCTTT	DHPS	68	903	10	3.4
137	AGTTGTGCCCCTCGGAGTGCGCCA	GPAA1	2	26	10	3.3
138	CCTAGACTGTACCTCCCATGGACC	COQ4	219	2814	10	3.3
139	TAGTGTTCCCTCCATCTATCGAAG	TMPRSS12	6	77	10	3.3
140	GTAGTACAATACCCCGAGTCGGAA	GJA4	35	443	10	3.3
141	CATGCGCTACTTAATTGAAGTGCC	BCMO1	13	163	10	3.3
142	TTATATTCCCAGTAGGGCTAGGAG	CLDN7	12	148	10	3.3
143	ACGATCAACCTGCGTTTTCCCGCA	APOPT1	175	2091	9	3.2
144	CGCAGGTTGCACAGAATGCTCGGT	EPB41L1	27	319	9	3.2
145	CGGCATTCCGTCAATTGCCGAACT	PMCH	67	777	9	3.2
146	CGCAAATACTTTCGGATGGCATCC	C1ORF64	212	2424	9	3.2
147	TCAGTACTAGGAAGGTCTCTACGA	MAX	73	828	9	3.1
148	GTCCGTTTAAGAACGTTTCGGCAC	C11ORF31	158	1789	9	3.1
149	TTATCATTCTGGGGATGGCAGGAG	PLEKHB2	124	1401	9	3.1
150	CCCTCCCAGTGTTGACTGTATTCC	GCNT3	60	667	9	3.1
151	GGGCGTGAGATAAAAGTGTAAAAT	MTERFD2	85	929	8	3.1
152	TAGGGTATAATAGATGATCCTGCC	ST6GALNAC6	29	315	8	3.1
153	CTTAGCCAATGGGTGCATCCGTGG	OR51G2	18	195	8	3.1
154	AGCAGACGTTGCATGCGCAATTCA	RANBP10	67	718	8	3.1
155	CCGCAGTCCCCTTCGCCGGAGATC	GFOD2	42	446	8	3.0
156	GCATGGGCCGAGCGCATTTCGCGG	FAM27E2	275	2793	8	3.0
157	ATTCGCGGCTATGCAGGGGCACTA	RHBDL2	5	49	8	2.9
158	CATAGTAGCGCACTACAGTTTAGC	REEP6	26	251	7	2.9
159	ACTTCGACGTCTGGAACCAGTCTC	C1ORF158	90	857	7	2.9
160	TTTGGCATCCCCCCTGTAGTGCGC	ZNF689	71	675	7	2.9
161	ACAGGATACATGATTACATGCCCC	SHMT1	11	102	7	2.8
162	TCTAAACGAACGCATCCCTGCCCT	PF4V1	34	313	7	2.8
163	TATAAGGCACCCAATAACCGAGAT	RORB	70	638	7	2.8
164	CTGCGACGCGGTACTGACGAATAT	C11ORF63	74	659	7	2.8
165	ACTGGGTCACAGTAGTGATTACCC	TGIF2	317	2810	7	2.8
166	CTTCGTGACAATACCTTTCGGAAT	CDK2	11	97	7	2.8
167	GCCCAGCTACACAACCAAGTTGCC	PYY	488	4288	7	2.8
168	GGGTCAGTAGTGGATGTACCAGTA	LOC554223	53	457	7	2.7
169	GCAAAGACACGTAGACGATAAGCC	FAM83A	62	515	6	2.7
170	ACACAAACGCTCATCAGCCCTGGC	CD300LB	127	1048	6	2.7
171	TGACGTCCGTCCCAGACCGTCTGC	GRB7	39	314	6	2.6
172	GAATTTGTCGACGTGCTTTGAGGA	TRIM52	65	521	6	2.6
173	CATATCACCAAATTTATTCCGAAC	KIRREL3-AS3	107	851	6	2.6

174	TTGACTTTGATGTATCAGATCTAC	***CD300C***	162	1253	6	2.6
175	ACAAATTCCGAGATAGACGTCCAA	DCTN3	127	981	6	2.6
176	CCAGAATTACGCACTTGTCGATGT	SLC39A7	45	345	6	2.6
177	TCTCAGTCTCCACTCGTCTTGAGA	SUOX	50	376	6	2.5
178	ACAAGATATTAACGCTCGGCTGGA	KIAA1467	19	139	6	2.5
179	ATGACTGTGTTAGGCGGCTCACGG	TIMM17A	128	915	6	2.5
180	TAGTATGACGCGAGCAGTTCTAAA	SH2D2A	123	871	6	2.5
181	CACTTATCGGGGTCATTCGAGGTC	ZCCHC2	44	310	5	2.5
182	TATCCCCCCTGGAGTCGCAGTCCT	LOC541471	399	2808	5	2.5
183	AATGATGTAGTCCGTCATCCTCAA	LINGO1	3	21	5	2.4
184	TTCCCCGTTCCTAGAAGGGGCAAA	CHRM5	2	14	5	2.4
185	TCCCGAGATTACATTTCAGACAAT	ADA	48	335	5	2.4
186	CGTTCACGTCATAGCGTTCCCGAA	AKR1C2	31	215	5	2.4
187	CAAGAGCTACGATCTACTCCCCCA	NR1D2	47	321	5	2.4
188	GACGGCAACTTCGGGAATCACTAG	PNMT	124	839	5	2.4
189	CACGCCAAAGAAACCTCGAAGCTG	CHCHD7	680	4594	5	2.4
190	AGTAGGTTCAACCGCAAACAGATC	NOA1	19	126	5	2.4
191	GTCAACGACCTAAGGAACTCGTGC	LAIR1	21	138	5	2.4
192	AAAAATGGGCGCTCTGAGACACAC	ZNF680	11	72	5	2.3
193	TGTAGAAGTTTCTGGATAAGCCAC	SLC50A1	130	849	5	2.3
194	GTGCTGACATCTAACCCGTCTAGA	HAND1	62	402	5	2.3
195	TCGTTAGTTGTCAAATGCCAAACC	STK32C	5	32	5	2.3
196	TGTCCCCATCACCATGAGTGCCGT	VMAC	146	933	5	2.3
197	ATGCTGGGAAGCGATAATCGCGTA	BCCIP	44	277	5	2.3
198	CAATCGACGCTAAAGTGACCAGGA	RPL14	158	982	5	2.3
199	TGGCGCATCCTAAAGTGTAAGATT	HSBP1	126	779	5	2.3
200	ATACCCTGTCGGTTGGTCAATCAC	ULK4	8	49	5	2.3
201	CACCTCATGGGGCGTAAGCCCAGG	CA6	168	1028	5	2.2
202	AATGCGTTCGTGACACTTACGCCT	PSMC4	5	30	5	2.2
203	CTTTCAGGTTGCACAGCGGACTTC	PRAMEF10	50	297	5	2.2
204	GTGCCCACCTTTAGACGTAATGGC	PPP1R1A	274	1610	5	2.2
205	TTCATTACCATAACTCGGTGGCCA	CCDC114	48	279	5	2.2
206	TGCTTTCTGCCCCCGTATTAGTAG	HSPB6	130	746	4	2.2
207	CCGTATATTTCTATTTATTTATCG	TGS1	25	141	4	2.1
208	GATTATACTTTCACGTGGACACGA	IGHD	60	337	4	2.1
209	CTGACGTGCCCTAATTCCCTGTGC	NDUFA10	75	421	4	2.1
210	GGACACTACTCCGTAAAGGTACGT	MPZL1	51	285	4	2.1
211	TGACAGTGGCCAGGCGACCCGCCG	LOC339535	17	95	4	2.1
212	GTGCACCCAGGGCCGTGACTGGAG	TMEM25	119	660	4	2.1
213	GTTCCAGTTGCCGCGCCGGGGTGC	NAALADL2	101	556	4	2.1
214	CCTCTGTCACAGGTACTCTCTGTT	CTC1	43	235	4	2.1
215	ATGGGTTCTGTAGGGCCGCCGCAA	ZDHHC15	158	859	4	2.1
216	ATAACCATTGAGGGTAATTTTTAC	C7ORF49	83	450	4	2.1
217	ACCCGAATAACATGTAATCTCCCT	EIF5A	68	364	4	2.1
218	ATAATCAGGGTGTGCCGATCCTGC	PPYR1	76	402	4	2.0

219	TCTTGAACCTCGAGATTATGACTC	SLC25A44	57	299	4	2.0
220	ACTATAGCACACTGAAGGTTTGAA	LIMK2	21	110	4	2.0
221	TATTTAGCACGCAAGAGCCGGAAC	GABRA5	13	68	4	2.0
222	CAAGTCCCGCTACGTGAGCGCCAA	OR2T2	16	83	4	2.0
223	ACACATTGTTACCGCCACGTTGAG	RPL15	83	429	4	2.0
224	GTGGCGCCAAGTCGCAATGGACTC	DNAJC7	12	62	4	2.0
225	CGCACATCAAGTCCCCAGTTCGTG	SYNGR1	141	714	4	2.0
226	GTCTCCTATTTACTACCTCCCTCC	TNFSF18	96	484	4	2.0
227	AGGTTTAAGGCTCCGCATCTAATC	CHCHD2	3	15	4	2.0
228	GGGGGATCTACGATATGACAGGCG	SLC25A22	62	307	4	1.9
229	CCCCCAATCGTGCTCCTTCACCTG	HN1L	52	257	4	1.9
230	TCTCAGCTTTCATATGACGGCCAC	DAP3	34	167	4	1.9
231	AAAAAAGTCGCCATGCCAGAACAA	SEMA4C	29	142	4	1.9
232	TTAAGGGTAACATGGCTACGCACT	UTP23	185	893	4	1.9
233	GCAGGCCTTACTGTACTCCTCAAG	ALG2	137	659	4	1.9
234	CATCTACGCACTTAACAACACTCT	DDX19A	101	483	4	1.9
235	ATCCGACAGTATGCGCCCTAGTGA	ECD	18	86	4	1.9
236	TTGTTCTAGCATATTTTATTACAA	42990	32	151	4	1.9
237	GTCATGATTAGTTTTATACGATGT	CHRM4	14	66	4	1.9
238	GTACTCCTACCTTATTCTCGACCG	DNAJB1	49	231	4	1.9
239	GTGCGGCTGTAGGATGTCGGGCCA	TSPAN15	9	42	4	1.9
240	GGTTCACAGTTTTTGAACTCAACC	CHI3L2	43	200	4	1.9
241	AAACTGTACGAACGTCTATCCGGT	SNAPC2	14	65	4	1.9
242	GGCTCATATTGGCAGGAGAAGAAG	CBFA2T2	130	603	4	1.8
243	ATATGCAGTGAATTAAGGCGATCA	SIVA1	218	998	4	1.8
244	TTCCTAAATACAGTTACCTAACCA	CATSPER4	35	160	4	1.8
245	GGACACGGGCGTGCCCGATTCACG	CCDC65	16	73	4	1.8
246	TCCTCGGTTTCTGACTGATCCCCC	GPR20	60	273	4	1.8
247	CTTTCCGCGGCGGTGGCGCCGTTG	GPER	5	22	3	1.8
248	CTGAAATGTTCCCGTACGGGTACG	CER1	199	875	3	1.8
249	CGATACCATTACCGACTTTCAATC	WISP2	58	254	3	1.8
250	TTCCAATAACGCTAAGACGACGGG	PARVG	55	240	3	1.8
251	GACCTACGAGGTCAGACATACTCG	RPS2	27	117	3	1.8
252	AGGACAGAGCCAACGAAAACGGAT	AIPL1	42	181	3	1.7
253	AGTATCTCTCAGCGAAATAGTGAC	ZCRB1	25	107	3	1.7
254	TACACGATACCCCGTGCTGAGACC	C1ORF87	44	187	3	1.7
255	TGGCCGTGCGGCGTCAATTGTCCA	RAB28	59	250	3	1.7
256	CCAACCCCTACGACAGTCGAGTGC	SUCNR1	225	946	3	1.7
257	AGAGGTTTGCTATCCCGTCCTCCG	EBAG9	114	475	3	1.7
258	ACGTTGCATCCCAAGCTTTGAGAG	CCDC146	72	298	3	1.7
259	TCATGTTACCATGCAAAAGTGATG	NUDT3	134	550	3	1.7
260	GCTCGCCCGCTCGGCTTAGGCTCA	WHAMMP3	29	119	3	1.7
261	TGACTTCAAATGTACGGAAGGTAA	C10ORF125	143	583	3	1.7
262	TGGCCCACCCGCCCTTACGGCATA	C7ORF34	500	2029	3	1.7
263	TGGTCAGTCATACAACAGGCAGAC	EXOC2	2	8	3	1.6

264	CCCATCTACTAGCATTGGGAGGTT	C12ORF4	1	4	3	1.6
265	CGTGCCTCGTCCCGATTTAGCTAT	GPR82	1	4	3	1.6
266	GCCCTCTAAAAATCTACTTCAGCC	TSPYL1	13	51	3	1.6
267	ATCACATGGAGAGCAATGTTGACC	CYCS	574	2244	3	1.6
268	ACCCCCATCCAACTTCCGGATCTA	MFF	11	43	3	1.6
269	CTAAGGACACAGGCTCCACGAAAT	CPA3	111	432	3	1.6
270	CTCTGAGACGCTGCAATCGACGAT	TMEM35	224	869	3	1.6
271	ACCTAGTCTGGCCTCACGTTAAGG	TMOD3	156	605	3	1.6
272	GCACGGCCCGTAGCCCTATCGCCC	FAM27L	71	272	3	1.6
273	TCTCAATACCCAATGCCCTTTTTG	ATG10	181	684	3	1.6
274	GCACAGTCTCAGAGTGCCACAACC	TAS2R3	331	1247	3	1.5
275	TGTGGTTCTCGGCCTTCACAGGTC	RPL14	240	899	3	1.5
276	CCAAGGACAAAGTCTAGAGAGCCT	EIF4E2	69	256	3	1.5
277	TATTACCGGGCCGTATTAGTTGAA	TEX2	31	115	3	1.5
278	CTTAAAACAACCCATCCTCCGGTG	PRAF2	102	375	3	1.5
279	GTGACGGTAGCCACATGTTCCTGC	RPL19	151	554	3	1.5
280	AGCTTAGCACTATAGGTAGCTATC	OSTM1	3	11	3	1.5
281	GCGGAGATACGACCCTACCACACC	COX4I2	232	846	3	1.5
282	CGCGGTAAGCACCTCATGCGCCGC	CEPT1	70	254	3	1.5
283	ACATCAGTACCCCCGCAGATCGTC	DMWD	128	463	3	1.5
284	TTCGCTAATCATTAAAAAAACGGA	NAGS	29	104	3	1.5
285	CGGACTTCGCGTGCGTAGGTCTTC	FGR	7	25	3	1.5
286	GCAATAACTGAACTTGTACAATAA	TYRP1	42	149	3	1.5
287	GCCGCTTTTGGATGTACCGAGTTG	C17ORF53	58	205	3	1.5
288	TGCCGCCATCCGATTAAGTCCCAT	TRIM13	31	109	3	1.4
289	TCGTAACGCCAGGTATCTCGGGTA	PCK1	4	14	3	1.4
290	CGAACTACTTACCTAATCGTGGGA	MST1R	141	493	3	1.4
291	CTTGTTCGTCGTGTTAGGATCGTT	CCDC42	70	244	3	1.4
292	TAAAGTCTGCATATGCCAAGCTGG	SNAP47	188	645	3	1.4
293	TTTTTAGACCATACGTGGGATTTT	GSTA1	14	48	3	1.4
294	CAACCTGAGAGTGTTGACCGAAGA	C14ORF79	319	1074	3	1.4
295	TGATAGCCGAGTGACCACCTTTTT	NRIP3	196	656	3	1.4
296	TAACCAACTCCCCTGTGCTCTGGG	SEC61B	86	287	3	1.4
297	GGCTTATTAGGACTCATCGCGCCC	TXLNA	3	10	3	1.4
298	TTTCTTGGCTTGCACTGTGACCGC	NUDT14	99	330	3	1.4
299	CCCAGTGGGGTCCGGGTCAACTCG	TMEM206	16	53	3	1.4
300	ATCATTCGCACAACCACGAACTCA	CCL4	1293	4240	3	1.3
301	AAAACGCGAACATGTACCTCGCAC	DGUOK	31	101	3	1.3
302	TGCCTTGCCGTAGTCAAACTCACC	ZNF416	8	26	3	1.3
303	AACGCCAAACCATATGCACCGTCC	C3AR1	56	182	3	1.3
304	AAGTCTATCAAAAGTCCCATCACT	ACPP	30	97	3	1.3
305	GCTGACCAGAAACTCTGACTATTT	LACRT	220	708	2	1.3
306	ATCACAGGCGGCGTAGCCGACCCG	BMS1P5	253	813	2	1.3
307	GATGCGGTGTGACGGATGTTCCCA	GOLGA7	183	587	2	1.3
308	GATTTGCACCTTAGACAGGGGGTC	TOLLIP	118	376	2	1.3

309	ACAGGTGTTTTGGCCGACTACTAA	C15ORF53	102	325	2	1.3
310	ATCCAAATGCGCGCCAGTTGCCTA	MRPS11	170	530	2	1.3
311	TCAGGGACACTTACAAGCCGGCGT	LINC00518	103	321	2	1.3
312	ATCAGACACGCCTATCCTACGAGG	SPATA8	161	501	2	1.3
313	GCTGCTAGCTATCAAGTTAAAATT	C22ORF31	53	162	2	1.2
314	CCGGCGTACCTCCTACCTAACATT	MRPL43	126	383	2	1.2
315	AAATCCTAGTAACGCCCCAATATA	RIMKLA	56	168	2	1.2
316	TCTCAATATACGGCGGTAAGTGCG	NANOG	1	3	2	1.2
317	CTTGTACGTCAGTAGATCATTTTC	WDR18	1	3	2	1.2
318	TGTCTCGTCCCATTAAAGGTGTCG	TREML2	1	3	2	1.2
319	CCTGGACACAATCTCTGCAAATTA	JPH1	25	74	2	1.2
320	TGCAGCTTTACAACATGCACTCTG	PDE6D	136	401	2	1.2
321	TTCGACGTAGATCTATGGGCGTGC	ANKRD49	70	206	2	1.2
322	CGTGTTGAAGCGCTGCGCAGTTTG	NPR3	82	240	2	1.2
323	GAAAACAGTATACCGCTGCCGACG	TRIB2	24	70	2	1.2
324	GTGTCATGCCCCCCGTTTACCGTT	PPIE	24	70	2	1.2
325	AAATTACCTACGATATTCCTATGA	GPR162	71	207	2	1.2
326	CTTGACCCATCCGACATATTACTC	MB21D1	101	294	2	1.2
327	CAGAGTACTCCGAGACTACAGGTC	C2ORF73	138	399	2	1.2
328	GTTGGCCATCACCTACGCAATTAC	CCDC28B	226	638	2	1.1
329	TCGATGTTAACGCCTCGAGCACTT	SLC25A10	106	299	2	1.1
330	GGACCCGAACGTCACTGCTATACC	DAD1	9	25	2	1.1
331	GAGACGCCGTACGACATTTTTAAA	PPIL1	28	76	2	1.1
332	GGCGAACTGTGAGTTTGTTGCACC	IL28A	258	684	2	1.0
333	TAGCGCTCCGCATCATCGACTTGC	TXNDC11	74	195	2	1.0
334	AAATTTGTATGCCACCGTCGCCTA	***FGF6***	352	921	2	1.0
335	TACTAAATTCACTGAAACCATTAC	***IL17A***	504	1309	2	1.0

Table 3-4. Enriched ORFs in PDL1 sorted population.

Gene Family Annotation	Cytokines and growth factors	Transcription factors	Homeodomain proteins	Cell differentiation markers	Protein kinases	Translocated cancer genes	Oncogenes	Tumor suppressors
Tumor suppressors	0	0	0	0	0	0	0	0
Oncogenes	0	1	0	0	0	3	3	
Translocated cancer genes	0	1	0	0	0	3		
Protein kinases	0	0	0	1	12			
Cell differentiation markers	1	0	0	7				
Homeodomain proteins	0	5	5					
Transcription factors	0	20						
Cytokines and growth factors	18							

Table 3-5. Gene family annotation for ORFs enriched>2fold.

Enriched Gene Set Name	# Genes in Gene Set (K)	# Genes in Overlap (k)	p-value	FDR q-value
GO_RESPONSE_TO_EXTERNAL_STIMULUS	1821	43	2.99E-12	6.63E-09
GO_CELL_CELL_SIGNALING	767	26	4.44E-11	4.93E-08
GO_REGULATION_OF_RESPONSE_TO_STRESS	1468	36	7.36E-11	5.44E-08
GO_REGULATION_OF_IMMUNE_SYSTEM_PROCESS	1403	34	3.50E-10	1.55E-07
HALLMARK_MYC_TARGETS_V1	200	7	5.31E-04	1.33E-02
HALLMARK_TNFA_SIGNALING_VIA_NFKB	200	7	5.31E-04	1.33E-02

Table 3-6. Gene set enrichment analysis for ORFs enriches >2 fold.

Bibliography

1. Massano, J., et al., Oral squamous cell carcinoma: review of prognostic and predictive factors. Oral Surg Oral Med Oral Pathol Oral Radiol Endod, 2006. 102(1): p. 67-76.
2. Koul, D., et al., Antitumor activity of NVP-BKM120--a selective pan class I PI3 kinase inhibitor showed differential forms of cell death based on p53 status of glioma cells. Clin Cancer Res, 2012. 18(1): p. 184-95.
3. Michaud, K., et al., Pharmacologic inhibition of cyclin-dependent kinases 4 and 6 arrests the growth of glioblastoma multiforme intracranial xenografts. Cancer Res, 2010. 70(8): p. 3228-38.
4. Burger, M.T., et al., Identification of NVP-BKM120 as a Potent, Selective, Orally Bioavailable Class I PI3 Kinase Inhibitor for Treating Cancer. ACS Med Chem Lett, 2011. 2(10): p. 774-9.
5. The Cancer Genome Atlas, N., et al., Comprehensive genomic characterization of head and neck squamous cell carcinomas. Nature, 2015. 517: p. 576.
6. Alexandrov, L.B., et al., Signatures of mutational processes in human cancer. Nature, 2013. 500: p. 415.
7. Cohen, E.E.W., et al., Pembrolizumab versus methotrexate, docetaxel, or cetuximab for recurrent or metastatic head-and-neck squamous cell carcinoma (KEYNOTE-040): a randomised, open-label, phase 3 study. Lancet, 2019. 393(10167): p. 156-167.
8. Bauml, J., et al., Pembrolizumab for Platinum- and Cetuximab-Refractory Head and Neck Cancer: Results From a Single-Arm, Phase II Study. J Clin Oncol, 2017. 35(14): p. 1542-1549.
9. Mehra, R., et al., Efficacy and safety of pembrolizumab in recurrent/metastatic head and neck squamous cell carcinoma: pooled analyses after long-term follow-up in KEYNOTE-012. Br J Cancer, 2018. 119(2): p. 153-159.
10. Ferris, R.L., et al., Nivolumab for Recurrent Squamous-Cell Carcinoma of the Head and Neck. N Engl J Med, 2016. 375(19): p. 1856-1867.
11. Concha-Benavente, F., et al., Identification of the Cell-Intrinsic and -Extrinsic Pathways Downstream of EGFR and IFNgamma That Induce PD-L1 Expression in Head and Neck Cancer. Cancer Res, 2016. 76(5): p. 1031-43.
12. Bu, L.L., et al., STAT3 Induces Immunosuppression by Upregulating PD-1/PD-L1 in HNSCC. J Dent Res, 2017. 96(9): p. 1027-1034.
13. Steuer, C.E., et al., A Correlative Analysis of PD-L1, PD-1, PD-L2, EGFR, HER2, and HER3 Expression in Oropharyngeal Squamous Cell Carcinoma. Mol Cancer Ther, 2018. 17(3): p. 710-716.
14. Gupta, D., et al., CRISPR-Cas9 system: A new-fangled dawn in gene editing. Life Sciences, 2019. 232: p. 116636.
15. Brenner, J.C., et al., Genotyping of 73 UM-SCC head and neck squamous cell carcinoma cell lines. Head Neck, 2010. 32(4): p. 417-26.
16. Ludwig, M.L., et al., The genomic landscape of UM-SCC oral cavity squamous cell carcinoma cell lines. Oral Oncol, 2018. 87: p. 144-151.
17. Badoual, C., et al., PD-1–Expressing Tumor-Infiltrating T Cells Are a Favorable Prognostic Biomarker in HPV-Associated Head and Neck Cancer. Cancer Research, 2013. 73(1): p. 128-138.

18. Tillman, B.N., et al., Fibroblast growth factor family aberrations as a putative driver of head and neck squamous cell carcinoma in an epidemiologically low-risk patient as defined by targeted sequencing. Head Neck, 2016. 38 Suppl 1: p. E1646-52.
19. Michmerhuizen N.M., L.E., Kulkarni A., Brenner J.C., Differential Compensation mechanisms Define Resistance to PI3K inhibitors in PIK3CA amplified HNSCC. Oto. Head and Neck Surgery, 2016(NIHMS799178).
20. Ma, Y.F., et al., Targeting of interleukin (IL)-17A inhibits PDL1 expression in tumor cells and induces anticancer immunity in an estrogen receptor-negative murine model of breast cancer. Oncotarget, 2017. 8(5): p. 7614-7624.
21. Akbay, E.A., et al., Interleukin-17A Promotes Lung Tumor Progression through Neutrophil Attraction to Tumor Sites and Mediating Resistance to PD-1 Blockade. Journal of thoracic oncology : official publication of the International Association for the Study of Lung Cancer, 2017. 12(8): p. 1268-1279.
22. Babina, I.S. and N.C. Turner, Advances and challenges in targeting FGFR signalling in cancer. Nature Reviews Cancer, 2017. 17(5): p. 318-332.
23. Wernig, G., et al., Efficacy of TG101348, a selective JAK2 inhibitor, in treatment of a murine model of JAK2V617F-induced polycythemia vera. Cancer Cell, 2008. 13(4): p. 311-20.
24. Tillman, B.N., et al., Fibroblast growth factor family aberrations as a putative driver of head and neck squamous cell carcinoma in an epidemiologically low-risk patient as defined by targeted sequencing. Head Neck, 2016. 38 Suppl 1: p. E1646-52.
25. Koole, K., et al., FGFR Family Members Protein Expression as Prognostic Markers in Oral Cavity and Oropharyngeal Squamous Cell Carcinoma. Molecular Diagnosis & Therapy, 2016. 20(4): p. 363-374.
26. Olsen, S.K., et al., Fibroblast Growth Factor (FGF) Homologous Factors Share Structural but Not Functional Homology with FGFs. 2003. 278(36): p. 34226-34236.
27. Cao, Y., R. Cao, and E.-M.J.J.o.M.M. Hedlund, R Regulation of tumor angiogenesis and metastasis by FGF and PDGF signaling pathways. 2008. 86(7): p. 785-789.
28. Marshall, M.E., et al., Fibroblast growth factor receptors are components of autocrine signaling networks in head and neck squamous cell carcinoma cells. Clinical cancer research : an official journal of the American Association for Cancer Research, 2011. 17(15): p. 5016-5025.
29. Guagnano, V., et al., Discovery of 3-(2,6-dichloro-3,5-dimethoxy-phenyl)-1-{6-[4-(4-ethyl-piperazin-1-yl)-phenylamin o]-pyrimidin-4-yl}-1-methyl-urea (NVP-BGJ398), a potent and selective inhibitor of the fibroblast growth factor receptor family of receptor tyrosine kinase. J Med Chem, 2011. 54(20): p. 7066-83.
30. Mohammadi, M., et al., Crystal structure of an angiogenesis inhibitor bound to the FGF receptor tyrosine kinase domain. 1998. 17(20): p. 5896-5904.
31. Song, M.M. and K. Shuai, The Suppressor of Cytokine Signaling (SOCS) 1 and SOCS3 but Not SOCS2 Proteins Inhibit Interferon-mediated Antiviral and Antiproliferative Activities. 1998. 273(52): p. 35056-35062.
32. Li, C.-W., et al., Glycosylation and stabilization of programmed death ligand-1 suppresses T-cell activity. Nature Communications, 2016. 7(1): p. 12632.
33. Kramer, R., et al., Inhibition of N-linked glycosylation of P-glycoprotein by tunicamycin results in a reduced multidrug resistance phenotype. Br J Cancer, 1995. 71(4): p. 670-5.
34. Li, C.W., et al., Eradication of Triple-Negative Breast Cancer Cells by Targeting Glycosylated PD-L1. Cancer Cell, 2018. 33(2): p. 187-201.e10.

35. Mann, J.E., et al., Analysis of tumor-infiltrating CD103 resident memory T-cell content in recurrent laryngeal squamous cell carcinoma. Cancer Immunol Immunother, 2019. 68(2):213-220.
36. Hoesli, R., et al., Proportion of CD4 and CD8 tumor infiltrating lymphocytes predicts survival in persistent/recurrent laryngeal squamous cell carcinoma. Oral Oncol, 2018. 77: p. 83-89.
37. Mann, J.E., et al., Surveilling the Potential for Precision Medicine-driven PD-1/PD-L1-targeted Therapy in HNSCC. J Cancer, 2017. 8(3): p. 332-344.
38. De Costa, A.M., et al., Characterization of the evolution of immune phenotype during the development and progression of squamous cell carcinoma of the head and neck. Cancer Immunol Immunother, 2012. 61(6): p. 927-39.
39. de Medeiros, M.C., et al., HNSCC subverts PBMCs to secrete soluble products that promote tumor cell proliferation. Oncotarget, 2017. 8(37): p. 60860-60874.
40. Kesselring, R., et al., Human Th17 cells can be induced through head and neck cancer and have a functional impact on HNSCC development. Br J Cancer, 2010. 103(8): p. 1245-54.
41. Nam, S.J., et al., Tumor-infiltrating immune cell subpopulations and programmed death ligand 1 (PD-L1) expression associated with clinicopathological and prognostic parameters in ependymoma. Cancer Immunol Immunother, 2018.
42. Lin, K., et al., EGFR-TKI down-regulates PD-L1 in EGFR mutant NSCLC through inhibiting NF-kappaB. Biochem Biophys Res Commun, 2015. 463(1-2): p. 95-101.
43. Grinberg-Bleyer, Y. and S. Ghosh, A Novel Link between Inflammation and Cancer. Cancer Cell, 2016. 30(6): p. 829-830.
44. Lim, S.O., et al., Deubiquitination and Stabilization of PD-L1 by CSN5. Cancer Cell, 2016. 30(6): p. 925-939.
45. Xue, J., et al., Type Igamma phosphatidylinositol phosphate kinase regulates PD-L1 expression by activating NF-kappaB. Oncotarget, 2017. 8(26): p. 42414-42427.
46. Gowrishankar, K., et al., Inducible but not constitutive expression of PD-L1 in human melanoma cells is dependent on activation of NF-kappaB. PLoS One, 2015. 10(4): p. e0123410.
47. Gillison, M.L., et al., Human papillomavirus and the landscape of secondary genetic alterations in oral cancers. Genome Res, 2019. 29(1): p. 1-17.
48. Brands, R.C., et al., Targeting VEGFR and FGFR in head and neck squamous cell carcinoma in vitro. Oncol Rep, 2017. 38(3): p. 1877-1885.
49. Sweeny, L., et al., Inhibition of fibroblasts reduced head and neck cancer growth by targeting fibroblast growth factor receptor. Laryngoscope, 2012. 122(7): p. 1539-44.
50. Koole, K., et al., FGFR Family Members Protein Expression as Prognostic Markers in Oral Cavity and Oropharyngeal Squamous Cell Carcinoma. Mol Diagn Ther, 2016. 20(4): p. 363-74.
51. Koole, K., et al., FGFR1 Is a Potential Prognostic Biomarker and Therapeutic Target in Head and Neck Squamous Cell Carcinoma. Clin Cancer Res, 2016. 22(15): p. 3884-93.
52. McDermott, S.C., et al., FGFR signaling regulates resistance of head and neck cancer stem cells to cisplatin. Oncotarget, 2018. 9(38): p. 25148-25165.

Chapter 4 Validation of a genome-scale CRISPR knockout screening protocol for identification of regulators of PDL1

Abstract

The immunosuppressive molecule PDL1 is expressed in HNSCC tumors and is a target for immunotherapy. Recent reports show that activity of known oncogenes can influence PDL1. Thus, we aimed to better understand the molecular underpinnings of PDL1 expression in HNSCC. We utilized a genome-scale CRISPR library and selected cells with diminished or enhance PDL1 expression to identify genetic knockouts conferring PDL1 up- or down-regulation. We successfully selected cells with altered PDL1 expression phenotypes, and validated that one of the candidate genes nominated by the screen, TLR2, can modulate PDL1.

Introduction

The ligation of PD-1 expressed on T-lymphocytes with PDL1, expressed on the surface of tumor cells, leads to repression of anti-tumor immunity and represents an essential target for immunotherapy. Previous studies have shown that PDL1 expression on the surface of tumors is induced in response to interferon gamma (IFNγ) released by T-lymphocytes, and that this induction relies on Jak2/Stat1 mediated transcription in HNSCC[1, 2]. More recently, other signals modulating the expression of PDL1 have been identified. Notably, in head and neck squamous cell carcinoma (HNSCC) cell lines, epidermal growth factor receptor (EGFR) activation was shown to positively regulate PDL1 expression on the cell surface [1]. Furthermore, EGFR is a known driver of HNSCC and RNA expression of PDL1 correlated with

that of EGFR in 23 tumor specimens [1]. Such observations led us to question whether additional pathways, including other oncogenic and pro-inflammatory signals, may contribute to immune escape via PDL1 upregulation, and whether these signals could be targeted to enhance response rates to immunotherapy.

Historically, large scale screening techniques such as those employing RNAi have yielded disappointing results due in part to technical challenges including lack of specificity [3]. Upon the discovery and advancement of CRISPR technology, however, new methods and applications for genome-scale functional screening have rapidly arisen [4]. In 2014, Shalem et al and Wang et al simultaneously published two of the first genome-scale screens utilizing a library of CRISPR constructs to generate pools of genetic knockouts in cultured cells [5, 6]. Since then, the field has rapidly expanded with diverse applications of this technology, from identifying genes essential for cell proliferation to nominating pathways conferring for resistance to therapies. Thus, CRISPR library screening represents a valuable tool to expand our understanding of various pathways. In the present study, we sought a more detailed understanding of the mechanisms regulating the expression of PDL1 in an effort to improve responses to therapies and identify new biomarkers for response. The Genome-scale CRISPR Knock-Out (GeCKO) v2 library consists of ~60,000 gRNAs designed to target Cas9 to over 19,000 different genes [7]. Using this library to generate a pool of genetic knockouts in HNSCC cell lines, we have validated a protocol for selecting cells with altered cell-surface PDL1 expression.

Materials and methods:

Cell culture: Cell lines were maintained in logarithmic growth phase in Dulbecco's Modified Eagle's Medium (DMEM) (Gibco #11965) containing 10% fetal bovine serum (FBS, Sigma), 1% NEAA (Gibco #15140122) and 7 μL/mL penicillin-streptomycin (Gibco #15140122) in a humidified atmosphere of 5% CO2 at 37°C. Cells were tested for mycoplasma contamination using the MycoAlert detection kit (Lonza).

Transduction of UM-SCC cell lines with Genome-scale CRISPR knock-out library: UM-SCC lines were transduced with the Human GeCKO CRISPR knockout pooled library version 2 (Addgene plasmid #52961). Conditions for transduction were established for a multiplicity of infection (MOI) of 0.3. Cells were subjected to 7 days of puromycin selection, then expanded and seeded for treatment and flow cytometry. To preserve at least 300x coverage, 30 million cells were seeded per treatment. Upon selection of the final populations of cells for sequencing, genomic DNA was extracted from the remaining cells using Gentra Puregene Cell Kit (Qiagen).

Treatment and staining of GeCKO library cell line for cell sorting: UM-SCC-49 GeCKO cells were seeded at 30 million per condition. 18h after seeding, media was replaced with plain media (Control) or media containing 10ng/mL IFNγ. After 72h incubation, cells were trypsinized and counted, and 30 million cells were incubated with a monoclonal antibody directed against PDL1 (ThermoFisher #14-5983-82) diluted to 1ug/mL in HBSS (Gibco) for 15 min in a suspension of 1 million cells per mL. 500,000 cells were also incubated without primary antibody as a control. Control and PDL1 stained cells were pelleted and resuspended in PE-conjugated rat anti-mouse secondary antibody (ThermoFisher #12-4015-82) diluted to 0.2ug/mL in HBSS. After 15 minute

incubation, cells were pelleted, resuspended at 2 million cells per mL in HBSS plus 0.5% FBS, and transported on ice for flow cytometry.

Serial cell sorting: Flow cytometry analysis and sorting was performed using an iCyt Synergy cell sorter (Sony Biotechnology) at the University of Michigan Flow Cytometry Core facility. A secondary antibody- only control was first analyzed to delineate positive vs. negative PDL1 immunostaining. For the first sort of the UM-SCC-49 GeCKO pool, gates were drawn to select the 10% of cells with lowest PE fluorescence ($PDL1^{low}$) and 10% with highest ($PDL1^{high}$). These populations were expanded separately in culture to 30 million cells each, then immunostained as above and subjected to cell sorting again, selecting the lowest 10% of cells from $PDL1^{low}$ and highest 10% of cells from $PDL1^{high}$. Again, these cells were expanded to 30 million in culture, immunostained for PDL1, and analyzed by flow cytometry a third time to ensure divergent phenotypes. "Positive" and "Negative" gates were drawn based on 0.1% and 99% of the control, respectively. At this point, all PDL1-negative ($PDL1^{low}$) and all PDL1-positive ($PDL1^{high}$) cells were selected. Following expansion in culture, genomic DNA was harvested from these final populations, as well as the initial unsorted UM-SCC-49 GeCKO pool.

GeCKO library preparation: Genomic DNA was extracted from the UM-SCC-49 GeCKO pools cells using the Gentra Puregene Cell Kit (Qiagen). 130ug genomic DNA per sample was divided into 13 reactions with 10ug input each and used to PCR amplify gRNA sequences using Herculase II Fusion DNA Polymerase (Agilent #600675). `The following primer sequences were used: Forward = AATGGACTATCATATGCTTACCGTAACTTGAAAGTATTTCG; Reverse = GGTCTTGAAAGGAGTGGGAATTGGCTCCGGTGCCCGTCAG.

The 13 reactions were combined, and 5 μL were used as input for the second round PCR reactions (4 reactions per sample) with the following primers to add sequencing adapters and barcodes to the PCR products: Forward= AATGATACGGCGACCACCGAGATCTACACTCTTTCCCTACACGACGCTCTTCCGATCT(1-9bp stagger)AAGTAGAGtcttgtggaaaggacgaaacaccg. Reverse= CAAGCAGAAGACGGCATACGAGATTCGCCTTAGTGACTGGAGTTCAGACGTGTGCTCTTCCGATCTataacggactagccttattttaac. The underlined sequence in the Forward primer indicates a representative 8 base pair barcode, which was different for each sample (control, $PDL1^{high}$, $PDL1^{low}$). Uppercase sequence indicates Illumina adapters. The forward primer contains the TruSeq Universal adapter, and the reverse primer consists of Illumina P7, 8 base pair index, and multiplexing PCR primer 2.0. Lowercase sequence indicates the priming sites for the lentiviral construct.

The PCR products were extracted and purified using Gel Extraction PCR Purification Kit (Qiagen) before submission to the University of Michigan DNA Sequencing Core for sequencing with Illumina MiSeq V3 Kit.*Analysis of CRISPR libraries:* Reads were demultiplexed by barcode and then mapped to the corresponding reference library using an in-house python script. We did not consider gRNAs represented by fewer than ten reads for further analysis. Read counts were normalized to the total number of reads for a given sample and the read count for each gRNA was then computed relative to the read count in the control to determine relative abundance in the sorted populations vs control.

SiRNA transfection: ON-TARGETplus siRNA SMARTpools were purchased from Horizon Discovery (TLR2, L-005120-01-0005; RELA, L-003533-00-0005; GAPD, L-004253-00-0005).

Non-targeting siRNA was purchased from Horizon Discovery (D-001810-02-05). Cells were seeded in six-well dishes at 100,000 cells per well. 18h post seeding, cells were serum starved for 3h, followed by transfection with 5uM siRNA per well with oligofectamine (Invitrogen #12252011) in a total of 1mL of OptiMEM (Gibco). After 6h, an additional 1mL standard media was added. For qPCR analysis, cells were harvested in 700uL QiaZOL (Qiagen) 24h after initial transfection. For analysis of PDL1 protein, cells were treated as indicated for an additional 48h, then total protein lysate was collected.

Cell line transcriptome analysis: RNA sequencing was performed for 43 HNSCC cell lines using Illumina stranded transcriptome library preparation kits as described in [8]. Heatmaps were generated using MeV software version 4.9 based on log_2(FPKM+1) values.

TCGA transcriptome analysis. Log_2(RSEM+1) values from TCGA Head and Neck Cancer cohort (n=566) were retrieved from the UCSC cancer genomics browser (xenabrowser.net). Correlations were calculated using Pearson r test, and linear regressions and box and whisker plots were generated using GraphPad Prism 8 software.

Western blotting: Cells were rinsed twice with ice cold PBS and lysed in a modified RIPA lysis buffer (150mM NaCl, 50mM Tris pH 8.0, 1mM PIPES, 1mM MgCl, 10% Glycerol, 1%NP40, 0.1% Triton X100) with HALT protease and phosphatase inhibitor cocktails (Thermo 186129, 1861277). Cells were spun at 14,000 rpm for 15 min and protein was quantified by BCA assay (Pierce). Separation by SDS-PAGE was performed and the antibodies were used for visualization of target proteins were purchased from Cell Signaling Technology as follows: PDL1 (#13684), β-actin (#4970), NFkB p65 (#8242), phospho(Ser-536)-NFkB p65 (#3033).

qPCR: RNA extraction from cell lysates preserved in QiaZOL was performed using RNeasy Spin Kit (Qiagen) according to manufacturer recommendations. cDNA templates were then synthesized using random primers and SuperScript III Reverse Transcriptase VILO kit (Invitrogen) according to manufacturer recommendations. Primers used for qPCR analysis are listed in Table 4-1. Amplification by qPCR was performed with Quantitect Sybr Green (Qiagen) on QuantStudio5 (Applied Biosystems) under the cycling conditions recommended by manufacturer.

Results

Selection of PDL1^{high} and PDL1^{low} cells

We elected to use a positive selection screening model to enrich for deficient or enhanced PDL1 expression (Figure 4-1A). UM-SCC-49 cells were transduced with the GeCKO v2A CRISPR library and subjected to puromycin selection. To identify genetic knockouts conferring altered PDL1 expression on the cell surface, we stained an IFNγ treated UM-SCC-49 GeCKO pool using a PE-tagged antibody directed against PDL1 and used flow cytometry to select cells with the highest (PDL1^{high}) and lowest (PDL1^{low}) PE fluorescence (Figure 4-1B). The selected populations were then expanded separately in culture. To enrich each population for the desired phenotype, we subjected each to further sorting by flow cytometry, selecting the 10% of cells with highest and lowest PE fluorescence for PDL1^{high} and PDL1^{low} populations, respectively. After expanding the final population in culture, sorting was repeated a second time for a total of three sorts. We validated successful enrichment for PDL1^{high} and PDL1^{low} phenotypes by comparing PE fluorescence in each of the final populations to each other and to an unsorted control pool. The unsorted UM-SCC-49-GeCKO pool stained for PDL1 surface expression

exhibited a median fluorescence intensity (MFI) equal to 100, with 16% of cells expressing PDL1 based on comparison to a control stained with secondary antibody only. PDL1^{low} cells exhibited a similar phenotype, with 17% expressing PDL1 (MFI=90.8) in response to IFNγ. In contrast, 99% of PDL1^{high} cells expressed PDL1 (MFI=813). These data are summarized in Figure 4-2B. Because it was not apparent from this analysis that PDL1^{low} had diverged phenotypically from the control population, we generated clonal cell lines from single cells isolated from the PDL1^{low} pool (Figure 4-2C). We found that these cell lines had dramatically diminished ability to upregulate PDL1 expression in response to IFNγ, indicating that we had indeed selected individual cells with dysregulated PDL1.

Next, barcodes from the initial UM-SCC-49 GeCKO library pool (control), PDL1^{high} pool, and PDL1^{low} pool were analyzed to determine enrichment of specific knockouts in sorted populations over the control. In the control pool, 44,892 gRNAs were identified (70% library coverage). Sequencing of barcodes from PDL1^{high} and PDL1^{low} pools identified 9922 (16% library coverage) and 7162 gRNAs (11% library coverage), respectively (Figure 4-3A). Distributions of reads across the detected gRNAs for each pool is shown in Figure 4-3B-D, and indicate that in the sorted populations, the majority of reads represent only a small proportion of gRNAs.

We set an arbitrary cutoff and only included gRNAs for which normalized read counts were greater than or equal to 10, and found that of these, 34% overlapped between PDL1^{high} and PDL1^{low}. We were surprised to find a large number of hits overlapping between the PDL1^{high} and PDL1^{low} pools. Because of this high degree of overlap, we next attempted to identify hits for which representation was enriched over the control pool in only one of the selected populations. gRNAs enriched >1.5x over the control in either sorted population are reported in Table 4-2

(PDL1^{Low}) and Table 4-3 (PDL1^{high}). In our final gRNA lists, we observed an interesting reciprocal relationship between some of the top hits in the PDL1^{high} and PDL1^{low} pools. A gRNA targeting Toll Like Receptor 2 (TLR2) was among the most abundant in the PDL1^{high} pool, while gRNAs targeting mir-105-1 and mir-105-2, thought to negatively regulate toll like receptors [9], were enriched in PDL1^{low}. Thus, we hypothesized that TLR2 may positively regulate PDL1 expression.

We therefore asked whether PDL1 and TLR2 were co-expressed in HNSCC tumors. We interrogated the TCGA HNSC dataset (n=566, https://www.cancer.gov/tcga) to assess RNA expression in human tumor samples. As expected, we found that expression of JAK2, a known driver of PDL1 downstream of IFNγ, correlates strongly with PDL1 expression in HNSCC (Pearson $r = 0.58$, $p < 0.0001$; Figure 4-4A). We also discovered a positive, albeit weaker, correlation between TLR2 and PDL1 (Pearson $r = 0.32$, $p < 0.0001$; Figure 4-4B). Hypothesizing that TLR2 may represent one of multiple signals converging on a downstream regulator of PDL1, we also noted that expression of other TLRs, including TLR7 and TLR8 (Figure 4-4C,D), correlated positively with that of PDL1. Because several TLRs, including those mentioned above, signal through Myd88, we also assessed whether PDL1 expression correlated with Myd88 expression and again identified a positive correlation (Pearson $r = 0.42$, $p < 0.0001$; Figure 4-4E). A correlation between Myd88 and PDL1 RNA expression was also observed in HNSCC cell lines (n=43; Pearson $r = 0.50$, $p = 0.0006$; Figure 4-4F), although no correlation between TLRs and PDL1 expression was evident in this dataset (not shown).

While these observations suggest a potential relationship between TLR activity and expression of PDL1, it is also possible that TLR upregulation and PDL1 expression are simply co-occurring features indicating elevated immune activity in the tumor microenvironment, as

PDL1 expression is often increased in inflamed tissues [10]. Thus, we sought to establish a causal link between TLR2 and PDL1 in cell lines. To validate that modulation of TLR2 can influence PDL1 expression, we knocked down TLR2 expression via siRNA (Figure 4-5A) and assessed PDL1 expression by immunoblot following treatment with IFNγ. We noted a decrease in the ability of IFNγ to induce PDL1 expression when TLR2 expression was diminished, indicating that our screening protocol successfully identified a gene capable of modulating PDL1 expression in UM-SCC-49 (Figure 4-5B). This decrease is quantified in Figure 4-5C.

We next sought to understand whether TLR2 could be activated to induce PDL1 expression. Pam3CSK4 is a synthetic lipopeptide that acts as a specific TLR1/2 agonist [11]. We treated wild-type UM-SCC-49 cells with Pam3CSK4, for 72h and observed no significant increase in total PDL1 expression evaluated by immunoblot (Figure 4-6A). However, when Pam3CSK4 was given simultaneously with IFNγ, the ability of IFNγ to induce PDL1 expression was enhanced (Figure 4-6A, quantified in 4-6B). Because activation of TLR2 is known to induce phosphorylation and activation of the p65 subunit of NFκB (also called RelA) [12], we also assessed phosphorylation of p65 on Serine 536 by immunoblot. We observed small increases in phosphorylated p65 in response to Pam3CSK4 or IFNγ alone, but a greater induction was observed with the combination. A modest increase in total p65 protein was also observed only in response to the combination.

Next, we considered the role of TLR2 in initiating an immune response. TLRs recognize pathogen associated molecular patterns (PAMPs) and initiate signaling cascades to drive various aspects of immune response, including production of pro-inflammatory cytokines. Previously, Wang et al showed that TLR2 is activated and PDL1 expression is increased following incubation of human monocytes with heat-killed Staphylococcus aureus (*S. aureus*) in culture

[13]. Given that HNSCC often arises in tissues with high exposure to pathogens, such as the oral cavity, we postulated that TLR2 may modulate PDL1 expression following activation by bacterial ligands. We therefore assessed total PDL1 protein in UM-SCC-49 cells treated with *S. aureus*, and found that indeed, *S. aureus* can induce expression of PDL1 (Figure 4-6C). Furthermore, *S. aureus* induced phosphorylation of p65, which has previously been described as an effector of TLR2 and as a driver of PDL1 in other models [14]. We therefore analyzed a small panel of IFNγ regulated and p65-regulated effectors, and showed that cells treated with Pam3CSK4 and *S. aureus* showed induction of p65 target IL6, but interestingly, there was minimal induction of PDL1 transcript expression in the absence of IFNγ. IFNγ appears to induce a distinct transcriptional profile at this time point, including HLAB and SOCS1 (Figure 4-6D, E).

We next examined the ability of TLR2 to regulate PDL1 in other HNSCC models. First, we assessed RNA expression of all TLRs in 43 HNSCC cell lines by RNAseq. TLR1, 2, 3, 4, and 6 were the most highly expressed (Figure 4-7A). We then tested several UM-SCC cell lines for PDL1 upregulation in response to either Pam3CSK4 or *S. aureus*, and discovered varying responses to these stimuli. UM-SCC-58, 59, and 97 are shown to represent the spectrum of responses (Figure 4-7B-D). UM-SCC-58, which exhibited lower expression of most TLRs, showed no increase in PDL1 expression in response to *S. aureus* or Pam3CSK4, although we observed similar results in UM-SCC-14a, which does express TLR2 mRNA. UM-SCC-59 appears to upregulate PDL1 in response to *S. aureus* but not the TLR2 specific agonist Pam3CSK4, suggesting that a different receptor might mediate this response. UM-SCC-97 modestly upregulates PDL1 in response to both *S. aureus* and Pam3CSK4. Both, UM-SCC-59 and -97 express similar TLR2 levels to UM-SCC-49.

Due to the ability of UM-SCC-97 to upregulate PDL1 in response to TLR2 agonists, we used this model to further interrogate the role of TLR activation in modulating PDL1. As we showed that *S. aureus* can induce expression of PDL1 in HNSCC cell lines, we also asked whether other common infectious bacteria might induce a similar response. PDL1 is generally thought to be upregulated in response to cytokine release by T-cells, but we found that even in the absence of T-cells, various bacterial strains known to activate TLR2 were able to induce PDL1 expression (Figure 4-7C). Additionally, siRNA knockdown of TLR2 in UM-SCC-97 blocked the upregulation of PDL1 in response to Pam3CSK4, indicating that the ligand indeed acts as a TLR2 agonist in this system (Figure 4-7D). We saw similar results with knockdown of the p65 (RELA) subunit of NFκB, indicating that the NFκB pathway may be an essential mediator of PDL1 induction following TLR2 activation.

Discussion

Here, we present validation of a genome-scale CRISPR knockout-screen to identify genes regulating the expression of PDL1 on the surface of UM-SCC-49 cells. Our study highlights both the promise and challenges of positive selection based screening of CRISPR libraries. While we were able to validate a PDL1 regulating signal from among the top hits of our screen, certain technical issues obscure our ability to interpret our screening results as a whole. Because the library was constructed with three gRNAs targeting each gene, we expected that for our strongest candidate PDL1 regulators, multiple gRNAs for the same gene would be identified. This was not the case, however, and limited our ability to statistically nominate candidate genes. We postulate that 1) highly variable initial representation of gRNAs in the initial library, and 2) limited ability of our selection method to detect small differences in PE fluorescence with

precision and accuracy may have contributed to the unexpected distribution of gRNAs in our sorted samples. Additionally, heterogeneity of the UM-SCC-49-WT cell line, including variability in the epigenome, could cause altered regulation of PDL1 in subpopulations regardless of genetic knockout status. We also may have been selecting for a survival and/or proliferative advantage as our cells were propagated in culture between sorts. For example, the $PDL1^{high}$ and $PDL1^{low}$ screens each nominated a unique gRNA targeting *KLHL30,* suggesting that knockout of this gene conferred an advantage under our growth conditions. Further validation of targets from this screen, and repetition of our screening protocol in this and other models, will be necessary to truly define the robustness of our method.

Another puzzling finding was that the GeCKO screen did not nominate the gene encoding PDL1 (*CD274*), despite the presence of *CD274* targeted gRNAs in the unsorted control library. Further investigation will be necessary to understand the cause of this observation. It is possible, despite the purported optimization of the GeCKO library for efficient and specific knockout, that *CD274* was not efficiently or specifically disrupted. Otherwise, this observation may necessitate further optimization of our sorting protocol.

We also provide evidence that activation of innate immune response genes, not only in immune cells but also intrinsically to HNSCC cells, can induce PDL1 expression. This finding suggests that tumor cells may be able to intrinsically upregulate PDL1 by overexpressing or activating TLRs. It is also possible that tumors arising in the context of inflammation may be more likely to utilize TLRs as a mechanism for PDL1 upregulation. Lyford-Pike et al showed that PDL1 is highly expressed in tonsillar crypts, a common site of infection, and postulate that this may represent and "immune privileged" environment hospitable to oncogenic virus infection and tumorigenesis [9]. The finding that TLR agonists and bacterial pathogens themselves may

directly promote upregulation of PDL1 in tumor cells brings an additional facet to this hypothesis.

This observation is of particular interest due to recent clinical trials using TLR agonists to treat cancer. Toll-like receptors reportedly exhibit both tumorigenic and anti-tumor effects, which are not fully understood and may be highly context-dependent. Stimulation of TLRs to treat bladder cancer dates back to the 1880s, and the TLR2/4 agonist Monophosphoryl lipid A is used in as a prophylactic vaccine adjuvant for HPV associated cervical cancer [15]. However, studies in other cancer types have reported an association between TLR expression and invasion and metastasis. Furthermore, knockdown or knockout of TLRs has led to tumor regression and reduced metastasis in in liver, breast and lung cancer models [15, 16]. Thus, elucidating the precise, likely multifactorial, impact of TLR modulation across the spectrum of HNSCC subtypes will be important in understanding the clinical implications of this work.

The present study is limited in that it does not address functional effects of TLR2 modulation of PDL1 expression in more complex systems. T-cell co-cultures and *in vivo* models will be necessary to determine the functional significance of our observation. Specifically, we will need to assess whether direct modulation of TLR2 on cancer cells impacts T-cell killing, and whether PDL1 mediates this effect. Due to the many established roles of TLRs in controlling immune responses, it is very likely that modulation of TLRs will have broader effects in vivo beyond simply PDL1 protein regulation, and understanding these will be crucial if our findings are to eventually be translated to the clinic.

Acknowledgements.

I would like to thank Megan Ludwig for the GeCKO library, Aditi Kulkarni for bioinformatics analysis, and Judy Kafelghazal and Julia Eisenberg for technical assistance.

Figures

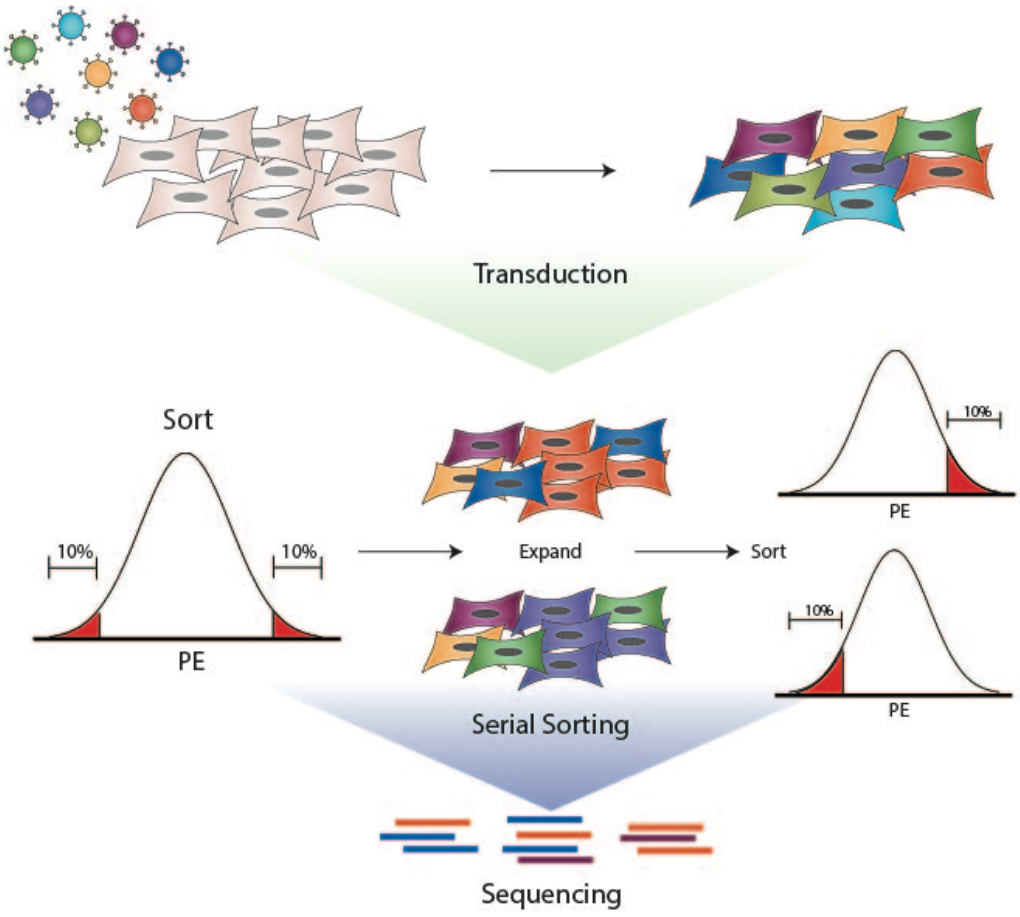

Figure 4-1 Establishing phenotypically distinct populations from UM-SCC-49-GeCKO pool.

Workflow is shown for generation of UM-SCC-49-GeCKO pool, cell sorting, and sequencing of final populations

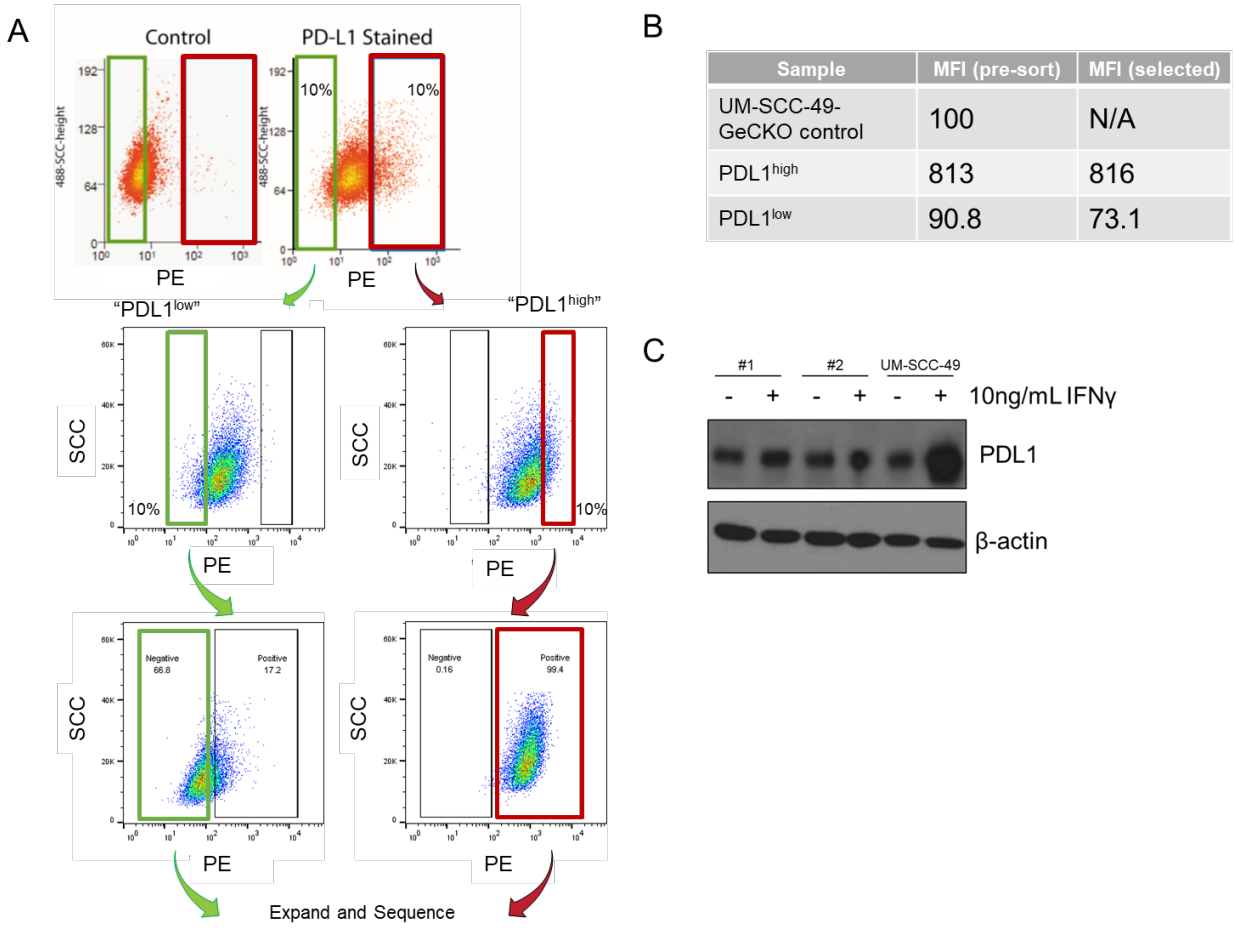

Sample	MFI (pre-sort)	MFI (selected)
UM-SCC-49-GeCKO control	100	N/A
PDL1^{high}	813	816
PDL1^{low}	90.8	73.1

Figure 4-2 Sorting of UM-SCC-49-GeCKO pool for PDL1 enhanced or deficient cells.

A) UM-SCC-49 cells infected with the GeCKO library were treated with 10ng/mL IFNg for 72h, trypsinized, and stained using a PE-conjugated antibody directed against PDL1. Cells were then subjected to cell sorting by flow cytometry (upper panels) to select the 10% of cells with the lowest PDL1 expression (green gate) and 10% with the highest (blue gate). PDL1^{low} cells were expanded in culture and sorted again for the 10% of cells with lowest PDL1 expression, while PDL1^{high} cells were expanded and sorted for the 10% with highest PDL1 expression (middle). The two populations were expanded again in culture and PDL1 surface expression analyzed a third time (lower panels). Green and red gates indicate populations of cells collected for PDL1^{low} and PDL1^{high} respectively. (B) Median fluorescence intensities (MFIs) are reported for indicated populations. (C) Individual cells were isolated and propagated from PDL1-low final sort, arbitrarily designated Clone #1 and #2. These and UM-SCC-49-wt were treated +/- IFNg for 72h and PDL1 was assessed by immunoblot.

A

Sample	Mapped reads ($x10^6$)	% library coverage	# gRNAs	# Unique gRNAs
Control	5.4	70.2	44,892	N/A
PDL1^{low}	4.0	11.2	7162	2692
PDL1^{high}	4.1	15.5	9922	5436

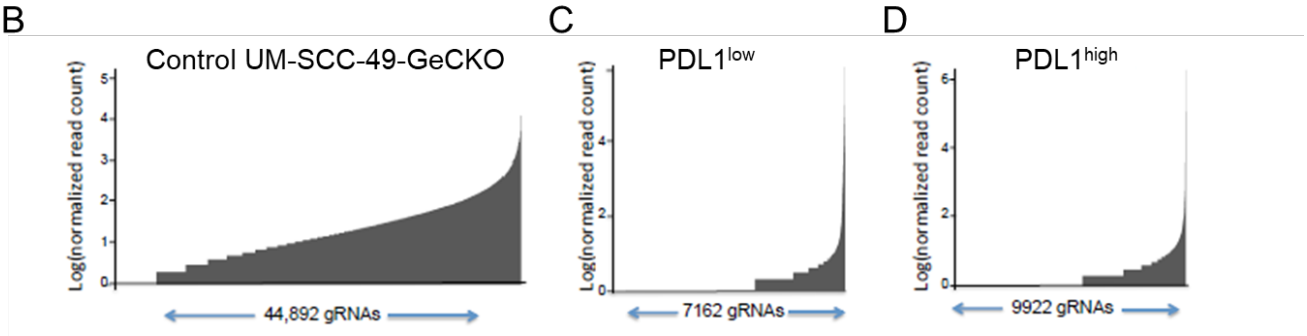

Figure 4-3. Sequencing of UM-SCC-49-GeCKO populations.

A) Mapping statistics from UM-SCC-49-GeCKO sequencing results. B-C) Distribution of read counts across gRNAs (normalized to total reads for each sample and log transformed).

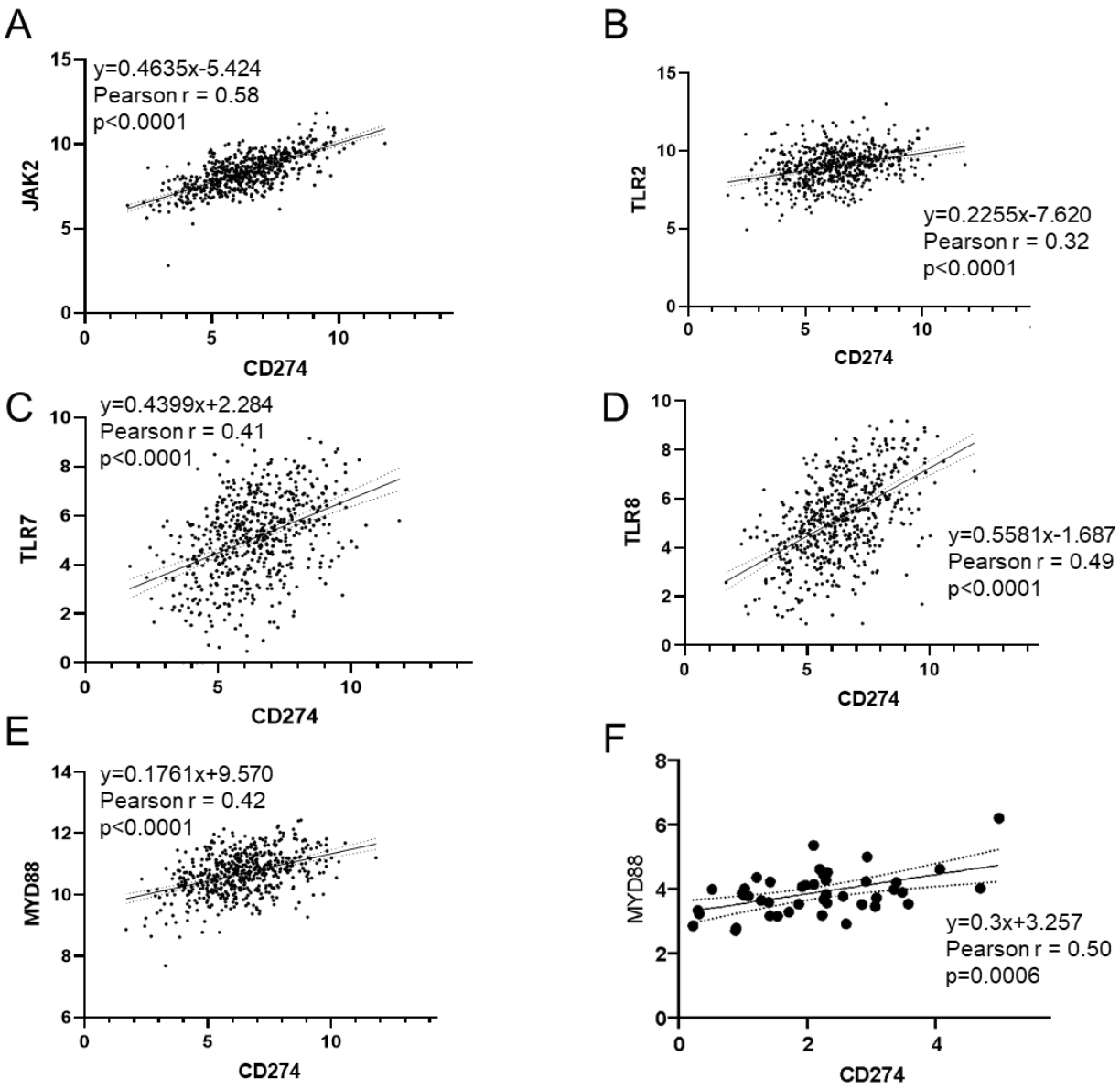

Figure 4-4. RNA expression in TCGA HNSC cohort.

A-E) TCGA Head and Neck Cancer samples were analyzed (n=566) for correlation between genes of interest (y-axis) and PDL1 (*CD274*; x-axis). Linear regression analysis was performed using (log_2(RSEM+1) and Pearson's r values are reported. F) Log_2(FPKM+1) values for PDL1 (*CD274*) and MYD88 RNA from HNSCC cell lines were analyzed (n=43).

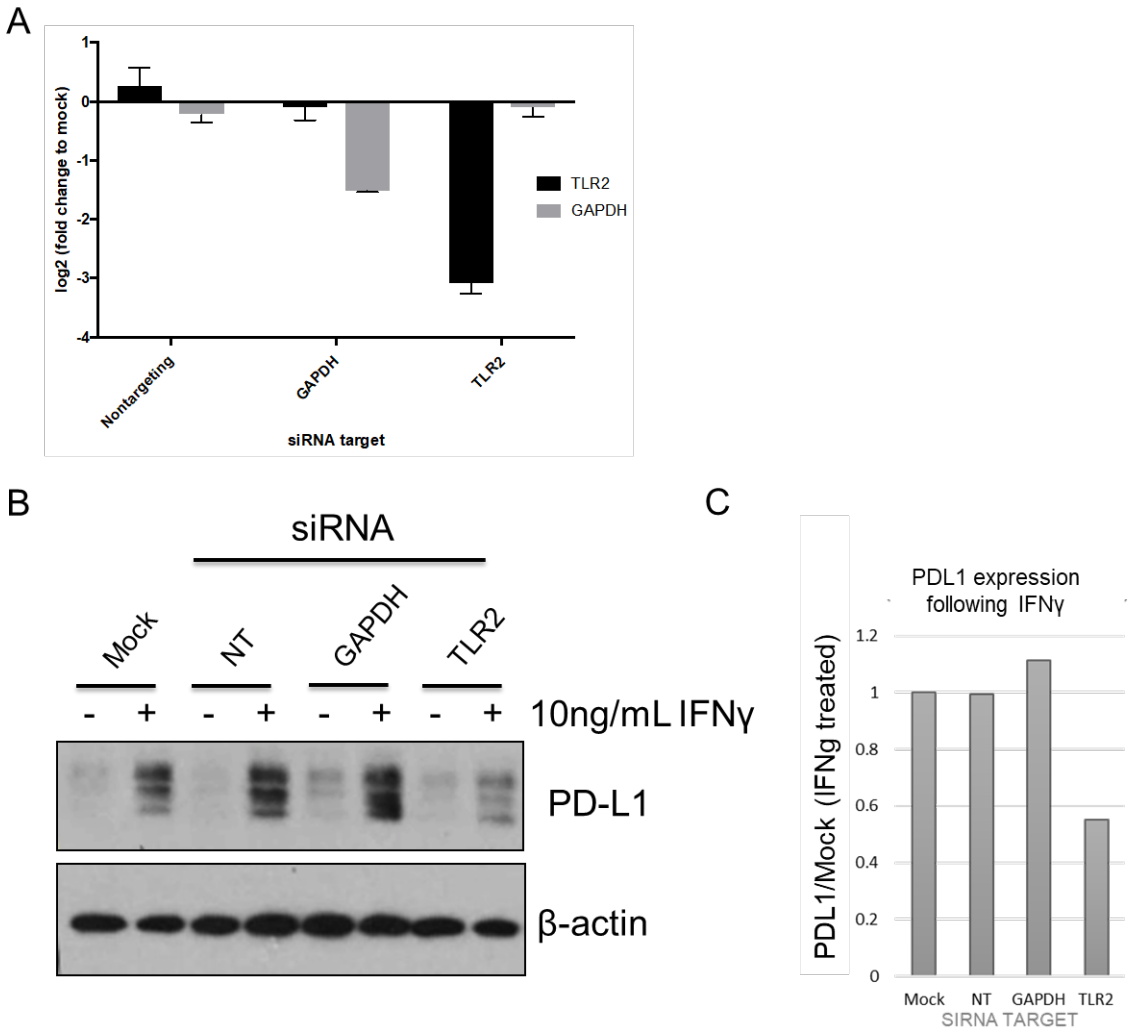

Figure 4-5. Knockdown of TLR2 in UM-SCC-49 reduces IFNg mediated upregulation of PDL1.

A) Knockdown of TLR2 and GAPDH was confirmed by qPCR. B) Cells were transfected with non-targeting (NT), GAPDH, or TLR2 siRNA for 24h were then treated -/+ IFNγ for 48h. PDL1 expression was assessed by immunoblot. C) Bands in (B) for IFNγ treated samples were quantified by densitometry. Densitometry units for PDL1 bands were normalized to respective β-actin bands. Normalized values were then divided by Mock.

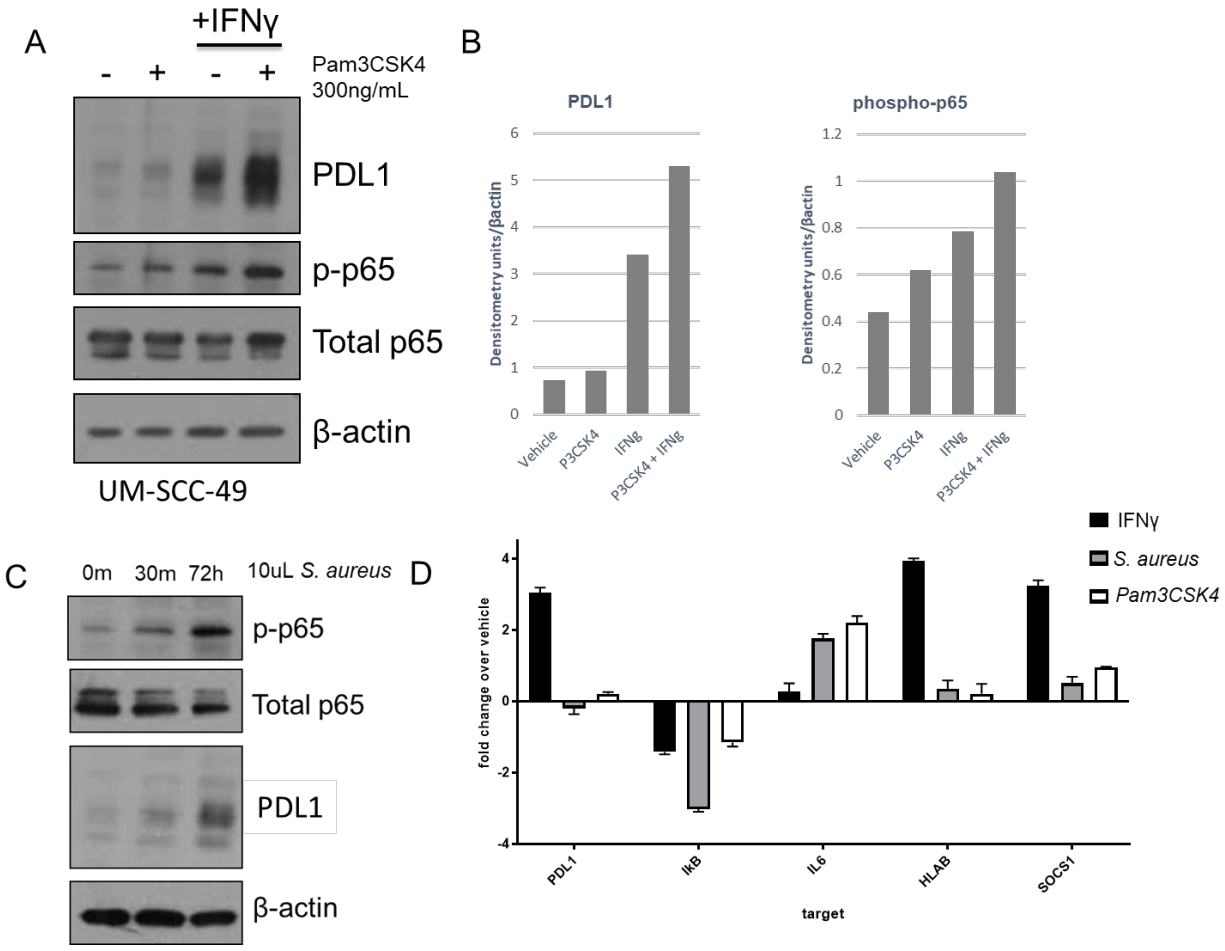

Figure 4-6. Effects of TLR2 activators in UM-SCC-49.

A) UMSCC49 cells were treated -/+300ng/mL Pam3CSK4 -/+ 10ng/mL IFNg for 72h. Protein lysates were analyzed by immunoblot and bands were quantified by densitometry in (B). C) UM-SCC-49 cells were treated for indicated timepoints with 0.075% S. aureus (Millipore) and lysates were analyzed by immunoblot. D) qPCR analysis of IFNg and TLR effectors and PDL1 expression in UM-SCC-49 treated with for 72h.

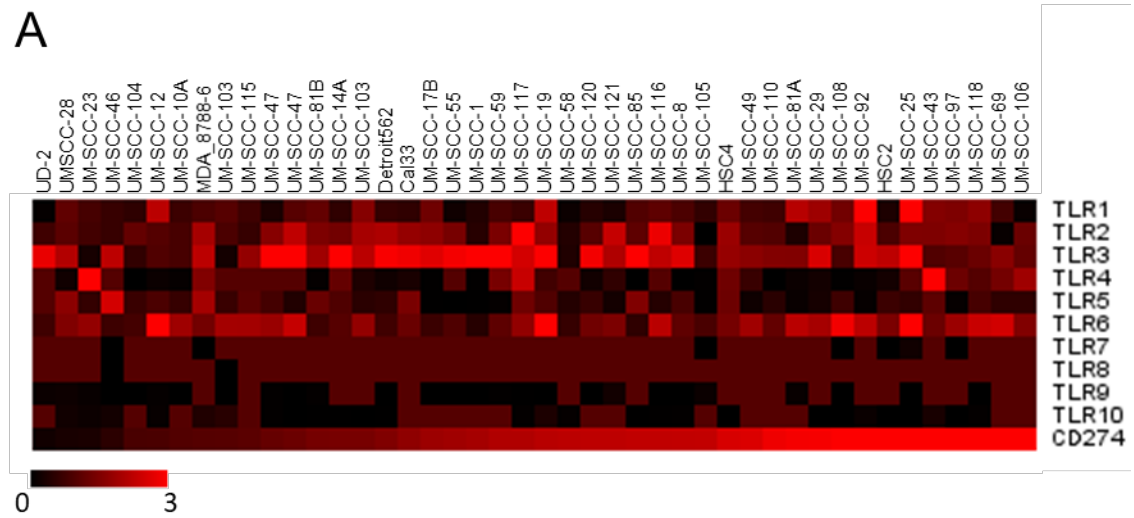
A
UD-2
UMSCC-28
UM-SCC-23
UM-SCC-46
UM-SCC-104
UM-SCC-12
UM-SCC-10A
MDA_8788-6
UM-SCC-103
UM-SCC-115
UM-SCC-47
UM-SCC-47
UM-SCC-81B
UM-SCC-14A
UM-SCC-103
Detroit562
Cal33
UM-SCC-17B
UM-SCC-55
UM-SCC-1
UM-SCC-59
UM-SCC-117
UM-SCC-19
UM-SCC-58
UM-SCC-120
UM-SCC-121
UM-SCC-85
UM-SCC-116
UM-SCC-8
UM-SCC-105
HSC4
UM-SCC-49
UM-SCC-110
UM-SCC-81A
UM-SCC-29
UM-SCC-108
UM-SCC-92
HSC2
UM-SCC-25
UM-SCC-43
UM-SCC-97
UM-SCC-118
UM-SCC-69
UM-SCC-106
TLR1
TLR2
TLR3
TLR4
TLR5
TLR6
TLR7
TLR8
TLR9
TLR10
CD274
0
3

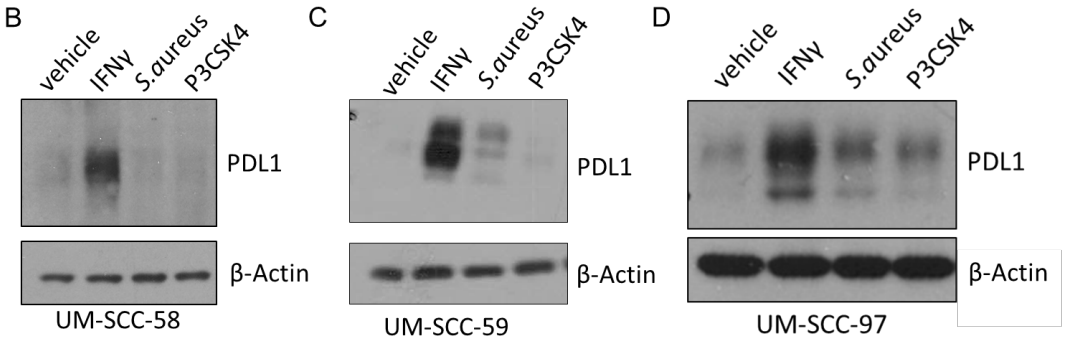
B
vehicle
IFNγ
S.aureus
P3CSK4
PDL1
β-Actin
UM-SCC-58
C
vehicle
IFNγ
S.aureus
P3CSK4
PDL1
β-Actin
UM-SCC-59
D
vehicle
IFNγ
S.aureus
P3CSK4
PDL1
β-Actin
UM-SCC-97

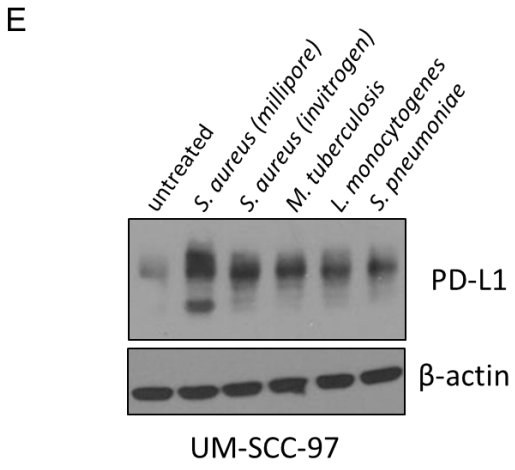
E
untreated
S. aureus (millipore)
S. aureus (invitrogen)
M. tuberculosis
L. monocytogenes
S. pneumoniae
PD-L1
β-actin
UM-SCC-97

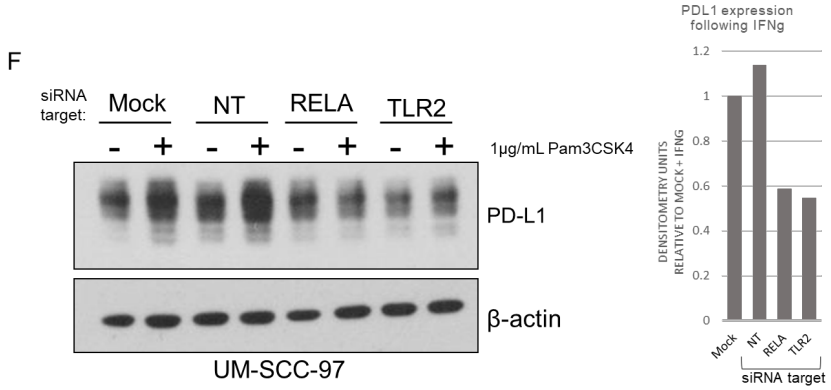

Figure 4-7. TLR2 signaling in HNSCC cell lines.

A) RNA expression (log2(FPKM+1)) of indicated genes in HNSCC cell lines. Cell lines are arranged from left to right in order of increasing expression of PDL1 (CD274). B-D) HNSCC cells were treated with vehicle control, 10ng/mL IFNγ, 0.075% S. aureus (Millipore), or 300ng/mL Pam3CSK4 for 72h. PDL1 expression was analyzed by immunoblot. E) UM-SCC-97 was incubated with heat-killed commercially available bacterial strains as indicated for 72h. F) Indicated siRNAs were transfected into UM-SCC-97 cells. 24h post transfection, cells were treated with Pam3CSK4 for an additional 48h. PDL1 was analyzed by immunoblot (left) and relative band intensity was quantified by densitometry (right).

Tables

Gene	Forward	Reverse
TLR2	AGCAGGATCCAAAGGAGACC	ACCAAGGTGGTTTGCTGAGT
GAPDH	AATGGGCAGCCGTTAGGAAA	GCCCAATACGACCAAATCAGA
PDL1	AGTCAATGCCCCATACAACAA	CGTCACTGCTTGTCCAGATGA
MYD88	GACTGCTCGAGCTGCTTACC	ACATTCCTTGCTCTGCAGGT

Table 4-1. Primer sequences for qPCR 3'-5'.

Rank	gRNA target	PDL1^{low}/Control	PDL1^{high}/Control
1	RNF130	130.4702	0.61437
2	UIMC1	97.62247	0.533461
3	KLHL30	97.47681	0
4	C1orf116	93.29673	0.604938
5	SLC2A6	93.00492	0.467358
6	TLR2	80.91354	0.363622
7	KIDINS220	74.24762	0.376101
8	COMP	73.34039	0.374752
9	STAB1	48.71035	0.181629
10	NFYB	45.65152	0.163268
11	DISP2	38.79179	0.872197*
12	SLC25A25	36.74726	0.14868
13	C7orf55	36.6708	0.194452
14	SSMEM1	34.35596	0.153269
15	TSPAN31	30.65758	0.121086
16	UNKL	27.33073	0.127668
17	ITSN1	14.07346	0.076536
18	HIRA	13.86975	0.066925
19	ZDHHC24	11.48397	5.910346
20	NODAL	11.19729	0.06114
21	TTL	7.2976454	0.027327

22	C1orf35	7.269804	0.038215
23	ULBP2	6.721698	0.028772
24	AXDND1	6.5365	0.040082
25	ZFP64	6.110201	0.042713
26	MAGEA6	5.625484	0.045438
27	PCDHGB6	5.256831	0.039738
28	FAM168B	4.806231	0.031167
29	FABP6	4.648937	0.03478
30	USP16	4.350071	0.028961
31	VPS25	4.180224	0.033329
32	SPATA31A2	4.175848	0.035267
33	NPR1	3.975242	0.033517
34	CKMT1A	3.801816	0.020674
35	CCDC117	3.520316	0.02719
36	KIF13B	3.131082	0.022894
37	FZR1	2.847764	0.022893
38	ZNRF3	2.696549	0.02445
39	STRN3	2.642702	0.026301
40	BLCAP	2.598926	0.020274
41	GMNC	2.586674	0.020701
42	KDM6A	2.56034	0.026508
43	OR5T2	2.554679	0.028434
44	CLNS1A	2.489466	0.021168

45	RAD50	2.088789	0.0218049
46	NARR	2.070283	0.020284
47	NARR	2.070283	0.020284*
48	HINT1	2.068037	0.018824
49	IRG1	2.043546	0.0089151
50	SLC9A6	2.043088	0
51	TTC34	1.554888	0.022822

Table 4-2. gRNAs ranked by enrichment in PDL1^{low} over control.

Rank	gRNA target	Chapter 1 PDL1^{high}/Control	Chapter 2 PDL1^{low}/Control
1	IZUMO3	223.6348	1.0669
2	hsa-mir-105-1	167.3409	1.178067
3	GLS	111.713	0.854239
4	FAT2	104.4253	0.590414
5	SCGB3A1	50.81308	0.337907
6	RAPGEF3	37.84282	0.242991
7	AP2A1	31.35016	0.214096
8	TRIM49	29.33133	0.181142
9	hsa-mir-105-2	9.937754	0.060283
10	FIGLA	6.562241	0.021861
11	POGLUT1	6.558918	0.06121
12	ZDHHC24	5.910346	11.48397
13	KCNIP2	5.604062	0.0485690
14	ZNF37A	4.446165	0.038013
15	TTC5	3.348804	0
16	SLC35F3	2.39854	0
17	FAM71C	2.325857	0
18	CXorf21	2.179963	0.014468
19	RBBP8	2.111634	0.04188
20	CCDC129	1.992549	0
21	SLC5A8	1.902974	0
22	CHST2	1.864696	0.068597
23	P2RY2	1.836203	0
24	SEMA6C	1.834026	0.015726
25	SPHK1	1.797793	0
26	KLHL30	1.794423	0.007607
27	hsa-mir-212	1.77299	0
28	CARNS1	1.744393	0
29	BRF2	1.744393	0
30	LMNB2	1.744393	0
31	MCL1	1.744393	0
32	GNA13	1.744393	0
33	NF2	1.722029	0.714116

Table 4-3. gRNAs enriched in PDL1high over control.

Bibliography

1. Concha-Benavente, F., et al., *Identification of the Cell-Intrinsic and -Extrinsic Pathways Downstream of EGFR and IFNgamma That Induce PD-L1 Expression in Head and Neck Cancer.* Cancer Res, 2016. **76**(5): p. 1031-43.
2. Sun, C., R. Mezzadra, and T.N. Schumacher, *Regulation and Function of the PD-L1 Checkpoint.* Immunity, 2018. **48**(3): p. 434-452.
3. Schuster, A., et al., *RNAi/CRISPR Screens: from a Pool to a Valid Hit.* Trends in Biotechnology, 2019. **37**(1): p. 38-55.
4. Smith, I., et al., *Evaluation of RNAi and CRISPR technologies by large-scale gene expression profiling in the Connectivity Map.* PLOS Biology, 2017. **15**(11): p. e2003213.
5. Shalem, O., et al., *Genome-scale CRISPR-Cas9 knockout screening in human cells.* Science, 2014. **343**(6166): p. 84-87.
6. Wang, T., et al., *Genetic screens in human cells using the CRISPR-Cas9 system.* Science, 2014. **343**(6166): p. 80-4.
7. Sanjana, N.E., O. Shalem, and F. Zhang, *Improved vectors and genome-wide libraries for CRISPR screening.* Nature methods, 2014. **11**(8): p. 783-784.
8. Mann JE, Kulkarni A, Birkeland AC, Kafelghazal J, Eisenberg J, Jewell BM, Ludwig ML, Spector ME, Jiang H, Carey TE, Brenner JC. *The molecular landscape of the University of Michigan laryngeal squamous cell carcinoma cell line panel.* Head Neck. 2019. Sep;41(9):3114-3124
9. Benakanakere, M.R., et al., *Modulation of TLR2 protein expression by miR-105 in human oral keratinocytes.* The Journal of biological chemistry, 2009. **284**(34): p. 23107-23115.
10. Lyford-Pike, S., et al., *Evidence for a role of the PD-1:PD-L1 pathway in immune resistance of HPV-associated head and neck squamous cell carcinoma.* Cancer Res, 2013. **73**(6): p. 1733-41.
11. Cheng, K., et al., *Specific activation of the TLR1-TLR2 heterodimer by small-molecule agonists.* Science Advances, 2015. **1**(3): p. e1400139.
12. Kumar, H., T. Kawai, and S. Akira, *Pathogen recognition by the innate immune system.* Int Rev Immunol, 2011. **30**(1): p. 16-34.
13. Wang, J., G. Roderiquez, and M.A. Norcross, *Control of adaptive immune responses by Staphylococcus aureus through IL-10, PD-L1, and TLR2.* Scientific reports, 2012. **2**: p. 606-606.
14. Li, H., et al., *LPS promotes the expression of PD-L1 in gastric cancer cells through NF-kappaB activation.* J Cell Biochem, 2018. **119**(12): p. 9997-10004.
15. Braunstein, M.J., J. Kucharczyk, and S. Adams, *Targeting Toll-Like Receptors for Cancer Therapy.* Targeted Oncology, 2018. **13**(5): p. 583-598.
16. Kim, S., et al., *Carcinoma-produced factors activate myeloid cells through TLR2 to stimulate metastasis.* Nature, 2009. **457**(7225): p. 102-6.

Chapter 5 Summary and Perspectives

Summary

Here, we have profiled various genetic, transcriptomic, and immunologic features of HNSCC, provided evidence for CD103+ TIL content as a potential prognostic biomarker, and validated multiple drivers of PDL1 expression. Because PDL1 expression is believed to play a role in HNSCC immune evasion but immunotherapies targeting this pathway are minimally effective, we sought to better understand the mechanisms contributing to this pathway in the hopes that we may eventually identify features of HNSCC that predict immunogenicity. We utilized cutting-edge genome wide screening techniques to select HNSCC cells with altered PDL1 expression and validated multiple hits nominated by these screens. Moving forward, we hope to further elucidate the precise mechanisms underpinning our observations and ultimately to advance the signals we discuss here as prognostic/predictive biomarkers or therapeutic targets to improve outcomes in HNSCC. The detailed landscape of the UM-SCC cell line panel we describe here will serve as a useful tool for integrating our findings with the heterogeneous characteristics of HNSCCs. In the future, we envision the development of a more comprehensive profile of tumor- intrinsic and extrinsic features influencing immunogenicity to inform precision immunotherapy strategies for diverse patient populations.

Section 1: Challenges and opportunities in immune modulation

It has been previously established that immune infiltration portends more favorable outcomes in HNSCC and other cancer types, suggesting that particular tumors may be better primed for immune-mediated clearance [1, 2]. This is especially true of HPV-associated tumors, which are known to carry a better prognosis than HPV negative tumors, bear a distinct immunologic phenotype marked by high levels of CD8+ T-lymphocytes, and respond better to anti-PD1 immunotherapy [3]. Here, we sought to better understand the prognostic value of specific subsets of tumor infiltrating lymphocytes (TILs) in recurrent laryngeal squamous cell carcinoma, which is typically HPV-negative [4]. While CD103 status was previously assessed in lung and ovarian cancers [5, 6], we were the first to investigate its significance in HNSCC. Our findings build upon previous reports by specifically identifying a CD103+/CD4+ TIL phenotype as an especially strong predictor of survival in this setting, supporting further investigation into the role of the CD103+ TIL population in HNSCC. Since the publication of our report, a large (464 participant) prospective evaluation of TILs in previously untreated HNSCC patients has been described [7], showing that TILs were independently associated with improved overall survival in each disease site, albeit to varying degrees. Furthermore, high CD4+ TIL counts were associated with decreased risk of death after primary chemoradiation, but not after surgery, further bolstering the concept that specific TIL populations may serve as predictive biomarkers and guide patient stratification. As the predictive/prognostic potential of TILs in HNSCC becomes clear, it will be useful to continue to more intricately characterize T-cell subsets to generate improved models for predicting outcomes. It will be of particular interest to investigate a relationship between TIL status and PDL1 expression in this setting, and to explore TIL status

as a predictive marker in patients treated with immunotherapy, as it is possible that tumors rich in specific T-cell subsets will derive greater benefit.

Considering the potential prognostic significance of immune infiltration in HNSCC and the idea that certain tumors may be better primed for immune response, we chose to investigate mechanisms modulating tumor immune checkpoints, with the ultimate goal of predicting or improving response to immunotherapy. Since the 2016 FDA approval of anti-PD1 therapies for R/M HNSCC, Pembrolizumab as a monotherapy has also been approved as first line treatment for HNSCC patients whose tumors express PDL1 [8]. However, while the approval of anti-PD1 therapy represents a landmark development in the management of a disease that has been, for several decades, strikingly devoid of therapeutic advances, the overall proportion of HNSCC patients who benefit from immunotherapy is small, and clinicians' capacity to prospectively select these patients is limited [9]. Some characteristics of HNSCC and other cancers have been shown to correlate with response to immunotherapy, including PDL1 expression, T-lymphocyte infiltration, HPV status, and tumor mutational burden [10-19]. Each is a rational approach to stratifying patients, but in practice falls short of reliably defining responsive populations. While PDL1 expression levels are currently used to guide clinical decisions surrounding anti-PD1 therapy, numerous studies on this topic have yet to reach a consensus as to how strongly this metric correlates with response [9, 20]. Interpretation of these results as a whole has likely been complicated by discordance in study design, as thresholds for PDL1 positivity vary widely, detection antibodies differ in specificity, and different methods of tissue sampling (tumor only vs tumor plus peritumoral sampling, for example) are used across studies. Additionally, PDL1 expression is intratumorally heterogeneous, further convoluting the results of these investigations. The as yet unmet challenges of defining a reliable threshold for PDL1 positivity

and establishing its role in predicting survival and therapeutic response highlight a need for improved biomarkers.

Our work suggests that common features of HNSCCs, such as FGFR activity, could potentially function in tumor cells to modulate immune checkpoints in addition to their documented roles in tumorigenesis. As we have identified novel PDL1 drivers that are also known to be dysregulated in cancer, we would next ask whether aberrant activity of these genes could mark highly immunosuppressive tumors and potentially serve as more reliable biomarkers for response to anti-PD1 therapy. TCGA reported FGFR1 and FGFR3 alterations among the most common genetic aberrations in HNSCC tumors [21]. Based on our findings, we next hypothesize that a subset of tumors with FGFR pathway dysregulation may also express more PDL1. Thus, we would next investigate a correlation between PDL1 expression and FGF/FGFR family alterations, including fusions, amplifications, mutations, and overexpression. It will be especially crucial to assess FGFR activity in this setting (e.g. phosphorylated FGF receptors) to bolster the claim that FGFRs induce high PDL1 levels. It would therefore be pertinent to analyze phosphorylated (activated) FGFRs in relation to PDL1 levels in human tumors by immunohistochemistry.

This work also aims to eventually inform rational combination immunotherapy approaches. We specifically pursued candidate pathways (FGFR and TLR) that have already been established as drug targets and for which clinical trials are underway, which could allow for more efficient translation of our findings to the clinic. The concept that immune checkpoints may be targeted indirectly via known drivers of cancer invites exciting new avenues for immune modulation and implies heretofore unexplored anti-tumor effects of current therapeutics. In recent months, multiple studies focused on other cancer types have also provided evidence for

the use of FGFR inhibitors in combination with anti-PD1 therapy. Li et al showed in cell line and murine models of colorectal cancer that FGFR2 activity induces PDL1 expression [22]. In September 2019, Palakurthi et al demonstrated that FGFR inhibition reduces PDL1 expression in murine models of non-small cell lung cancer (NSCLC) and that FGFR inhibition in combination with anti-PD1 yielded a survival benefit over either treatment alone [23]. Thus, we speculate that targeting of FGFR activity may also serve to improve the efficacy of immunotherapy regimens for HNSCC. Also yet to be investigated is the influence of genetic aberrations in the FGFR pathway in mediating the phenotypes described above. FGFR mutations and fusions are not especially common in HNSCC (4.2% of tumors) and most affect FGFR3 [21], but it is possible that these features may denote a specific subset of patients more or less likely to respond to immunotherapy alone or to combination FGFR/anti-PD1 therapy. Further exploration of the FGFR mutant population would therefore be of particular interest and could lead to development of a biomarker more perspicuous than those that are currently in use, which are challenging to reliably quantify.

Our observation that TLR2 may directly modulate PDL1 is also of interest given recent trials of TLR agonists in HNSCC. Multiple trials currently underway are investigating TLR8 and TLR9 agonists in combination with the biologic cetuximab, which targets EGFR [24, 25]. Rationalizing this approach is the observation that cetuximab can induce antibody-dependent cellular cytotoxicity in addition to inhibiting EGFR activity, and that this effect could be enhanced by activation of TLRs [25]. The results of our study, however, suggest that the potential for PDL1 upregulation under these conditions could be an important consideration, and may support either more scrupulous patient selection for TLR agonist therapy or even the addition of PD1 inhibition to this regimen.

Another point for future inquiry would be the role of the microbiome in modulating response to immunotherapy, and whether this could be influenced by tumor-intrinsic aberrant expression or activity of TLRs. Myriad roles for specific bacterial taxa in modulating anti-tumor immune responses have been described in melanoma, and the abundance of certain bacteria has been associated with such metrics as survival, response to immunotherapy or chemotherapy, and risk of treatment toxicities in several human cancers and in murine models [26-28]. Generally, it appears that components of the normal gut microbiota confer therapeutic response and survival benefits, while imbalances may lead to detrimental immune inhibitory effects [26, 29]. These studies exclusively consider the gut microbiome, and center around the ability of microbes to modulate local and systemic immune responses. The impact of the oral microbiome in HNSCC is unclear, and the concept that bacteria may act directly on tumor cells to modulate immunogenicity has not been thoroughly explored. Recently, periodontal bacteria *Porphyromonas gingivalis* and *Fusobacterium nucleatum* have been implicated in carcinogenesis [30]. Both are also known to activate TLR2 [31, 32], leading us to speculate that these species might directly contribute to immune evasion in tumor cells expressing TLR2 during oral carcinogenesis. Modeling this *in vivo* will be vital to understanding the complexity of interactions between oral bacteria, the local and systemic immune system, and the tumor itself.

Section 2: Positive-selection based genome-wide screening

We describe here the application of two different genome-scale screening techniques toward the identification of genes and pathways regulating PDL1 expression in cell lines. Functional screening at this scale has historically relied on sh- or si-RNA libraries, which are wrought with complications such as off-target effects [33]. The efficiency and specificity

offered by CRISPR technology has revolutionized library screening and presents a plethora of opportunities to apply this concept towards improving our understanding of critical biological processes. Our report adds to the array of studies demonstrating the utility of these libraries in elucidating drivers of particular phenotypes. The open reading frame screen we present here is also among the first applications of whole-genome overexpression screening in mammalian cells. However, our results also highlight some important technical challenges that will need to be addressed as we expand our usage of these systems.

The overexpression screen discussed in Chapter 3 revealed multiple intriguing genes potentially driving PDL1 expression, five of which we were able to validate. Future experiments will define the mechanisms through which these genes modulate PDL1 and expand our analysis of the enriched gene list to validate and advance other hits. Shortly after we completed our screen, an interesting report was published involving the most enriched gene we identified: *ERO1L*. Tanaka et al demonstrated that in breast cancer cell lines, ERO1L promotes PDL1 expression both through a HIF1alpha dependent transcriptional mechanism and through facilitation of oxidative protein folding [34]. This finding lends support to the idea that our screening protocol was able to select positive PDL1 regulators. It will be of interest to our group to explore a similar relationship between ERO1L and PDL1 in HNSCC, and to understand whether this could be assessed as a biomarker or could represent a novel therapeutic target.

Of particular relevance to our work was the 2017 discovery of CMTM6 as a critical regulator of PDL1 in pancreatic cancer cells using genome-wide CRISPR screening with FACS based selection [35, 36]. This finding was recapitulated in breast cancer, melanoma, and lung cancer models. Burr et al and Mezzadra et al reported that CMTM6 specifically regulated cell surface expression of PDL1 and was required for endocytic recycling of PDL1 [35, 36]. Given

the similarity of our experimental design to that described by Burr et al, we expected concordance between our findings. Surprisingly, *CMTM6* was not represented in the list of enriched gRNAs nominated by our CRISPR screen. While this finding could be the result of biological differences between these two systems, we postulate that it could be due to poor representation of *CMTM6* gRNAs in the control pool. Only one of three *CMTM6* gRNAs was detected at all in the control pool (60 reads ; Appendix 1), and this gRNA was not detected in either PDL1 sorted population. Similar issues were evident with regard to other genes we expected to be nominated by our screen, such as the interferon gamma receptor (*IFNGR*) and *STAT1*. We found that *IFNGR* gRNAs were poorly represented in the unsorted control pool (0, 3, and 6 reads), and only one *STAT1* gRNA was detected (7 reads). It is possible that these knockouts confer such an insurmountable survival disadvantage that cells harboring these gRNAs are rapidly lost from the population.

Another point of interest is the lack of overlap among genes nominated by the two screening mechanisms, despite use of the same cell line model and selection conditions. We expected, for example, to identify some of the same targets in the $PDL1^{low}$ pool as in the selected ORF pool. We will need to better understand the efficiency of functional ORF overexpression and of genetic knockout in our systems in order to interpret this finding. It is possible that, with poor efficiency, many of the cells we selected were random false positives with either no alteration functionally expressed, or exhibiting an off target effect conferring a survival advantage. These cells may have overgrown many of the true positive cells over the course of serial sorting and expansion. We will need to repeat these screens multiple times in UM-SCC-49 to clarify false discovery rates. It will then be useful to screen additional cell lines to identify recurring pathways across diverse models.

Section 4: Future directions

Our immediate next step will be to elucidate the mechanisms of candidate PDL1 drivers nominated by our screens. To understand how the FGFR pathway, for example, influences PDL1 expression, we will perform proteome and transcriptome analyses following stimulation of cells with FGF ligands and following FGFR inhibition. It will be of particular interest to examine proteome and transcriptome changes in IFNγ stimulated cells while FGFRs are inhibited, as this may reveal novel crosstalk mechanisms between these pathways. It will also be important to replicate these experiments in multiple genetic backgrounds to determine whether these mechanisms are widely utilized and whether further advancement of this work could be broadly clinically applicable. It is possible that by examining the mechanism(s) through which candidate drivers modulate PDL1, we will identify a novel signaling node for PDL1 regulation utilized by multiple signaling pathways.

To fully understand the functional significance of FGFR and TLR signaling in anti-tumor immunity, it will be crucial to study these pathways in more complex systems. The logical next step will be to knock out or knock down our candidate drivers of PDL1 expression and assess T cell activation and T cell mediated killing in a co-culture assay using Jurkat T cells, or potentially HLA-matched patient-derived T-cells. Eventually, we can assess the impact of modulating these pathways *in vivo*. Several questions could be addressed with an *in vivo* model deficient in, for example, TLR. We would first ask whether modulation of TLR2 specifically in tumor cells impacts tumor growth and survival. We would also investigate the impact of altered TLR2 activity in the contexts of traditional HNSCC therapy (radiation, cisplatin) and in the context of anti-PD1 immunotherapy to understand whether this signal could represent a

prognostic or predictive biomarker. It would then follow to ask whether TLR inhibitors or agonists can impact outcomes. To follow up on our TLR2 observation specifically, it would be interesting to examine the role of the microbiome. It is possible that the presence of particular bacteria could influence tumor immunogenicity by activating TLRs.

An important limitation of our studies that must be addressed *in vivo* is the systemic impact of modulating candidate PDL1 drivers, as our current model exclusively examines these pathways in cancer cell lines. For example, while it may be possible to combat immunosuppression using FGFR or TLR inhibitors, it is likely that these will also affect other cell types in the microenvironment, which could lead to unforeseen pro- or anti-tumorigenic effects. FGFR inhibition, for example, also induces stromal fibroblast senescence and reduces MDSC recruitment [37]. It is also likely that our candidate PDL1 drivers support tumorigenesis in numerous ways beyond PDL1 mediated immune evasion, as is certainly the case for the FGFR signaling pathway. Thus, it may be that our PDL1 regulation data indicate just one of many factors rationalizing the modulation of these genes in HNSCC, and could indicate a feasible alternative or ancillary method of immune checkpoint targeting to improve outcomes.

Taken together, we hope the work presented here will serve as a starting point for new inquiries into the pathways modulating immunogenicity in HNSCC and that we can eventually apply a more sophisticated understanding of these signals to improve patient outcomes.

Bibliography

1. Lei, Y., et al., *Telltale tumor infiltrating lymphocytes (TIL) in oral, head & neck cancer.* Oral oncology, 2016. **61**: p. 159-165.
2. Fu, Q., et al., *Prognostic value of tumor-infiltrating lymphocytes in melanoma: a systematic review and meta-analysis.* Oncoimmunology, 2019. **8**(7): p. 1593806.
3. Wang, H.-F., et al., *The Double-Edged Sword-How Human Papillomaviruses Interact With Immunity in Head and Neck Cancer.* Frontiers in immunology, 2019. **10**: p. 653-653.
4. Ludwig, M.L., et al., *Changing the paradigm: the potential for targeted therapy in laryngeal squamous cell carcinoma.* Cancer biology & medicine, 2016. **13**(1): p. 87-100.
5. Ganesan, A.-P., et al., *Tissue-resident memory features are linked to the magnitude of cytotoxic T cell responses in human lung cancer.* Nature Immunology, 2017. **18**(8): p. 940-950.
6. Webb, J.R., et al., *Tumor-Infiltrating Lymphocytes Expressing the Tissue Resident Memory Marker CD103 Are Associated with Increased Survival in High-Grade Serous Ovarian Cancer.* Clinical Cancer Research, 2014. **20**(2): p. 434.
7. Spector, M.E., et al., *Prognostic Value of Tumor-Infiltrating Lymphocytes in Head and Neck Squamous Cell Carcinoma.* JAMA Otolaryngology–Head & Neck Surgery, 2019. **145**(11): p. 1012-1019.
8. Cramer, J.D., B. Burtness, and R.L. Ferris, *Immunotherapy for head and neck cancer: Recent advances and future directions.* Oral Oncology, 2019. **99**: p. 104460.
9. Davis, A.A. and V.G. Patel, *The role of PD-L1 expression as a predictive biomarker: an analysis of all US Food and Drug Administration (FDA) approvals of immune checkpoint inhibitors.* Journal for ImmunoTherapy of Cancer, 2019. **7**(1): p. 278.
10. Wang, J., et al., *HPV-positive status associated with inflamed immune microenvironment and improved response to anti-PD-1 therapy in head and neck squamous cell carcinoma.* Scientific Reports, 2019. **9**(1): p. 13404.
11. Turajlic, S., et al., *Insertion-and-deletion-derived tumour-specific neoantigens and the immunogenic phenotype: a pan-cancer analysis.* The Lancet Oncology, 2017. **18**(8): p. 1009-1021.
12. Gajewski, T.F., et al., *Cancer Immunotherapy Targets Based on Understanding the T Cell-Inflamed Versus Non-T Cell-Inflamed Tumor Microenvironment*, in *Tumor Immune Microenvironment in Cancer Progression and Cancer Therapy*, P. Kalinski, Editor. 2017, Springer International Publishing: Cham. p. 19-31.
13. Rosenberg, J.E., et al., *Atezolizumab in patients with locally advanced and metastatic urothelial carcinoma who have progressed following treatment with platinum-based chemotherapy: a single-arm, multicentre, phase 2 trial.* Lancet, 2016. **387**(10031): p. 1909-20.
14. Taube, J.M., et al., *Association of PD-1, PD-1 ligands, and other features of the tumor immune microenvironment with response to anti-PD-1 therapy.* Clin Cancer Res, 2014. **20**(19): p. 5064-74.
15. Yarchoan, M., A. Hopkins, and E.M. Jaffee, *Tumor Mutational Burden and Response Rate to PD-1 Inhibition.* N Engl J Med, 2017. **377**(25): p. 2500-2501.

16. Rizvi, N.A., et al., *Cancer immunology. Mutational landscape determines sensitivity to PD-1 blockade in non-small cell lung cancer.* Science, 2015. **348**(6230): p. 124-8.
17. Yarchoan, M., et al., *PD-L1 expression and tumor mutational burden are independent biomarkers in most cancers.* JCI insight, 2019. **4**(6): p. e126908.
18. Gibney, G.T., L.M. Weiner, and M.B. Atkins, *Predictive biomarkers for checkpoint inhibitor-based immunotherapy.* The Lancet. Oncology, 2016. **17**(12): p. e542-e551.
19. Vassilakopoulou, M., et al., *Evaluation of PD-L1 Expression and Associated Tumor-Infiltrating Lymphocytes in Laryngeal Squamous Cell Carcinoma.* Clin Cancer Res, 2016. **22**(3): p. 704-13.
20. Wu, P., et al., *PD-L1 and Survival in Solid Tumors: A Meta-Analysis.* PLOS ONE, 2015. **10**(6): p. e0131403.
21. The Cancer Genome Atlas, N., et al., *Comprehensive genomic characterization of head and neck squamous cell carcinomas.* Nature, 2015. **517**: p. 576.
22. Li, P., et al., *FGFR2 Promotes Expression of PD-L1 in Colorectal Cancer via the JAK/STAT3 Signaling Pathway.* The Journal of Immunology, 2019: p. ji1801199.
23. Palakurthi, S., et al., *The combined effect of FGFR inhibition and PD-1 blockade promotes tumor-intrinsic induction of antitumor immunity.* Cancer Immunology Research, 2019: p. canimm.0595.2018.
24. Miyauchi, S., et al., *Immune Modulation of Head and Neck Squamous Cell Carcinoma and the Tumor Microenvironment by Conventional Therapeutics.* Clinical Cancer Research, 2019. **25**(14): p. 4211.
25. Rajasekaran, N., et al., *Enhancement of antibody-dependent cell mediated cytotoxicity: a new era in cancer treatment.* ImmunoTargets and therapy, 2015. **4**: p. 91-100.
26. Fessler, J., V. Matson, and T.F. Gajewski, *Exploring the emerging role of the microbiome in cancer immunotherapy.* Journal for ImmunoTherapy of Cancer, 2019. **7**(1): p. 108.
27. Viaud, S., et al., *The intestinal microbiota modulates the anticancer immune effects of cyclophosphamide.* Science, 2013. **342**(6161): p. 971-6.
28. Routy, B., et al., *Gut microbiome influences efficacy of PD-1–based immunotherapy against epithelial tumors.* Science, 2018. **359**(6371): p. 91.
29. Iida, N., et al., *Commensal bacteria control cancer response to therapy by modulating the tumor microenvironment.* Science, 2013. **342**(6161): p. 967-70.
30. Chattopadhyay, I., M. Verma, and M. Panda, *Role of Oral Microbiome Signatures in Diagnosis and Prognosis of Oral Cancer.* Technology in cancer research & treatment, 2019. **18**: p. 1533033819867354-1533033819867354.
31. Jia, Y.P., et al., *TLR2/TLR4 activation induces Tregs and suppresses intestinal inflammation caused by Fusobacterium nucleatum in vivo.* PLoS One, 2017. **12**(10): p. e0186179.
32. Makkawi, H., et al., *Porphyromonas gingivalis Stimulates TLR2-PI3K Signaling to Escape Immune Clearance and Induce Bone Resorption Independently of MyD88.* Front Cell Infect Microbiol, 2017. **7**: p. 359.
33. Schuster, A., et al., *RNAi/CRISPR Screens: from a Pool to a Valid Hit.* Trends in Biotechnology, 2019. **37**(1): p. 38-55.

34. Tanaka, T., et al., *Cancer-associated oxidoreductase ERO1-alpha promotes immune escape through up-regulation of PD-L1 in human breast cancer.* Oncotarget, 2017. **8**(15): p. 24706-24718.
35. Burr, M.L., et al., *CMTM6 maintains the expression of PD-L1 and regulates anti-tumour immunity.* Nature, 2017. **549**(7670): p. 101-105.
36. Mezzadra, R., et al., *Identification of CMTM6 and CMTM4 as PD-L1 protein regulators.* Nature, 2017. **549**(7670): p. 106-110.
37. Katoh, M., *FGFR inhibitors: Effects on cancer cells, tumor microenvironment and whole-body homeostasis (Review).* Int J Mol Med, 2016. **38**(1): p. 3-15.